Dissertation
submitted to the
Combined Faculties for the Natural Sciences and for Mathematics
of the Ruperto-Carola University Heidelberg, Germany
for the degree of
Doctor of Natural Sciences

presented by
Lisa Schardt, M.Sc.
born in Siegen, Germany

Oral examination: 03.05.2017

The impact of Cyclosporine A on human epidermal keratinocytes

Referees:
Prof Dr Peter Angel
Prof Dr Petra Boukamp

This work was conducted in the Division of Skin Carcinogenesis at the German Cancer Research Center, Heidelberg, Germany, from July 2012 to February 2017.

Eidesstattliche Erklärung

Ich erkläre hiermit, dass ich die vorgelegte Dissertation selbst verfasst und mich keiner anderen als der von mir ausdrücklich bezeichneten Quellen und Hilfen bedient habe. Diese Dissertation wurde in dieser oder anderer Form weder bereits als Prüfungsarbeit verwendet, noch einer anderen Fakultät als Dissertation vorgelegt. An keiner anderen Stelle ist ein Prüfungsverfahren beantragt.

Heidelberg,

……

Lisa Schardt

DANKSAGUNG

Zu allererst möchte ich mich bei Prof. Petra Boukamp bedanken, dafür, dass Sie immer für uns da war, für uns eingestanden ist und vor allem dafür dass Sie mit Ihrer Begeisterung für die Wissenschaft mich auch immer wieder bestärkt und mitgerissen hat. Vielen Dank für deine herzliche Betreuung und für etliche inspirierende Diskussionen.

Des Weiteren möchte ich mich bei Prof. Peter Angel bedanken, für die Bereitschaft zur Begutachtung meiner Doktorarbeit, so wie für seine Expertise und sein konstruktives Feedback während meiner TAC Meetings. Auch möchte ich mich bei Prof. Martin Leverkus bedanken, der mit seinem Enthusiasmus und seinen konstruktiven Beiträgen zur Diskussion während meiner TAC Meetings diese sehr bereichert hat.

Ganz oben auf meiner Dankesliste stehen auch alle meine Kollegen der A110-Gruppe, Angelika Krischke, Angelika Lampe, Anja Bort, Christine Leufke, Elisa Specker, Elizabeth Pavez Loriè, Elke Laport, Gaby Blaser, Hans-Jürgen Stark, Heinrich Steinbauer, Herman Stammer, Iris Martin, Katharina Nöske, Katrin Schmidt, Larissa Brunner, Lena Postawa, Leonard Nevaril, Lutz Langbein, Manuel Berning, Marco Nici, Marion Eryilmaz, Marius Tham, Milena Barf, Philipp Scholz, Sabrina Bauer, Silke Prätzel-Wunder und Svenja Ewert. Vielen Dank für eine wunderbare Zeit am DKFZ. Durch euch konnte ich viele schöne Erinnerungen während meiner Promotionszeit sammeln.

Mein Besonderer Dank gilt der ZK2-Crew (Anja, Manuel und Marius). Ohne euch wäre die Zeit nur halb so toll gewesen. Vielen Dank für die unvergesslichen und schönen gemeinsamen Zellkultur-Sessions :) Auch möchte ich mich bei Manuel und Marius bedanken, dafür dass sie sich meiner am Anfang angenommen haben und mich in die Geheimnisse der OTKs eingeführt haben. Vielen Dank für eure Hilfe und unsere Diskussionsrunden, welche mir nicht nur oft weitergeholfen haben, sondern auch eine große Freude waren. Auch möchte ich nochmal bei den A110-leftovers Anja und Iris bedanken, die mit mir bis zum Schluss die Stellung gehalten haben und ohne sie es ganz bestimmt nicht so schön ‚zu Ende gegangen' wäre :)

Für die Unterstützung bei verschiedenen Methoden und die großzügigen Spenden an Antikörpern bedanke ich mich bei: Iris Martin (für die Hilfe in etwaigen Zellkultur Notlagen und Unterstützung bei meinen Experimenten), Lena und Larissa (für ihre tatkräftige Unterstützung meiner Experimente), Hanna Niehues (für Ihren LCE3 Antikörper), Masashi Narita (für seinen LCE2 Antikörper), Silke Prätzel-Wunder und Lutz Langbein (für etliche Keratin Antikörper), Evelyn Jäger (für Ihre Unterstützung durch die MassSpec Analyse), Brigitte Schoell (für Ihre Unterstützung durch die M-FISH Analyse), Dr. Sabine Rosenberger (für Ihre Unterstützung durch die TEER Analyse) und der DKFZ Genomics and Proteomics Core Facility (für die Durchführung der Genexpressionsanalysen).

Mein persönlicher Dank gilt meiner Familie, die mich in jeder Lebenslage stets unterstützt hat, so wie Lars-Lennart Oettl der mir nicht nur während der Promotion immer Rückhalt gegeben hat.

CONTENT

LIST OF FIGURES

LIST OF TABLES

ZUSAMMENFASSUNG

Das erhöhte Auftreten des kutanen Plattenepithelkarzinoms in Patienten mit Organtransplantat wird häufig mit dem Immunsuppressivum Cyclosporin A (CsA) assoziiert. Zusätzlich zu seinem therapeutischen Einfluss auf die Immunüberwachung, werden immer mehr Hinweise auf einen immun-unabhängigen Mechanismus von CsA auf nicht-Immunzellen publiziert. Jedoch sind diese beschriebenen Effekte zum Teil höchst unterschiedlich und die Langzeiteffekte von CsA auf humane Keratinozyten innerhalb eines Gewebekontext sind weitestgehend unbekannt.

Mit Hilfe von 3D organotypischen Hautkulturen (OTKs), die eine Langzeitbehandlung mit CsA in einer physiologisch relevanten Umgebung erlauben, konnten wir zeigen, dass CsA die Stratifizierung und die Differenzierung von moderat differenzierenden HaCaT Zellen, so wie die von schlecht differenzierenden HaCaT-RAS A-5 Zellen, verbessert hat. Dies wurde durch die Histologie, durch Immunfluoreszenz-Färbungen von Differenzierungsmarkern, so wie an Hand von differentiell regulierter Gene, die Teil des GO-terms ‚epidermal development' sind, gezeigt. Verbesserte Differenzierung konnte auch durch einen erhöhten transepithelialen elektrischen Widerstand nachgewiesen werden. Dieser steht im direkten Zusammenhang mit der epidermalen Barrierefunktion. Wir konnten jedoch weder erhöhte Proliferation noch invasives Wachstum nach CsA-Behandlung feststellen. Um zu überprüfen ob UV-Bestrahlung als Co-Karzinogen invasives Wachstum von CsA-behandelten HaCaT oder HaCaT-RAS A-5 Zellen zulässt, wurden OTKs parallel zu der kontinuierlichen CsA-Behandlung kontinuierlich mit UV bestrahlt. Auch diese Kombination aus UV+CsA konnte die Zellen nicht tumorigen transformieren. Stattdessen haben wir festgestellt, dass die UV-Bestrahlung und die Kombination UV+CsA ein ähnliches Regulationsmuster der ‚epidermal development' Gene hervorruft, wie das der alleinigen CsA-Behandlung. Daher lässt es sich mutmaßen, dass die CsA-Behandlung und die UV-Bestrahlung einen gemeinsamen regulatorischen Mechanismus induziert haben.

Generell überleben HaCaT Zellen in OTKs nur für einen begrenzten Zeitraum. Nach 4 bis 5 Wochen werden die Epithelien atrophisch. CsA hat jedoch in reproduzierbaren Experimenten die Lebensdauer dieser HaCaT Epithelien verlängert, in dem es mehr vitale basale und suprabasale Keratinozyten erhalten hat. Wie durch eine Genexpressionsanalyse und anschließender Ingenuity® Pathway Analysis indiziert wurde, hat CsA den Zelltod reduziert, möglicherweise durch den HGF oder Integrin Signalweg.

Da es notwendig war verschiedene Seren für unsere Experimente zu benutzen, haben wir festgestellt, dass in einem bestimmten Serum HaCaT Zellen, zusätzlichen zu den oben beschriebenen Charakteristika, invasiv gewachsen sind wenn diese mit CsA behandelt wurden. Dies wurde durch die

Unterbrechung der Basalmembran und die Infiltration von HaCaT Zellen in die darunter liegende Dermis gezeigt. Darüber hinaus wurden mehr Gene differentiell reguliert, im Vergleich zum anderen Serum, das keine CsA-induzierte Invasion zugelassen hat.

Zusammengefasst zeigen unsere Daten, dass CsA grundsätzlich nicht unter allen Bedingungen Keratinozyten zu Krebszellen transformiert. Stattdessen haben unsere Daten demonstriert, dass CsA die Differenzierung von Keratinozyten verbessert, vor allem in Zellen mit aberranter epidermaler Differenzierung, sowie deren Langlebigkeit fördert. Durch Zufall haben wir jedoch festgestellt, dass abhängig von bestimmten Serumfaktoren, CsA auch Invasion/Tumorigenität induzieren kann. Dies spiegelt auch die Situation einiger Patienten mit Organtransplantat wider, die innerhalb kürzester Zeit etliche Plattenepithelkarzinome, auch ‚cutaneous carcinomatous catastrophe' genannt, bekommen. Mit Hilfe unserer Daten ist unsere Studie nun für tiefergehende Analysen bereit, um Signalwege zu identifizieren die HaCaT Zellen für die Invasion sensibilisieren. Mit diesem Wissen könnten schlussendlich biologische Targets entdeckt werden, die diesem verheerenden Nebeneffekt von CsA entgegenwirken könnten.

SUMMARY

Increased incidence of cutaneous squamous cell carcinomas (cSCCs) in organ transplant recipients is frequently associated with the immunosuppressive drug Cyclosporine A (CsA). Besides its therapeutic effect on the immune surveillance, evidence is accumulating for an immunity-independent mechanism of CsA on non-immune cells. However, the effects described so far are highly diverse and its long-term influence on human keratinocytes within a tissue context is largely unknown.

Using a 3D organotypic skin culture model (OTC), for long-term treatment of keratinocytes within a physiologically relevant environment, we showed that CsA improved the stratification and differentiation of moderately differentiating HaCaT cells and of poorly differentiating HaCaT-RAS A-5 cells. This was demonstrated by histology and immunofluorescent stainings for differentiation markers, as well as differential RNA expression of several genes associated with the GO-term 'epidermal development'. Improved differentiation was also demonstrated by an enhanced transepithelial electrical resistance, a trait directly correlated with the epidermal barrier function. However, CsA did not induce enhanced proliferation or invasion of neither HaCaT nor HaCaT-RAS A-5 cells grown in OTCs. In order to determine, whether UV irradiation as a co-carcinogen would enable invasive growth of CsA-treated HaCaT or HaCaT-RAS A-5 cells, OTCs were continuously irradiated with UV in combination with continuous CsA treatment. However, this did not induce tumorigenic transformation. Instead we found that UV irradiation and the combination of UV+CsA induced a similar regulation pattern of 'epidermal development' genes as did CsA alone, suggesting a common regulatory mechanism induced by CsA treatment and UV irradiation.

In general, HaCaT epithelia only survive for a restricted time span in OTCs. After 4 to 5 weeks the epithelia become atrophic. Importantly, CsA reproducibly extended the life span of the HaCaT epithelia, by retaining more vital basal and suprabasal keratinocytes. As indicated from an expression array and Ingenuity® Pathway Analysis, CsA reduced cell death in these OTCs, possibly through HGF or Integrin signaling.

Having to use different serum batches for our experiments, we finally discovered that by the addition of a specific fetal calf serum HaCaT cells, in addition to the above described characteristics, became invasive when treated with CsA. Invasion was demonstrated by disruption of the basement membrane and penetration of HaCaT cells into the underlying dermal equivalent. This was associated with a tremendous increase in differentially expressed genes as compared to the serum conditions that did not allow for CsA-induced HaCaT invasion.

Together, our data confirm that in general CsA is not directly transforming keratinocytes into cancer cells under every condition. Instead our data suggest that CsA improves keratinocyte differentiation,

in particular in cells with aberrant epidermal differentiation and promotes their longevity. By chance, however, we experienced that, depending on certain serum factors, CsA could also rapidly induce invasion/tumorigenicity – thus simulating a situation typical for a subgroup of transplant recipients, who rapidly develop multiple cSCCs, also termed cutaneous carcinomatous catastrophe. With these findings our study is now suited for an in depth analysis to unravel the pathways sensitizing HaCaT cells for invasive growth. This knowledge may finally help to identify targets to counteract this devastating CsA-dependent side effect.

1. INTRODUCTION AND AIM

1.1. Introduction

1.1.1. Cutaneous squamous cell carcinomas

Cutaneous squamous cell carcinomas (cSCCs) are epithelial tumors arising from the squamous epithelium of the skin. Next to basal cell carcinomas (BCC), which also originate from epidermal cells, cSCCs are the second most frequent cancer type. In the United States it was estimated that up to 400,000 new cases of cSCCs were diagnosed in 2012, of which up to 12,572 patients developed nodal metastasis and up to 8791 died of cSCCs (Karia *et al.* 2013). Taking into account that cSCCs are not obliged to be registered and that misunderstanding may occur with patient records stating death by skin cancer, without further clarification of the type of skin cancer, numbers might even be underestimated for cSCCs (Garrett *et al.* 2016). Moreover, cSCCs cases are increasing in the population. National incidence estimates from the United States demonstrated a steady increase in the number of nonmelanoma skin cancers, which include BCCs and cSCCs as the major tumor types. Taking data from databases from Medicare and Medicaid Services, cases of cSCCs in the United States were estimated based on skin cancer treatments: From 2006 to 2012 procedures for skin cancers increased by 14% (Rogers *et al.* 2015). A similar trend was also reported by the Spanish cancer register in Girona. Moreover, the Spanish register showed a higher risk for men to develop cSCCs in comparison to women (Rubio-Casadevall *et al.* 2016). The general metastasize rate of cSCCs is about 3.7% and the mortality rate is up to 2.1% (Chrysalyne D. Schmults 2013). Given the high number of cases of cSCCs the total number of deaths by cSCCs is comparable to that of melanoma deaths in areas like the southern states of the United States (LeBoeuf & Schmults 2011; Karia *et al.* 2013). In line with the increase in cSCCs and the associated risk of metastasis it is also discussed to rename the commonly used term nonmelanoma skin cancer by keratinocyte carcinomas, thereby naming the disease by their cellular origin and not by excluding them from melanoma (Karimkhani *et al.* 2015).

Surgical excision is the primary care of cSCCs and up to 90% of the cases proceed without further complications afterwards (Bahner & Bordeaux 2013). However, cases of high risk cSCCs, also called cutaneous catastrophic carcinomas, and patients with metastasis are in the need of other treatment options (Berg & Otley 2002; Carucci 2004; Abikhair *et al.* 2016). Adequate systemic therapies or even targeted systemic medications, which could improve the survival rate of these patients, are currently not available (Sapijaszko *et al.* 2015). This is partly due to the lack of corresponding studies with high risk cSCCs patients, but is especially true due to a lack of appropriate targets for targeted therapy (Sapijaszko *et al.* 2015; Harwood *et al.* 2016). One factor which hampers the development of a

systemic targeted drug is the fact that cSCCs are genetically very heterogeneous and have the highest number of mutations compared to other malignancies (Durinck *et al.* 2011). cSCC development is said to occur in a multistep process (Boukamp 2005a) and precursor stages of cSCCs comprise actinic keratosis, SCC in situs and keratoacanthomas. Though the latter is still controversially discussed (Burnworth *et al.* 2006; Burnworth *et al.* 2007; Leufke *et al.* 2014). However, more than 80% of precursors do not progress into invasive cSCCs (Ratushny *et al.* 2012). Cumulative exposure of UV irradiation, including accumulation of UV dependent DNA changes, is one of the major risk factors of cSCC development. Accordingly, most cSCCs arise in sun-exposed areas, such as the face or scalp (Boukamp 2005b). The mean age of cSCC appearance is about 76 years, being indicative for a multistep development of cSCCs and the necessity of accumulation of genomic changes (Smith *et al.* 2004). One very common mutation in cSCCs is the mutational inactivation of the p53 tumor suppressor gene, being found in about half of all cSCCs (Brash *et al.* 1991; Boukamp 2005b; Benjamin *et al.* 2008). However, also in non-lesional skin 25% of skin samples show p53 immunoreactivity, arguing that p53 mutations on their own are not the sole driver of cSCCs, although they might facilitate the development (Stark *et al.* 1994; Khorshid *et al.* 1996). Moreover, p53 mutant mice develop spontaneous tumors within the first 6 months; however they do not develop skin tumors in that period (Donehower *et al.* 1992). In contrast mice with an epidermal p53 knockout, who in contrast to the p53 mutant mice survive beyond the first 6 months, develop spontaneous tumors from hair follicle (Martinez-Cruz *et al.* 2008). Even more frequently than p53 mutations, mutations either in the NOTCH1 or in the NOTCH2 gene are found, namely in up to 75% of cSCCs (Wang *et al.* 2011). However, like for p53 mutations, NOTCH mutations were also found in 20% of normal sun-exposed skin samples, showing that cSCCs emergence needs more than one driver mutation (Martincorena *et al.* 2015). Other mutations in cSCCs, include mutations in HRAS, cyclin D1, MYC, FAT1 and CDKN2A (Pierceall *et al.* 1991; Boukamp 2005a; Burnworth *et al.* 2007; Martincorena *et al.* 2015).

1.1.2. cSCCs in organ transplant recipients

In 1954 the first successful allogeneic kidney transplantation among monozygotic twins was performed. In the late 1950's and 1960's the implementation of immunosuppressive medications enabled the first syngeneic transplantations with kidney (1958), liver (1963) and heart (1967) from genetically different donors (Katsanos & Donickier 2009). With advances in transplantation medicine and the resulting extended organ transplant recipient life expectancy, long-term complications of immunosuppression therapy became manifested. Due to the suppressed immune system organ transplant recipients have a 2-4-fold increased risk of developing malignancies (Adami *et al.* 2003; Krynitz *et al.* 2013). Noteworthy, the risk for cSCCs is even increased 56-100-fold (Lindelof *et al.* 2000;

Berg & Otley 2002; Adami *et al.* 2003). However, not all skin cancers are equally affected. The incidence of melanoma is only increased by 2.1-8-fold (Kubica & Brewer 2012) and the risk for BCC development in organ transplant recipients is estimated to be 6-fold compared to the normal population (Krynitz *et al.* 2016). Consequently organ transplant recipients, in contrast to the immunocompetent population, have more cSCCs than BCCs (Euvrard *et al.* 2003). This switch in ratio might be due to the fact that cSCCs could be under stricter immunosurveillance than BCCs (Walter *et al.* 2010).

Probably due to different intensities of drug regimens, risk estimations for cSCCs vary depending on the type of transplant. For example, in a Swedish cohort with 10,746 organ transplant recipients transplanted from 1970-2008, the risk for cSCCs in kidney recipients was 120-fold, 32-fold in liver recipients and 198-fold in heart or lung recipients (Krynitz *et al.* 2013). On average, organ transplant recipients are up to 10-12 years younger (54-58.2 years) in comparison to the immunocompetent population (64-70.4 years) when diagnosed with the first cSCC (Ong *et al.* 1999; Smith *et al.* 2004; Lott *et al.* 2010). The mean time for the first cSCCs after transplantation is about 6.2 ± 2.5 years, as calculated for an Australian cohort (Ong *et al.* 1999). Moreover, the cumulative incidence rate is increasing with time after transplantation, reaching as high as up to 73% after 20 years (Bouwes Bavinck *et al.* 1996). In more detail, the incidence rates, which are varying for different cohorts and locations, are as follows: After 10 years the cumulative incidence is at 10% in Europe, 35% in the United States and up to 45% in Australia (Berg & Otley 2002). After 20 years the risk rises to 20% in Sweden, 40% in the Netherlands (Bouwes Bavinck *et al.* 1996), 54-61% in the UK (Bordea *et al.* 2004; Harwood *et al.* 2013), 54% in New Zealand (Mackenzie *et al.* 2010) and 70-73% in Australia (Bouwes Bavinck *et al.* 1996; Ramsay *et al.* 2002). Noteworthy, those organ transplant recipients who develop a primary cSCC after transplantation are much more likely to develop multiple cSCCs in comparison to the normal population. While in the normal population the cumulative incidence of a subsequent cSCC is about 18% after 3 years, in organ transplant recipients the risk is much higher (Wisgerhof *et al.* 2010): After the first diagnosis of cSCC, 25% of organ transplant recipients develop a second cSCC after 13 month (Lindelof *et al.* 2000) and after 3 years the cumulative incidence is at 34-60%, depending on the cohort and type of transplant (Lindelof *et al.* 2000; Marcil & Stern 2000; Mackenzie *et al.* 2010). 5 years after the first cSCC up to 64-80% of organ transplant recipients will develop further cSCCs (Marcil & Stern 2000; Mackenzie *et al.* 2010). Furthermore, in patients who will develop multiple SCC, the occurrence of the first SCC is earlier than in patients which only develop a single SCCs (Bordea *et al.* 2004).

The occurrence of more than 10 cSCCs and BCC per patient within one year is also called cutaneous catastrophic carcinomas and is more frequent in organ transplant recipients than in the normal

population. In some cases organ transplant recipients develop more than 100 cSCCs per year (Berg & Otley 2002). For example in a Dutch kidney transplant cohort 25% of the organ transplant recipients developed more than 10 nonmelanoma skin cancers (Wisgerhof *et al.* 2010). These numbers also illustrate why organ transplant recipients need a tight dermatologic follow-up examination. Especially those which were already diagnosed with actinic keratosis or cSCCs before transplantation and organ transplant recipients, who already developed multiple cSCCs after transplantation, should have a follow up interval of 6 or 2-4 months, respectively (Berg & Otley 2002). While not only the number of cSCCs in organ transplant recipients increases, the risk of metastasis also rises from 3.7% in the general population to 8% in organ transplant recipients (Berg & Otley 2002; Chrysalyne D. Schmults 2013). Next to a higher metastasis rate, the danger of cSCCs in organ transplant recipients is also highlighted by the number of deaths from cSCCs after transplantation. For example in the case of an Australian heart transplant cohort 15% of deaths 4 years after the transplantation were due to advanced cSCCs, while in comparison 10% were due to malignant melanoma (Ong *et al.* 1999). Similarly, in an Canadian renal transplant cohort, 12% of the transplant patients, who developed cancer after transplantation, died of cSCCs, while only 2% died of malignant melanoma at the time point of the retrospective study (Tremblay *et al.* 2002). The high occurrence of cSCCs in organ transplant recipients not only is a massive psychological burden for these patients, but also very costly for the national health insurance (Ruegg *et al.* 2012). Many risk factors for cSCCs and multiple cSCCs in organ transplant recipients, like UV exposure and fair skin type, are common with the immunocompetent population. However, some are also specific for organ transplant recipients and might explain the higher number of cSCCs in this population (Table 1.1). One such example is the length and type of immunosuppression.

Table 1.1 Known risk factors for cSCC development in organ transplant recipients

Factors specific for organ transplant recipients s	Environmental Factors	Genetic Factors
Immunosuppression (length, level, type)[1, 2]	Older age[1, 2, 3]	Fair skin type[1, 2, 3]
cSCCs history before transplantation[1]	Latitude[1]	Light eye color[1, 2, 3]
Year of transplantation (<1984)[3]	UV exposure[1, 2, 3]	Hair color[1, 2, 3]
Multiple transplantations[3]		
Transplant type[3, 4]		

[1] (Fortina *et al.* 2009), [2] (Ponticelli *et al.* 2014), [3] (Euvrard *et al.* 2006), [4] (Krynitz *et al.* 2013)

1.1.3. Immunosuppression therapy in organ transplant recipients

Moving from genetically identically donors to genetically diverse donors in the 1960's was enabled by the use of steroids and azathioprine which led to a 50% graft survival after one year (Watson & Dark

2012). However, a breakthrough was accomplished with the introduction of new immunosuppressive drugs, like the discovery of the calcineurin inhibitor CsA in the mid 1970's, and its release in the beginning of the 1980's. This caused an increase in kidney graft survival of up to 90-95% after one year (Watson & Dark 2012) and consequently also caused an increased survival of renal organ transplant recipients in comparison to the standard treatment with azathioprine (Group 1986). With time other immunosuppressive medications were established and included in the regimens. In the mid 1990's another calcineurin inhibitor named tacrolimus was released (Johansson & Moller 1990). It showed an even stronger positive outcome on graft survival than CsA (Fung *et al.* 1991). However, it also had some more intense side effects like neurotoxicity (Mueller *et al.* 1994). A bit later mycophenolates were available for immunosuppressive therapy. These were well tolerated and more potent than azathioprine (Ensley *et al.* 1993; Sollinger 1995). However, they were not as strong as calcineurin inhibitors and they were only approved as a combination therapy with calcineurin inhibitors, substituting azathioprine and/or steroids (Stegall *et al.* 1997). At the end of the 1990's mTOR inhibitors were developed. While mTOR inhibitors are less nephrotoxic than both calcineurin inhibitors, they still can induce life-threatening pneumonitis (Cravedi *et al.* 2010; Errasti *et al.* 2010). Generally, a combination of medications is needed and the regimen has to be adapted to the individual patient. Drugs might get decreased or substituted with other drugs to avoid or minimize side effects, but it always has to be balanced with the risk of organ rejection. Predictive markers for organ rejection may also help to minimize and adapt immunosuppression, but are not identified yet (Hanlon *et al.* 2013). Figure 1.1 shows the trend in immunosuppression therapy after 1992 demonstrating the response of azathioprine, steroid and CsA, in comparison to newer, more potent or more tolerable drugs like tacrolimus, mTOR inhibitors and mycophenolates. As the graph starts with 1995 it does not show, that in the 1980's azathioprine and steroids were the standard regimens, with up to 80-90% in case of kidney organ transplant recipients (Durando & Reichel 2005). While early graft survival tremendously increased in the last decades due to the above mentioned drugs, side effects and lower long-term graft survival still cause a demand for new drugs. Newer developments include antibodies or new calcineurin inhibitors, which might have less side effects (Hardinger & Brennan 2013). Additionally, new alternatives to the classic immune therapy are as well explored at the moment. One new field of research is the administration of donor-derived mesenchymal stem cells, which *in-vitro* and in the rat model can be used as an immunomodulatory and potentially pro-tolerogenic tool (Popp *et al.* 2008).

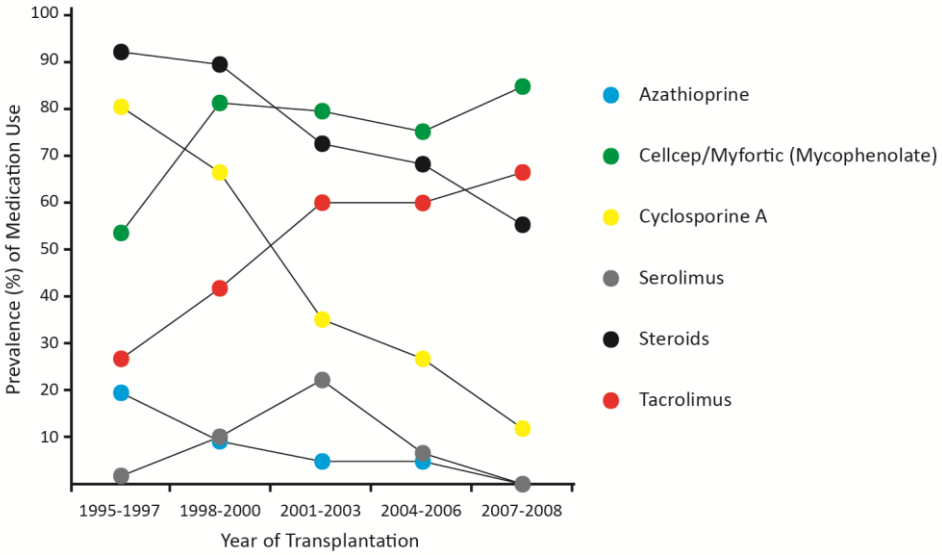

Figure 1.1 Trend in immunosuppressive medication in organ transplant recipients from 1995 to 2008. Adapted from (Coghill *et al.* 2016).

1.1.4. cSCCs in organ transplant recipients treated with Cyclosporine A

As mentioned before immunosuppression is a risk factor for cSCCs development in organ transplant recipients (Fortina *et al.* 2009; Ponticelli *et al.* 2014). Noteworthy, not all immunosuppressive drugs have the same impact on cSCC occurrence and some like mTOR-inhibitors even show a decrease in cSCC incidence in organ transplant recipients (Feldmeyer *et al.* 2012). Generally, the effort is made to decrease immunosuppressive drugs and, if possible, to substitute for immunosuppressive drugs which are not in suspicion of causing or enhancing cancer. One drug which is associated with increased cSCCs numbers, however, is Cyclosporine A (CsA) (Hiesse *et al.* 1995; Petter Jensen 1999; Herman *et al.* 2001). Moreover, CsA usage was linked to the development of cutaneous catastrophic carcinomas (Abikhair *et al.* 2016). These patients develop up to 100 new cSCCs per year (Berg & Otley 2002) and in 80% of these patients cSCCs appear within 10 month after transplantation in 80% (Abikhair *et al.* 2016). Consequently, several studies were performed to compare different regimens and it was demonstrated that withdrawal from CsA caused a reduction of cSCCs (Campistol *et al.* 2006; Hofbauer 2010; Caroti *et al.* 2012). Moreover, the conversion from CsA did reduce the vascularization and thickness of cSCCs in organ transplant recipients (Rival-Tringali AL1 2009). Alternatively, lowering of the CsA dose also reduced the numbers of cSCCs, but also increased the frequency of cellular rejection (Dantal *et al.* 1998). In comparison to the previous mentioned publications, some newer studies could not determine an association with cSCCs development when looking at CsA usage vs. no CsA usage in organ transplant recipients (Ingvar *et al.* 2010; Coghill *et al.* 2016). However, a correlation of CsA with cSCCs was also found for other disorders, as for example psoriasis. Patients with severe psoriasis are also partly treated with CsA and in these cases an increased risk in cSCCs development was shown as well (Paul *et al.* 2003).

1.1.5. CsA – Mode of action

The fungal (Tolypocladium Inflatum) metabolite CsA was discovered in the 1970's and was shown to inhibit lymphocyte proliferation and thereby allowing murine skin transplantation (Borel *et al.* 1976). After the approval of CsA by the FDA in the early 1980's, it replaced azathioprine and steroids as a standard regimen in kidney transplantation by nearly doubling the graft survival rate. Subsequently CsA allowed for subsequent milestone in transplantation of other organs like heart and liver (Watson & Dark 2012). CsA is a calcineurin inhibitor, which forms a complex with cyclophilin A within the cell. This complex binds and inhibits the calcium- and calmodulin-dependent phosphatase calcineurin. In the steady state calcineurin is dephosphorylating cytosolic nuclear factor of activated T-cells (NFAT). Dephosphorylated NFAT, which on its own has weak DNA binding capacities, is translocated into the nucleus where it, depending on the cell type and cell context, connects with one or more binding partners. These binding partners, collectively named NFATn, are dependent on other signaling pathways, like for example the MAP kinase pathway. Upon interaction and binding of the DNA, NFAT and NFATn initiate cell type specific gene transcription (Figure 1.2) (Medyouf & Ghysdael 2008; Crabtree & Schreiber 2009). The immunosuppressive action of CsA is mainly accredited to the prevention of a T-cell mediated immune response. Upon donor-derived antigen recognition by T-cells, Ca^{2+} is released into the cytoplasm, which leads to calcineurin activation and subsequent NFAT dephosphorization. In the nucleus, activated NFAT binds to the transcription factors AP-1 and NF-kB amongst others and induces the production of IL-2, which is needed for the T-cell mediated immune response. The absence of IL-2, in case of CsA treatment, then leads to reduction of naïve T-cell maturation and proliferation, as well as reduction of memory T-cell activation (Hermann-Kleiter & Baier 2010; Espinosa *et al.* 2016).

In addition to its impact on the calcineurin/NFAT pathway, CsA has also other, calcineurin-independent, implications. Through binding to cyclophilin D CsA can inhibit the mitochondrial permeability transition pore formation and thereby is able to prevent cell death in neural precursor cells (Sachewsky *et al.* 2014). The calcineurin-independent mechanisms are not shared by other calcineurin inhibitors like for example tacrolimus, which acts by binding to another immunophilin, namely to FK506 binding protein (Chang & Johnson 2002).

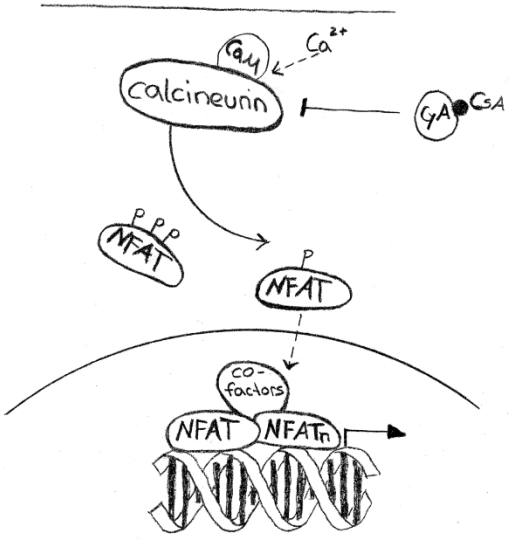

Figure 1.2 The calcineurin/NFAT signaling pathway.
CaM: calmodulin, CyA: cyclophilin A, CsA: Cyclosporine A, NFAT: nuclear factor of activated T-cells, NFATn: NFAT binding partners.

1.1.6. Experimental implications of CsA's role in cSCCs development

With the achievements in transplantation medicine and long-term survival in the beginning of the mid 1970's, other aspects of the long-term medication were revealed with time (Watson & Dark 2012). Quite early it was shown that CsA administration in mouse models facilitated growth and metastasis of transplanted tumors (Eccles *et al.* 1980; Servilla *et al.* 1987). While in the beginning this was mainly attributed to the immunosuppressive properties of CsA, in 1999 Hojo *et al.* showed that CsA has as well a cell-autonomous impact on A-549 cells, inducing TGF-β-dependent cell transformation favoring invasion. Moreover, the use of immunodeficient mice, lacking T-cells, B-cells and natural killer cells, strengthened the conclusion for an immune-independent and TGF-β-dependent impact of CsA on tumor development. On the one hand Hojo *et al.* demonstrated a CsA-induced increase in pulmonary metastasis growth of different tail vein-injected cancer cell lines, on the other hand a decrease of pulmonary metastasis growth by the combinatorial treatment with CsA and an anti-TGF-β antibody (Hojo et al. 1999). While that specific study did not focus on skin cells, others specifically looked for CsA-dependent cSCCs development. While CsA on its own seems not to cause any skin tumor development (Han *et al.* 2012), its impact on UV-induced tumors is differently described in different publications. A very early study on UV-induced skin tumors in albino HRA/Skh-1 mice demonstrated an earlier on set of skin tumors in CsA-treated mice, but not an increase in numbers or size of these tumors (Kelly *et al.* 1987). In contrast, Duncan *et al.* showed that CsA is decreasing the number of UV-induced skin tumors, while it increases the tumor size and aggressiveness in SKH-1 hairless mice (Duncan *et al.* 2007; Wulff *et al.* 2008). Later Han *et al.* showed that CsA causes an earlier onset of UV-induced skin tumors and higher numbers of tumors in

immunocompromised nude mice (Han *et al.* 2012). The latest study by Voskamp *et al.* showed that CsA decreases UV-induced skin tumors, as well as decreases the tumor size in SKH-1 hairless mice (Voskamp *et al.* 2013). Probably due to different treatment regimens these studies had different outcomes concerning the impact of CsA on UV-induced cSCCs. The UV treatment scheme, the applied CsA doses, as well as differences in mice models, might play an important role in the outcome of those different experiments. However, Voskamp *et al.* as well emphasized the differences between CsA injection, gavage and dietary CsA administration, which as well might have an impact on the experimental outcome (Voskamp *et al.* 2013).

Additional hints for an immuno-independent impact of CsA on keratinocytes came from studies on the calcineurin pathway. It was shown that mice with a keratinocyte specific deletion in calcineurin were more prone to chemically-induced carcinogenesis (Wu *et al.* 2010). Notwithstanding NFATc1 deletion in follicular stem cells caused a decreased rate of chemically-induced skin malignancies (Goldstein *et al.* 2015). One proposed molecular mechanisms by which CsA is promoting cSCC formation was ATF3-dependent inhibition of p53 and subsequent inhibition of senescence (Wu *et al.* 2010). Moreover, it was shown that UVA irradiation independently potentiated ATF3 expression in keratinocytes (Dziunycz *et al.* 2014). Hints for other cell autonomous mechanisms, including inhibition of DNA repair and inhibition of apoptosis (Yarosh *et al.* 2005), enhanced survival (Ji *et al.* 2012) and enhanced migration (Kashyap & Rabinovitz 2012), were found in cultured keratinocytes. Concerning the impact of CsA on proliferation of keratinocytes, published studies showed contradictory results. While a positive proliferative impact of prolonged CsA treatment is claimed by *Han et al.* (Han *et al.* 2010), others showed an anti-proliferative effect of CsA (Fisher *et al.* 1988; Voskamp *et al.* 2013).

In addition to a cell autonomous impact on the keratinocytes, other cell types in the skin might be involved in cSCC development. While CsA is suppressing the immune system to prevent organ rejection, CsA is not completely eliminating all immune cells. Accordingly, all types of immune cells including T-cells can be found in cSCCs from organ transplant recipients (Krynitz *et al.* 2010). In line CsA was shown to enhance UV dependent inflammation and facilitated cSCC development via enhancement of angiogenesis (Duncan *et al.* 2007; Yajima *et al.* 2008; Zhou & Ryeom 2014). Moreover, recently Abikhair *et al.* reported that CsA induces IL-22 expression in T-cells and expression of the corresponding receptor in cSCC cells. Together this increased the proliferation and invasion of SCC cells. Thus Abikhair *et al.* presented a mechanism in which close dependence and distinct responses of different cell types to CsA favored cSCC development (Abikhair *et al.* 2016).

1.2. Aim and rational of the study design

CsA is associated with the enhanced occurrence of cSCCs in organ transplant recipients. Since its discovery in the 1970's, many clinical and experimental studies addressed the impact of CsA on tumorigenesis. However, despite all those studies, the consequences of CsA on human skin keratinocytes are still poorly understood. Effects of CsA were investigated primarily on cultured (2D conventional culture) cells or in mouse models. Utilizing human three-dimensional (3D) organotypic skin cultures (Berning *et al.* 2015), which provide a more *in-vivo*-like situation with all its consequences on tissue-dependent gene regulation, might thus provide more physiologically relevant information about the role of CsA on human skin keratinocytes, while it also avoids species-specific differences.

As cSCCs development commonly requires a latency period of 5 to 10 years, a direct transformation of normal keratinocytes by CsA appears unlikely. Therefore, keratinocytes were used which already have gained genetic alteration that made them more similar to pre-stages in the multistep process of cSCCs. These included the HaCaT cells, spontaneously immortalized human keratinocytes, which exhibit UV signature mutations in the p53 gene, as well as chromosomal aberrations, which are similarly found in cSCCs (Boukamp *et al.* 1988). While these cells are non-tumorigenic, we also included the HaCaT-RAS A-5 cells, which because of transfection with the H-Ras^{G12V} oncogene gained the ability to form benign cysts in nude mice, thus representing a benign-tumorigenic variant of the HaCaT cells (Boukamp *et al.* 1990). Investigating these cells in the *in-vivo*-like organotypic cultures, the following questions were addressed:

1. What are the consequences of continuous CsA treatment on epithelial morphology of the non-tumorigenic HaCaT and the benign-tumorigenic HaCaT-RAS A-5 keratinocytes?
2. What are the consequences of CsA on epithelial tumorigenesis (proliferation, invasion)?
3. How is the epithelial gene expression changed upon continuous CsA treatment?

As for immunocompetent patients, cSCCs in organ transplant recipients primarily appear in sun exposed areas (Smith *et al.* 2004). Thus, UV irradiation might be an important co-factor for CsA-enhanced cSCCs development:

4. Does a combination of UV and CsA further change the epithelial morphology and/or the gene expression and is this combination necessary for tumorigenic conversion?

2. RESULTS

2.1. Determination of a CsA dose for further experiments

For a first impression of the impact of CsA on keratinocytes several experiments with different doses of CsA were performed with cultured cells. Moreover, experiments were performed to determine an *in-vitro* CsA dose for OTCs, which is comparable to the *in-vivo* blood concentration in organ transplant recipients.

2.1.1. CsA impact proliferation and apoptosis of cultured cells

HaCaT keratinocytes were treated with CsA in conventional cultures (2D) and analyzed using the CellTiter-Blue® assay, which measures the amount of fluorescent resorufin metabolized from added resazurin. HaCaT keratinocytes were treated with increasing amounts of CsA (50 ng ml^{-1} - 100 µg ml^{-1}) or the corresponding amount of its solvent DMSO for 72h. Fluorescent signals of doses up to 0.5 µg ml^{-1} CsA and the corresponding amount of 0.002% DMSO were not deviating from each other. Starting with 1 µg ml^{-1} CsA had a reducing impact on signal intensity when compared with lower CsA concentrations or the corresponding DMSO concentration. Signal intensity of 2.5 -7.5 µg ml^{-1} CsA were similar to each other and further reduced the signal when compared to 1 µg ml^{-1} CsA. A drastic decrease in signal intensity was determined for doses starting at 15 µg ml^{-1} CsA. Signal intensities of DMSO-treated HaCaT keratinocytes were not impacted up to the amount of 0.03% DMSO, which corresponds to 7.5 µg ml^{-1} CsA. Signal intensities of 0.06% and 0.1% DMSO, corresponding to 15 and 25 µg ml^{-1} CsA, were similar to each other, but lower in comparison to lower DMSO doses. 0.2% and 0.4%, corresponding to 50 and 100 µg ml^{-1} CsA, drastically decreased the signal intensity (Figure 2.1A). Additionally, a SYBR Green incorporation assay was performed to assess cell numbers after CsA treatment. CsA treatment did not have an immediate impact on cell numbers of HaCaT or HaCaT-RAS A-5 cells after 24h or 48h. However, after 72h CsA a non-significant decrease in cell numbers was observed (Figure 2.1B). A FACS-assisted apoptosis assay was performed in order to test whether the decrease in cell numbers might result from apoptosis. In HaCaT cells treated with DMSO around 18% apoptotic cells were detected. A dose of 1 µg ml^{-1} decreased the rate to 16%. 2.5 µg ml^{-1} CsA and 10 µg ml^{-1} CsA slightly increased the rate to 20-21%. HaCaT-RAS A-5 cells treated with DMSO had a slightly smaller rate of apoptosis in comparison to HaCaT cells: 15%. 0.25 µg ml^{-1} CsA and 10 µg ml^{-1} CsA decreased the rate to about 10-12%. However, 2.5 µg ml^{-1} CsA had no impact in comparison to the DMSO-treated cells. In contrast, a concentration of 100 µg ml^{-1} CsA clearly elevated the apoptosis rate in HaCaT-RAS A-5 keratinocytes to 32%. Due to technical issues the measurement for 100 µg ml^{-1} CsA in HaCaT cells is not available (Figure 2.1C).

Summarized, the CellTiter-Blue® and the SYBR Green assay suggested that CsA is decreasing the proliferation rate of keratinocytes. Moreover, measurement of apoptotic cells excluded the possibility that cell numbers decreased due to induction of apoptosis.

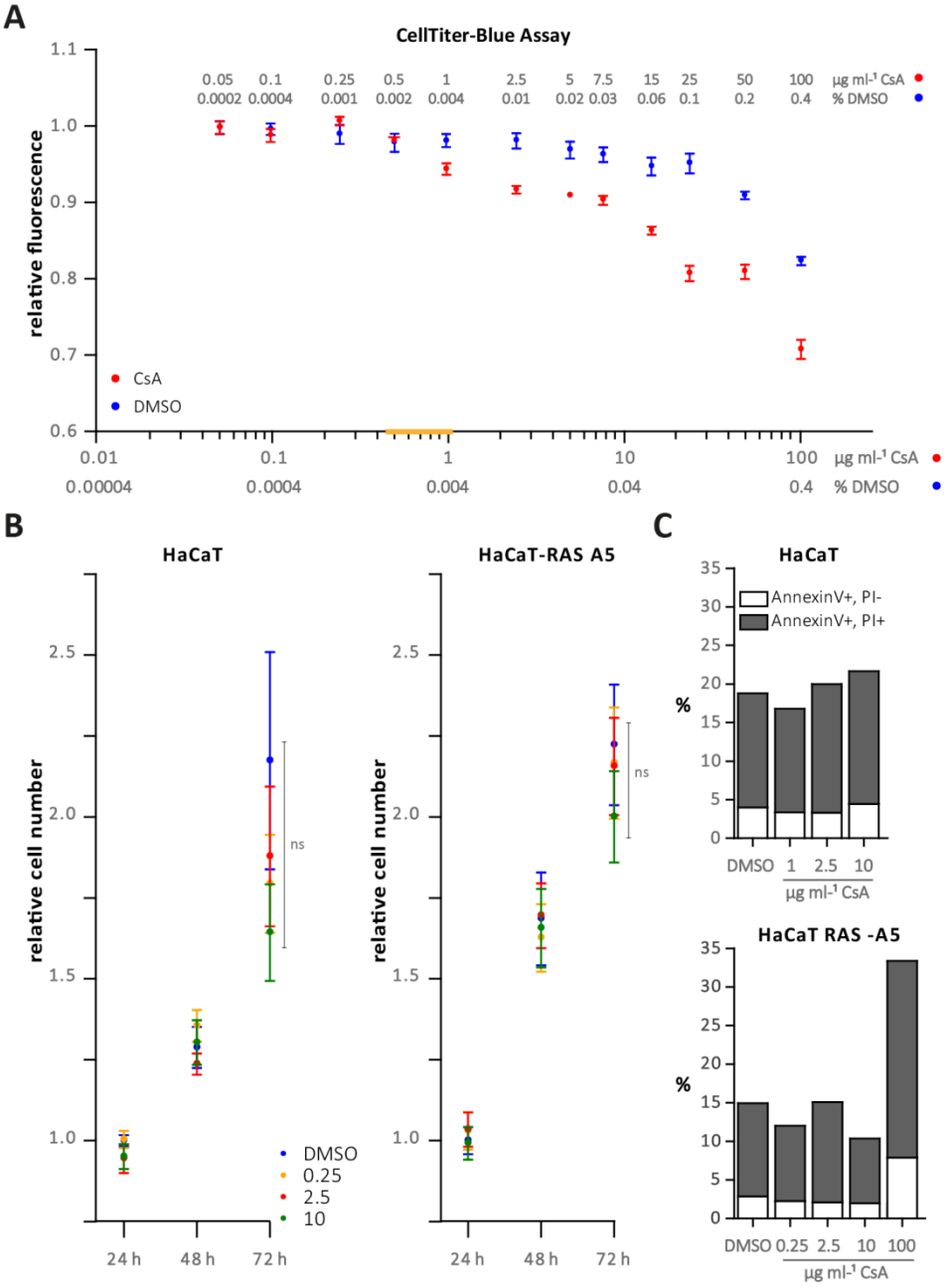

Figure 2.1 CsA impact on proliferation and apoptosis of cultured cells.
(A) *CellTiter-Blue® assay*. Monolayer HaCaT keratinocytes were treated with different doses of CsA or the solvent DMSO alone for 72h. The relative fluorescence of metabolized resazurin (additive) was measured. The graph shows the mean (n=8) and the standard error of the mean. Data points of DMSO or CsA were normalized to the mean of the lowest DMSO or CsA concentration, respectively. The orange bar marks the range of CsA within the epithelium of OTCs treated with 10 µg ml^{-1} CsA via growth medium supplementation, which was taken as standard concentration in subsequent experiments. **(B)** *SYBR Green incorporation*. Relative cell numbers (fluorescence intensity) of cultured HaCaT and HaCaT-RAS A-5 keratinocytes after CsA or DMSO (0.04%) treatment. Data points represent the mean and the standard error of the mean (n=8). Values from each CsA concentration or DMSO were normalized to the mean of the 24h value of DMSO or the corresponding CsA concentration, respectively. **(C)** *FACS-assisted apoptosis assay*. Cultured HaCaT and HaCaT-RAS A-5 cells

were treated with CsA or DMSO (0.04%) for 24h. The graph shows single cell analysis for AnnexinV (early apoptosis marker) and PI (late apoptosis marker). The plot shows the mean percentage of positive cells per total cell number. Per sample 3800 – 6000 single cells were analysed.

2.1.2. Continuous long-term treatment of cultured HaCaT cells

CsA might have a genotoxic impact, as described for lymphocytes (Oliveira *et al.* 2004; Ozturk *et al.* 2008). To assess a genotoxic impact of CsA on HaCaT cells, cultured cells were treated for 9 weeks. Maintenance and splitting of HaCaT cells was done according to standard cell culture procedures. CsA was added together with fresh medium three times a week.

After 9 weeks of continuous CsA treatment multiplex fluorescence *in situ* hybridization (M-FISH) was performed to assess chromosomal changes. New chromosomal aberrations, which were not present within the control (DMSO) treated HaCaT keratinocytes, were counted. Two different doses of CsA were applied: 0.25 and 2.5 µg ml^{-1} CsA. This long-term treatment of HaCaT keratinocytes was performed twice. Due to a change of serum within the laboratory, both experiments were done in individual sera, serum A and serum B. Serum B was also used for the previous described short-term assays (Figure 2.1). In serum A about 9 new chromosomal aberrations per metaphase appeared in the DMSO-treated HaCaT cells. This number increased to 19 and 21 new aberrations per metaphase for 0.25 µg ml^{-1} CsA and 2.5 µg ml^{-1} CsA, respectively. In serum B the number of new aberrations per metaphase in DMSO HaCaT cells was higher than for serum A, namely 19. New aberrations for 0.25 µg ml^{-1} CsA increased to 31 per metaphase, but decreased to 9 for 2.5 µg ml^{-1} CsA (Figure 2.2A). The increase in new chromosomal aberrations in serum A, neither had an impact on the morphology of HaCaT keratinocytes (Figure 2.2B), nor was the impact on proliferation changed upon CsA treatment (Figure 2.2C) when compared to short-term treatment with CsA as described in Figure 2.1B.

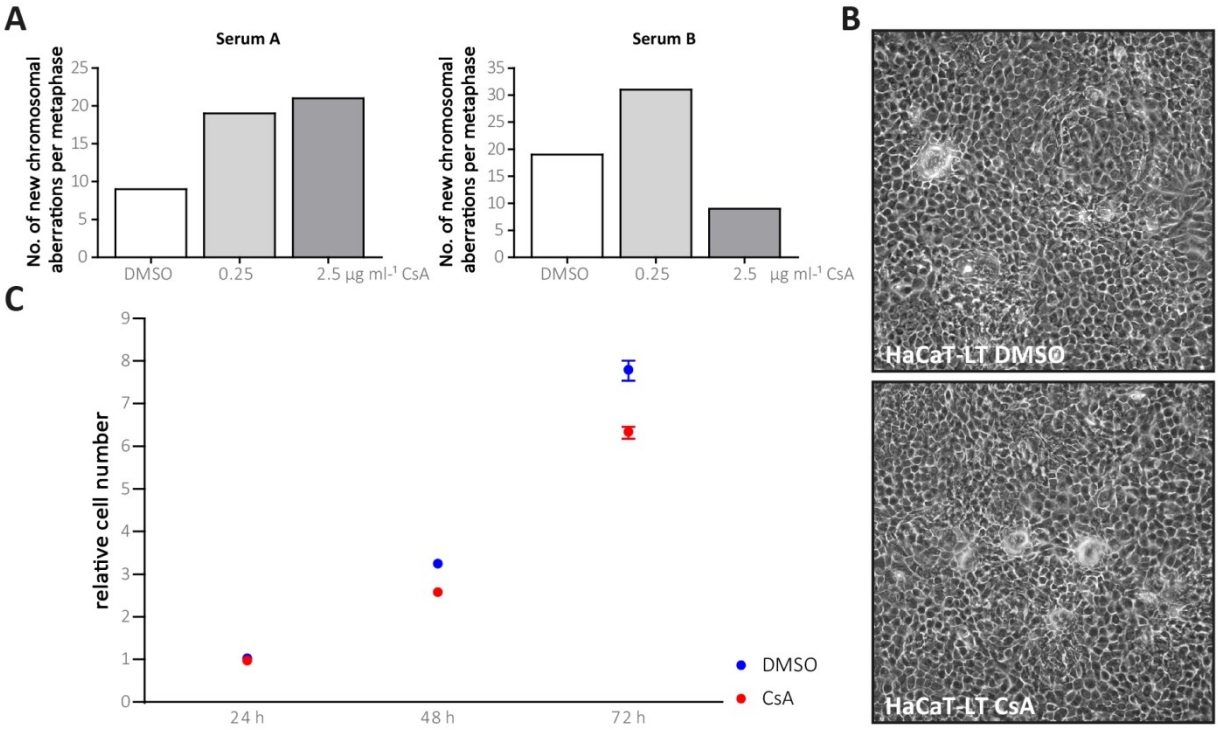

Figure 2.2 Long-term CsA treatment of cultured HaCaT keratinocytes.
Cultured HaCaT cells were treated for 9 weeks with 0.25 or 2.5 µg ml^{-1} CsA or DMSO (0.04%). **(A)** *Multiplex fluorescence in situ hybridization*. The graph shows the mean of new chromosomal aberrations per metaphase spread. In total 30 metaphase spreads were analysed per treatment. **(B)** *Light microscopy* images from cultured HaCaT cells after 9 weeks of continuous treatment with DMSO as control (HaCaT-LT DMSO) or 2.5 µg ml^{-1} CsA (HaCaT-LT CsA) in serum A. **(C)** *SYBR Green incorporation*. Relative cell number of HaCaT-LT after CsA or DMSO (0.04%) treatment in serum A after 24h, 48h and 72h. Data points represent the mean and the standard error of the mean of one experiment with four biological replicates each. Values from CsA or DMSO were normalized to the mean of the corresponding CsA or DMSO 24h value, respectively.

2.1.3. CsA is reaching the epithelium in HaCaT- and HaCaT-RAS A-5-OTCs – MassSpec measurements

OTCs lack perfusion by blood vessels and drug distribution is merely possible by diffusion. In order to treat OTCs with CsA, CsA was supplemented to the growth medium, feeding the cells from below by diffusion. In order to determine whether and how much CsA is reaching the dermis and the epidermis via diffusion, mass spectrometry measurements were performed in the dermal, as well as in the epidermal part of OTCs after 3 weeks of continuous CsA treatment. No CsA could be detected for the dermal or epidermal samples treated with DMSO in HaCaT-OTCs. Supplementation of 0.25 µg ml^{-1} CsA in HaCaT-OTCs, led to 0.04 µg ml^{-1} CsA and 0.07 µg ml^{-1} CsA within the dermal and epidermal samples, respectively. The supplementation of 2.5 µg ml^{-1} CsA, led to 0.57 µg ml^{-1} CsA and 0.44 µg ml^{-1} CsA in the dermal and epidermal samples, respectively. The highest amount of CsA within the epithelium was measured after the supplementation of 10 µg ml^{-1} CsA, namely 0.937 µg ml^{-1} CsA. In the dermal sample, the same supplementations led to an amount of 0.23 µg ml^{-1} CsA. Similar to HaCaT-OTCs, no CsA was detected in HaCaT-RAS A-5-OTCs treated with DMSO. Supplementation of 0.25 µg ml^{-1} CsA and 2.5 µg ml^{-1} CsA led in both cases to around 0.017 µg ml^{-1} CsA in the dermal and

0.047 µg ml^{-1} CsA in the epidermal samples. The amount of CsA after 10 µg ml^{-1} CsA supplementation in HaCaT-RAS A-5-OTCs was similar to HaCaT-OTCs, namely 0.214 µg ml^{-1} CsA in the dermal and 1.1 µg ml^{-1} CsA in the epidermal sample (Figure 2.3). These measurements were comparable to the HaCaT samples, except for the amount of CsA in the epidermis after 2.5 µg ml^{-1} CsA supplementation, which was higher in HaCaT epithelia. Measurements after 2.5 µg ml^{-1} CsA supplementation were only done once, in contrast to 10 µg ml^{-1} CsA supplementation, which was measured in 3 independent samples. Therefore it is not explicitly evidenced whether HaCaT epithelia manifested more CsA than HaCaT-RAS A-5 cells after 2.5 µg ml^{-1} CsA supplementation.

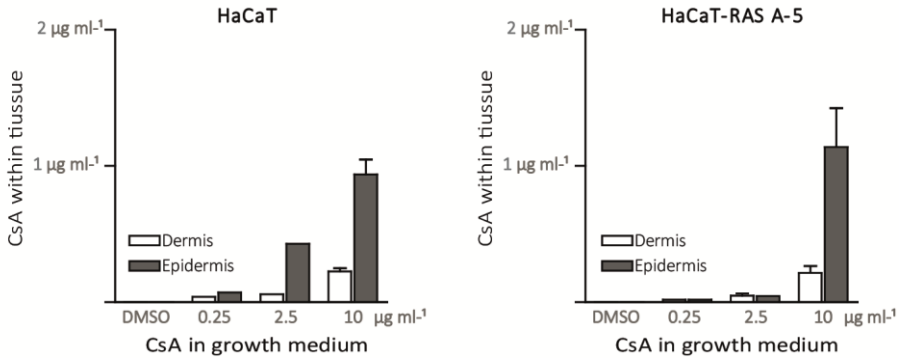

Figure 2.3 Mass spectrometry measurements of CsA concentration within HaCaT- and HaCaT-RAS A-5-OTCs. Measurements were done separately with dermal or epidermal compartments of corresponding OTCs. The graphs represent the mean and the standard error of the mean from two experiments (DMSO: n=2, 10 µg ml^{-1} CsA: n=6) or from one experiment (0.25 and 1x 2.5 µg ml^{-1} CsA: n=1, 2.5 µg ml^{-1} CsA in HaCaT-RAS A-5: n=2).

2.1.4. Impact of 10 µg ml^{-1} CsA and higher doses on HaCaT- and HaCaT-RAS A-5-OTCs

The blood CsA concentration in organ transplant recipients is about 25 ng ml^{-1} – 1.25 µg ml^{-1}, depending on type of graft and time point of blood measurements (Saigal *et al.* 2002; Sommerer *et al.* 2006), whereas it was shown that CsA can accumulate within the skin reaching levels of about 2.8 µg ml^{-1} (Fisher *et al.* 1988). Mass spectrometry measurements showed that at least a dose of 10 µg ml^{-1} CsA (in cell culture medium) is needed to reach a level within the *in-vivo* blood range (25 ng ml^{-1} – 2.8 µg ml^{-1}) in the epithelial cells. Accordingly OTCs were prepared and treated with 10 µg ml^{-1} CsA and higher doses (25-100 µg ml^{-1} CsA) to analyze the overall morphology of these cultures. H&E histological stainings revealed that increased DMSO (0.04%-0.4%) had no morphologic impact on HaCaT- and HaCaT-RAS A-5-OTCs. HaCaT-OTCs treated with 10 µg ml^{-1} CsA and 25 µg ml^{-1} CsA had a more structured morphology when compared to the corresponding DMSO-treated HaCaT-OTC, but did not show any obvious sign of atrophy. Treatment with 50 µg ml^{-1} CsA and 100 µg ml^{-1} CsA led to atrophic epithelia and to an acantholytic morphology. HaCaT-RAS A-5-OTCs treated with 10 µg ml^{-1} CsA had, similar to HaCaT-OTCs a more structured and as well a more differentiated epithelium when compared to the DMSO-treated HaCaT-RAS A-5-OTC. In contrast to HaCaT-OTCs, in HaCaT-RAS A-5-OTCs an atrophic and acantholytic epithelium was already triggered by 25 µg ml^{-1} CsA (Figure 2.4).

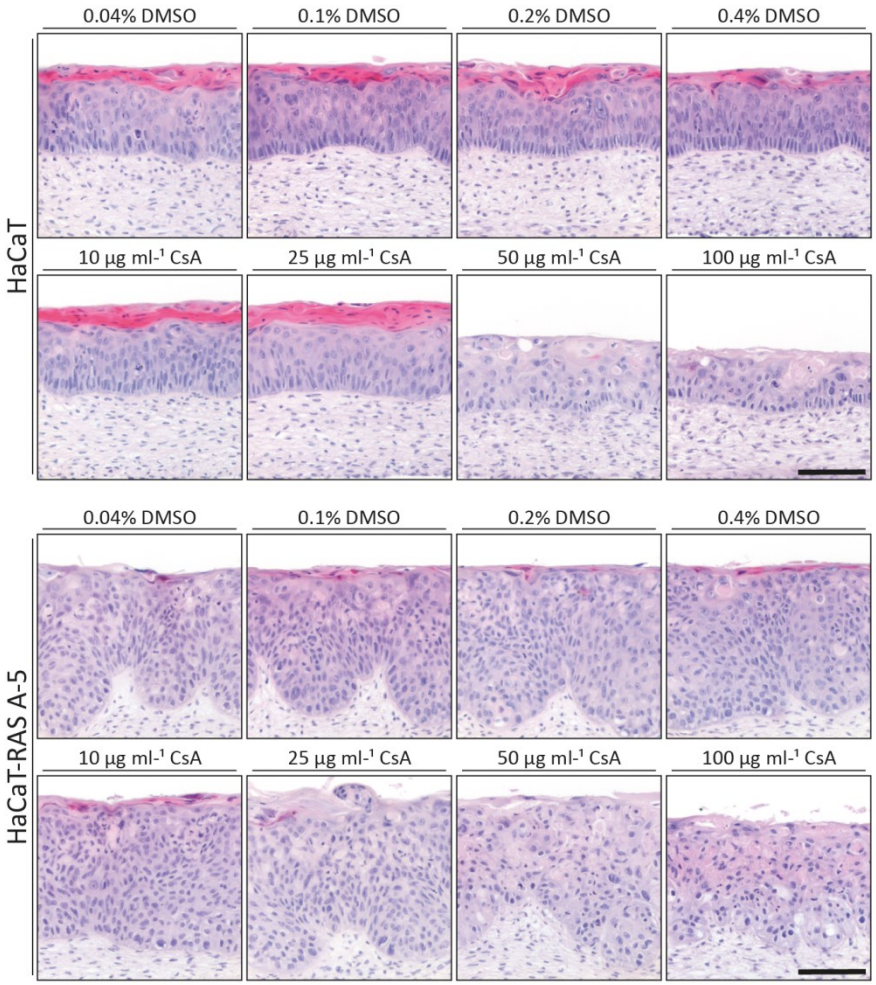

Figure 2.4 Impact of high CsA doses on HaCaT- and HaCaT-RAS A-5-OTCs.
HaCaT- and HaCaT-RAS A-5-OTCs were treated with the indicated concentrations of CsA or the corresponding amount of the solvent DMSO via growth medium supplementation. OTCs were harvested after 2 weeks (HaCaT-OTCs) or 3 weeks (HaCaT-RAS A-5 OTCs) and processed for H&E histological staining. Scale bars: 100 µm.

2.2. Continuous CsA treatment of HaCaT- and HaCaT-RAS A-5-OTCs

As a minimum dose of 10 µg ml^{-1} CsA is needed to reach a CsA level (Figure 2.3) comparable to *in-vivo* blood levels (Saigal *et al.* 2002; Sommerer *et al.* 2006) and doses starting with 25 µg ml^{-1} CsA led to atrophic growth in HaCaT-RAS A-5-OTCs (Figure 2.4), 10 µg ml^{-1} CsA was taken as standard supplementation to the growth medium for all further experiments with OTCs.

In order to get an impression on the impact of continuous CsA on keratinocytes over time and to assess the impact in a realistic physiologic environment time series of CsA-treated HaCaT- and HaCaT-RAS A-5-OTCs were prepared. HaCaT or HaCaT-RAS A-5 keratinocytes were allowed to build an epithelium in the OTCs without CsA treatment for one week. CsA was then added to the OTCs and continuously treated for 1, 2 and 3 weeks.

2.2.1. Continuous CsA improved epithelial organization of HaCaT- and HaCaT-RAS A-5-OTCs and decreased the proliferation of keratinocytes

Morphology and overall appearance from continuously CsA-treated HaCaT- and HaCaT-RAS A-5-OTCs were assessed by H&E histological staining. From earlier studies it is known that HaCaT-OTCs form a multi-layered parakeratotic epithelium (Berning *et al.* 2015). Moreover, in comparison to OTCs built with normal human keratinocytes, the organization of the stratified epithelium of HaCaT-OTCs is rather disorganized (Berning *et al.* 2015). In accordance, control HaCaT-OTCs treated with DMSO showed this typical HaCaT organization at all time points (before treatment start and after 1, 2 and 3 weeks of treatment). Treatment with CsA had a rather minor impact on the HaCaT growth pattern. Histology of early OTCs revealed that CsA did not alter the diameter of the epithelium, nor could invasion be detected. However, after 2 and 3 weeks of CsA treatment the epithelial stratification seemed more organized with all strata being more separated from each other. Moreover, after 3 weeks of treatment the vital cell layers, stratum basale and spinosum, as identified by intense nuclei staining, appeared thicker and better organized in CsA-treated HaCaT-OTCs (Figure 2.5).

HaCaT-RAS A-5 cells form a hyper-proliferative multi-layered, parakeratotic epithelium, with invading buds penetrating into the underlying dermal equivalent when grown in OTCs. In addition, in comparison to HaCaT epithelia, HaCaT-RAS A-5 epithelia are less differentiated (Berning *et al.* 2015). Also for these cells, DMSO treatment did not alter the expected morphological appearance of HaCaT-RAS A-5 epithelia. Furthermore, and similar to CsA-treated HaCaT cells, CsA treatment enhanced the tissue organization and increased differentiation (Figure 2.5).

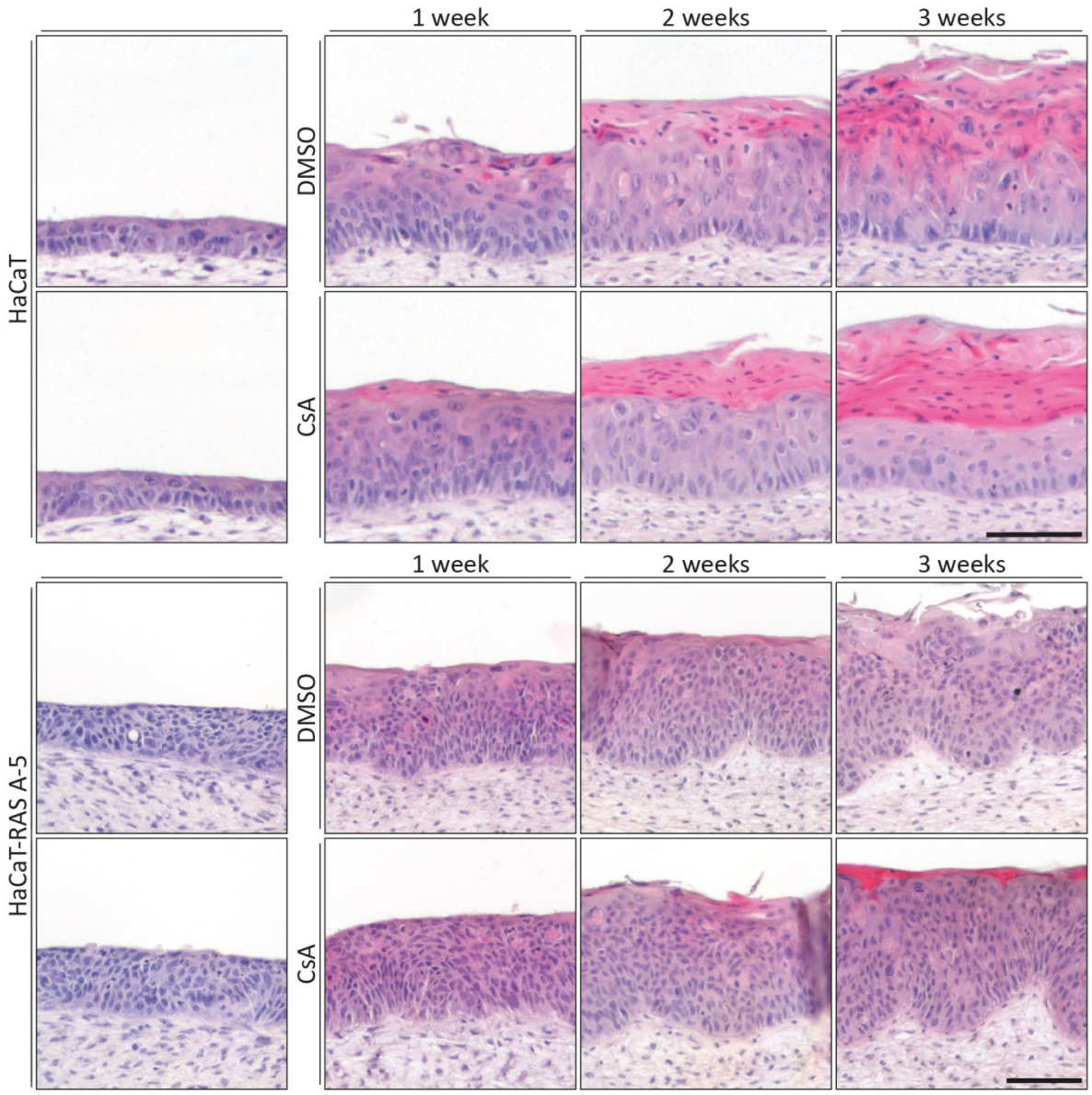

Figure 2.5 H&E histological staining of HaCaT- and HaCaT-RAS A-5-OTCs after 1-3 weeks of continuous CsA treatment.
HaCaT- and HaCaT-RAS A-5-OTCs were harvested and processed for H&E histological staining one week after epithelia seeding and after 1, 2 and 3 weeks of treatment. OTCs were treated with 10 µg ml^{-1} CsA or the solvent DMSO (0.04%). Scale bars: 100 µm.

H&E histological stainings revealed no thickening of the epithelia upon CsA treatment. In order to further exclude an impact on proliferation, cryosections of HaCaT- and HaCaT-RAS A-5-OTCs were stained for the proliferation marker Ki67. Immunofluorescent stainings showed that especially suprabasal proliferation was diminished after CsA treatment (Figure 2.6A). The Proliferation index ($Ki67^+$ per length of basement membrane) demonstrated a decrease in proliferation of HaCaT and HaCaT-RAS A-5 cells after 2 and 3 weeks of continuous CsA treatment (Figure 2.6B).

Summarized, CsA led to an improvement of tissue organization and differentiation of HaCaT and HaCaT-RAS A-5 epithelia, while it reduced cell proliferation of both cell types, especially in suprabasal cell layers.

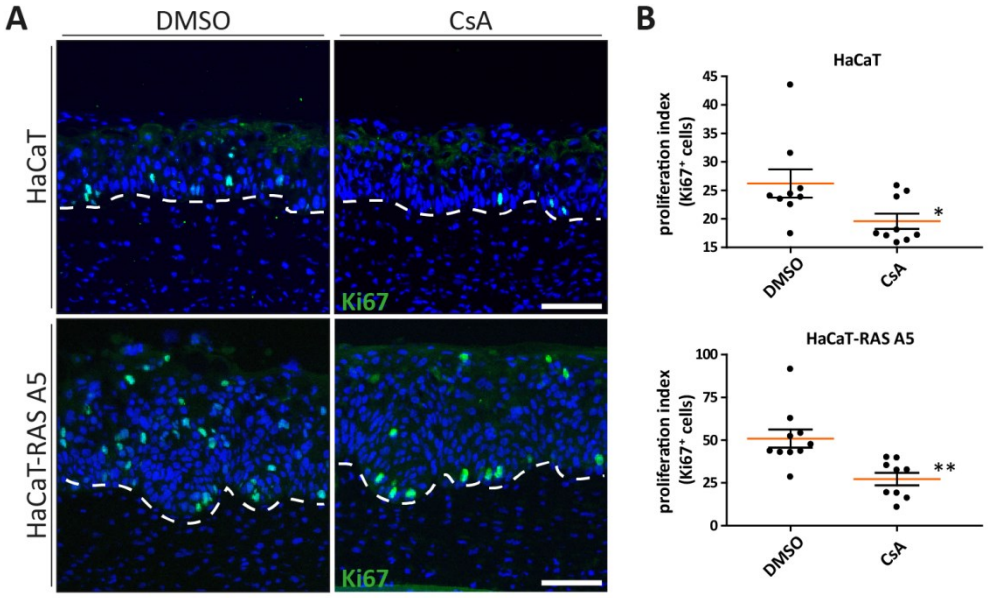

Figure 2.6 Proliferation of HaCaT and HaCaT-RAS A-5 keratinocytes within OTCs upon continuous CsA. Cryosections from HaCaT- and HaCaT-RAS A-5-OTCs, treated with 10 µg ml^{-1} CsA or DMSO (0.04%) for 2 (HaCaT) or 3 (HaCaT-RAS A-5) weeks, were stained for Ki67 (green). **(A)** *Immunoflourescent staining*. Pictures show representing sections stained for Ki67 (green) and nuclei (blue). The dotted line marks the basement membrane. Scale bars: 100 µm. **(B)** *Proliferation index (Ki67$^+$ cells)*. Each data point represents the number of Ki67$^+$ cells per length of basement membrane. n=9 (from 3 OTCs). The orange bar marks the mean and the error bars represent the standard error of the mean. *: p-value of 0.03, **: p-value of 0.002 (two-sided, unpaired t-test).

2.2.2. Genome wide RNA expression analysis from continuously CsA-treated HaCaT and HaCaT-RAS A-5 epithelia

In order to reveal changes on a transcriptional level, genome wide RNA expression profiles were performed from epithelia of HaCaT and HaCaT-RAS A-5 cells, which were treated with CsA for 2 or 3 weeks, respectively. As HaCaT-OTCs have a shorter lifespan than HaCaT-RAS A-5-OTCs, RNA was extracted already after 2 weeks in order to get a view at a time point of maximal vitality of the control OTCs.

2.2.2.1. RNA expression profiles from CsA-treated HaCaT and HaCaT-RAS A-5 epithelia were distinct from their corresponding control samples

Expression profiling was done from three biological replicates per condition. Evaluation of the raw data from RNA from HaCaT and HaCaT-RAS A-5 epithelia was done as follows: Raw data from both treatment groups (DMSO and CsA) were normalized together and non-metric multidimensional scaling (NMDS) and hierarchical clustering were applied to assess the quality of the data. For both experiments (HaCaT epithelia and HaCaT-RAS A-5 epithelia) all triplicates from one treatment groups

(DMSO and CsA) separated along the first dimension using NMDS (Figure 2.7A). In agreement, hierarchical clustering split all samples into DMSO or CsA as depicted in the dendrogram (Figure 2.7B). Both analyses showed that biological replicates clustered well, implying a similar expression pattern. Furthermore, differential gene expression was determined and filtered by p-value ≤ 0.01. The 20 highest and lowest differentially expressed genes are listed in the appendix (Tables 7.1 and 7.2).

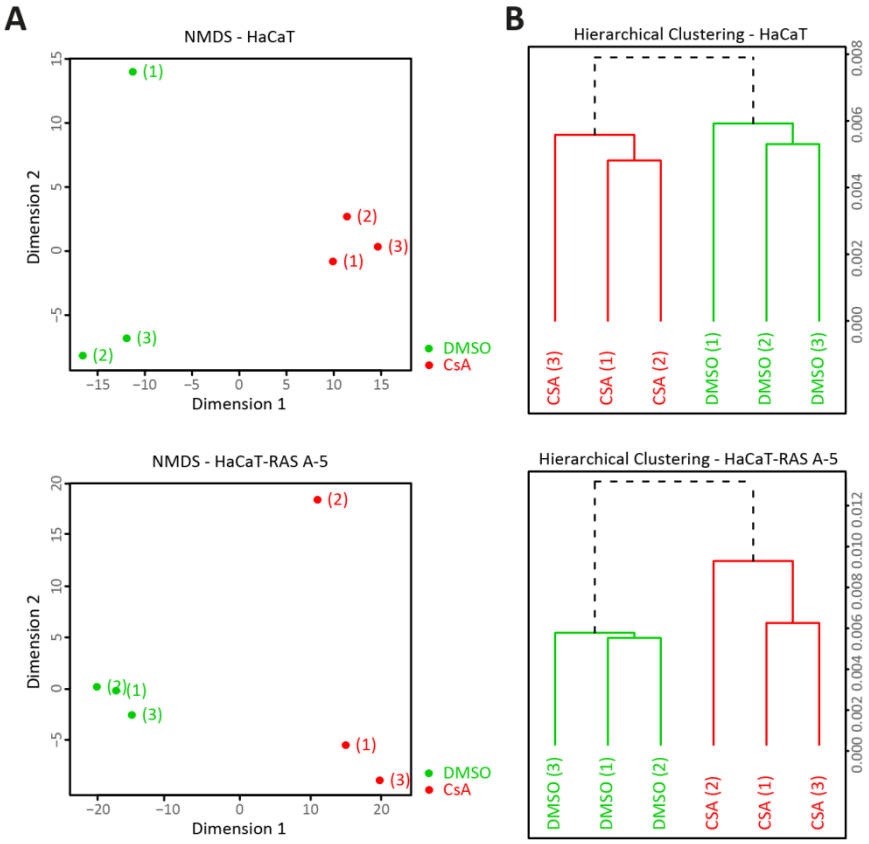

Figure 2.7 Visualizations of biological replicates from RNA expression profiles from CsA-treated HaCaT and HaCaT-RAS A-5 epithelia by NMDS and hierarchical clustering.
(A) *Non-metric multidimensional scaling* (NMDS) and **(B)** *hierarchical clustering* were applied to assess the discriminability of the 3 biological replicates from both treatment groups (DMSO and CsA). Clustering and visualization was performed with Chipster from normalized data.

In total 507 genes were differentially regulated in case of the RNA from CsA-treated HaCaT epithelia. Of these genes 25% (128/507) were regulated above 1.5-fold. A bit above half of these genes were down-regulated (58%, 75/128). This was as well the case for the total number of differentially expressed genes, from which 55% (278/507) were down-regulated. The total number of differentially expressed genes in epithelia from CsA-treated HaCaT-RAS A-5 was comparable to HaCaT epithelia, namely 521. However, fold changes of differentially expressed genes was stronger affected in HaCaT-RAS A-5 epithelia, in which 63% (327/521) of all differentially expressed genes were above 1.5-fold regulated (Figure 2.8A). The higher magnitude of fold changes in HaCaT-RAS A-5 epithelia can also be

seen in the scatterplot (Figure 2.8B). 44% (HaCaT: 156/507) or 43% (HaCaT-RAS A-5: 156/521) of all differentially expressed genes were regulated in both data sets (Figure 2.8C).

A

Numbers of differentially expressed genes

	HaCaT		HaCaT-RAS A-5	
No. of genes	Total	≥ 1.5-fold	Total	≥ 1.5-fold
Total	507	128	521	327
Up-regulated	229	53	199	139
Down-regulated	278	75	322	188

B

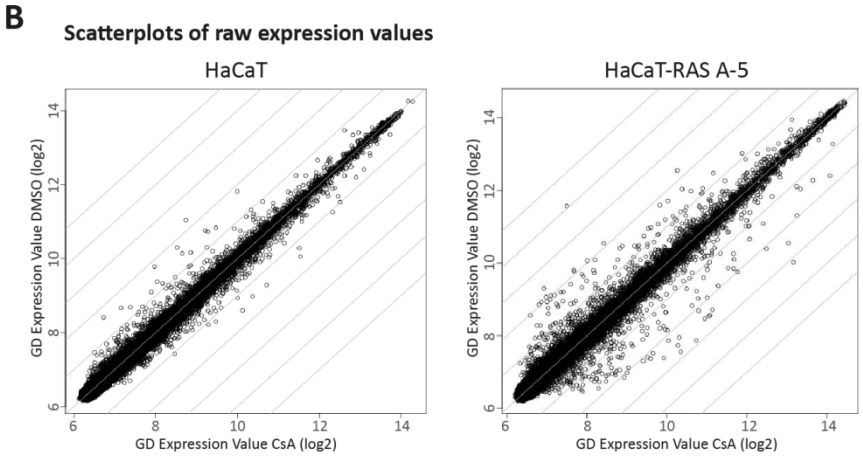

C

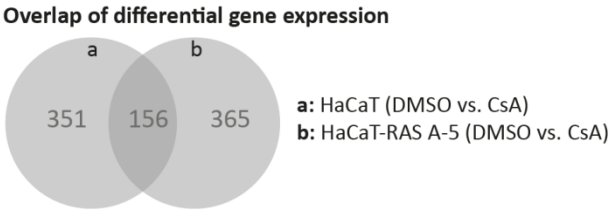

Figure 2.8 Number and magnitude of differentially expressed genes (DMSO vs. CsA) from HaCaT and HaCaT-RAS A-5 epithelia.
(A) *Differentially expressed genes (DMSO vs. CsA).* Whole genome RNA expression profiles from HaCaT and HaCaT-RAS A-5 epithelia treated with DMSO or CsA. The table shows the total number of differentially expressed genes and the number of differentially expressed genes with a fold change ≥ 1.5. Differentially expressed genes were calculated with Chipster (filtered by p-value ≤ 0.01). **(B)** *Scatterplot of relative gene expression.* Each dot shows the mean of the relative expression value (log2) from 3 biological replicates for one gene. Y-axis (DMSO), x-axis (CsA). Dots on line of origin = no differential gene expression. Data for the scatterplot were neither normalized nor filtered. **(C)** *Overlap of differential gene expression* from both data sets (HaCaT and HaCaT-RAS A-5 epithelia).

2.2.2.2. CsA treatment affected many genes from the GO-term: 'epidermal development'

From the 20 highest up- and down- regulated genes from CsA-treated HaCaT and HaCaT-RAS A-5 epithelia expression profiles, 10/40 genes (HaCaT) and 12/40 genes (HaCaT-RAS A-5) were part of the GO-term (GO-0008544) 'epidermal development' (underlined in Tables 7.1 and 7.2). Accordingly, the complete gene expression profile sets HaCaT and HaCaT-RAS A-5 epithelia were filtered by this GO-term. Both resulting lists were combined and a heat map was created (Figure 2.9). In total 38 genes were part of the term 'epidermal development' from the CsA-treated HaCaT RNA expression profile and 47 genes in case of the CsA-treated HaCaT-RAS A-5 RNA expression profile. The heat map

revealed that genes, which were regulated in both gene sets, were either both up- or both down-regulated, suggesting a common regulation pattern. Most genes were up-regulated. However, some, as for example keratin 15 (KRT15) and E74 like ETS transcription factor 3 (ELF3), were down-regulated in both cell types. In addition, especially one specific gene group seemed to be responding to CsA, namely late cornified envelope (LCE) genes.

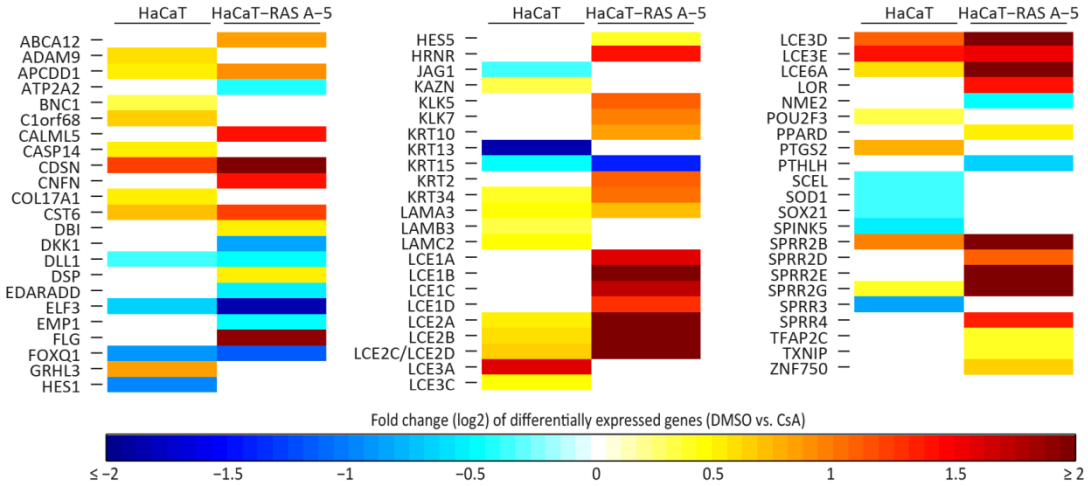

Figure 2.9 Heat map of differentially expressed genes from genome wide RNA expression profiles from HaCaT and HaCaT-RAS A-5 epithelia (DMSO vs. CsA) sorted by the GO-term 'epidermal development'.
Differentially expressed genes (DMSO vs. CsA) from CsA-treated HaCaT and HaCaT-RAS A-5 RNA expression profiles were filtered by p-value (≤0.01) and the GO-term 'epidermal development' (GO-0008544). Fold changes (log2) are depicted by the indicated color. The rows are sorted alphabetically.

2.2.3. Differentially expressed genes could be validated by qRT-PCR and IF staining

From the list of differentially expressed genes involved in 'epidermal development' 7 genes were selected for validation by qRT-PCR with RNA from 2-4 independent experiments as well as immunofluorescent stainings from one representing experiment. It is suggested that calcineurin inhibition by CsA is causing down-regulation of certain differentiation genes, like for example filaggrin (FLG) in keratinocytes (Santini *et al.* 2001). Therefore, OTCs built with normal human keratinocytes were prepared and treated with CsA for 3 weeks. RNA and cryosections from these NHEK-OTCs were included in the validation experiments.

LCE proteins comprise 3 groups LCE1, LCE2 and LCE3. From groups LCE2 and LCE3 one gene each was chosen for validation by qRT-PCR, namely LCE2A and LCE3A. Additionally localization of LCE2 and LCE3 (Niehues *et al.* 2015) was highlighted by immunofluorescent staining. According to the RNA expression profile data HaCaT cells showed no increase in LCE2A and a 2.9-fold increase for LCE3A. For HaCaT-RAS A-5 cells the profile revealed an increase in LCE2A (5.6-fold) and no regulation for LCE3. Using qRT-PCR, LCE2A was down-regulated (0.7-fold) and LCE3A was up-regulated (1.7-fold) in NHEK epithelium. As expected from the gene expression array data, fold changes measured by qRT-PCR for LCE2A and LCE3A were higher in HaCaT-RAS A-5 cells (LCE2A: 32-fold regulation; LCE3A: 4-

fold regulation) than in HaCaT cells (LCE2A: 1.3-fold regulation; LCE3A: 2.1-fold regulation) (Figure 2.10A). Immunofluorescent staining of control (DMSO) NHEK epithelia nicely revealed LCE2 deposition in the stratum corneum and granulosum and LCE3 within early differentiating cells in the stratum spinosum as well as stratum granulosum. This correlated to previous published stainings in human skin (Niehues *et al.* 2015). Due to the fact that LCE2 and LCE3 were strongly deposited in NHEK control epithelia, potential minor changes could not be detected in CsA-treated NHEK epithelia by immunofluorescent staining. In case of HaCaT epithelia the control OTCs showed a similar distribution of LCE proteins to the NHEK epithelia; LCE2 were only in the outermost layers and LCE3 in differentiating cells excluding the outermost layers. However, the amount of deposited LCE2 and LCE3 was much less and LCE3 appeared later in comparison to NHEK epithelia with several suprabasal cells very weakly or not stained for LCE3. In control HaCaT-RAS A-5 epithelia, LCE2 was nearly absent; nevertheless those proteins present were also deposited in the outermost layers of the epithelium. LCE3 proteins were also deposited in the suprabasal cells underneath the outermost layer; however it even appeared later than in HaCaT epithelia. Interestingly, and in line with the increased RNA expression in CsA-treated HaCaT and HaCaT-RAS A-5 epithelia, the immunofluorescent staining detected more LCE proteins deposited in differentiating cells in HaCaT and HaCaT-RAS A-5 epithelia. Noteworthy, the distribution, with LCE2 in the outermost and LCE3 in suprabasal cells, but underneath LCE2, was maintained (Figure 2.10B).

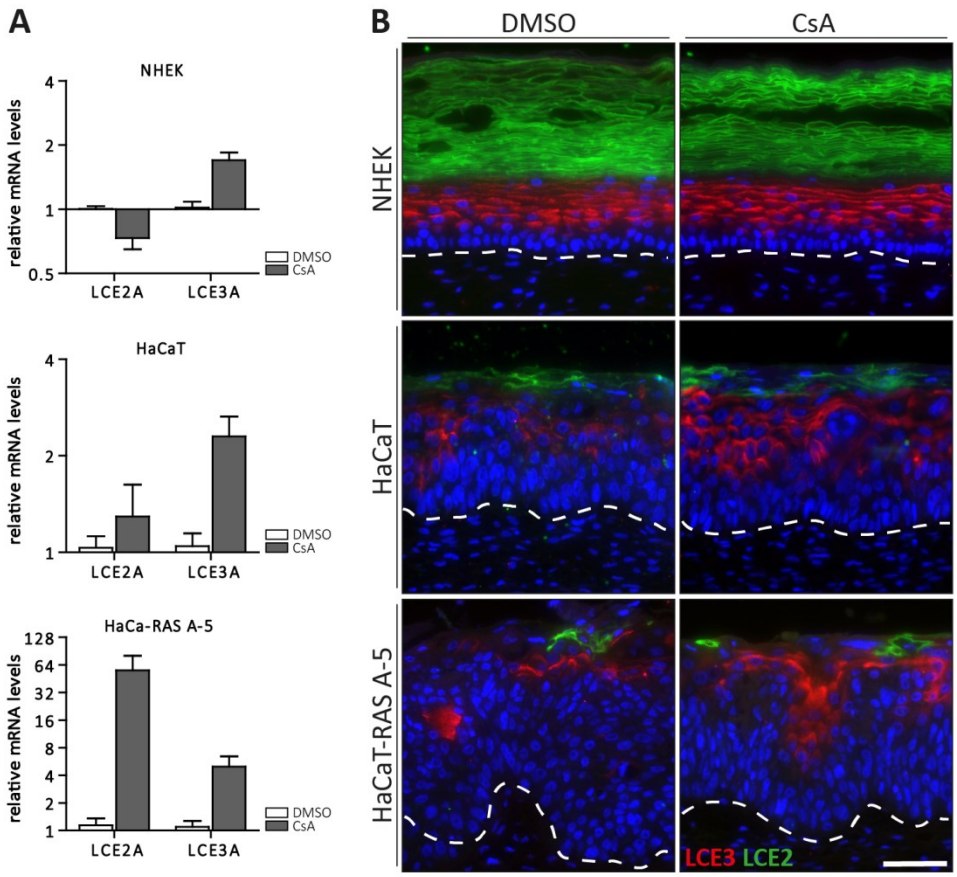

Figure 2.10 Relative gene expression and protein localization of LCE2A/LCE2 and LCE3A/LCE3 in NHEK, HaCaT and HaCaT-RAS A-5 epithelia treated with CsA.
(A) *Relative RNA expression*. RNA isolated from indicated epithelia treated with DMSO (0.04%) or CsA (10 µg ml^{-1}) for 3 weeks was quantified by qRT-PCR. The graphs show the mean and standard error of the mean. NHEK: n=9 (from 3 independent experiments), HaCaT and HaCaT-RAS A-5: n=11 (from 4 independent experiments). **(B)** *Immunofluorescent staining* for LCE2 (green) and LCE3 (red) on cryosections from the indicated OTCs treated with DMSO (0.04%) or CsA (10 µg ml^{-1}) for 2 (HaCaT) or 3 (NHEK and HaCaT-RAS A-5) weeks. Sections were counterstained by DAPI to stain nuclei (blue). The dotted line marks the basement membrane. Scale bar: 50 µm.

Another example was the keratin 10 (KRT10) gene, a commonly used marker for early epidermal differentiation. KRT10 was not differentially expressed in HaCaT cells based on the genome wide RNA expression array data set, while a 1.7-fold up-regulation was seen for HaCaT-RAS A-5 cells. Measurements by qRT-PCR revealed no changes in RNA regulation for NHEK epithelia. In HaCaT epithelia KRT10 RNA expression slightly increased (1.3-fold) and in HaCaT-RAS A-5 epithelia exhibited 4-fold up-regulation of KRT10 RNA (Figure 2.11A) upon CsA treatment. In control (DMSO) NHEK and HaCaT epithelia KRT10 was deposited in all suprabasal cell layers. In contrast in control HaCaT-RAS A-5 epithelia KRT10 deposition was limited to the upper part of the epithelium, while many suprabasal keratinocytes were not stained for KRT10. No major difference in KRT10 protein deposition could be detected for CsA-treated NHEK and HaCaT epithelia by immunofluorescent staining in comparison to the control. Noteworthy, in CsA-treated HaCaT-RAS A-5-OTCs KRT10 deposition was increased; after

CsA treatment most suprabasal layers could be stained for KRT10, while the basal cell layer and several cells from the first and second suprabasal cell layer remained KRT0 negative (Figure 2.11B).

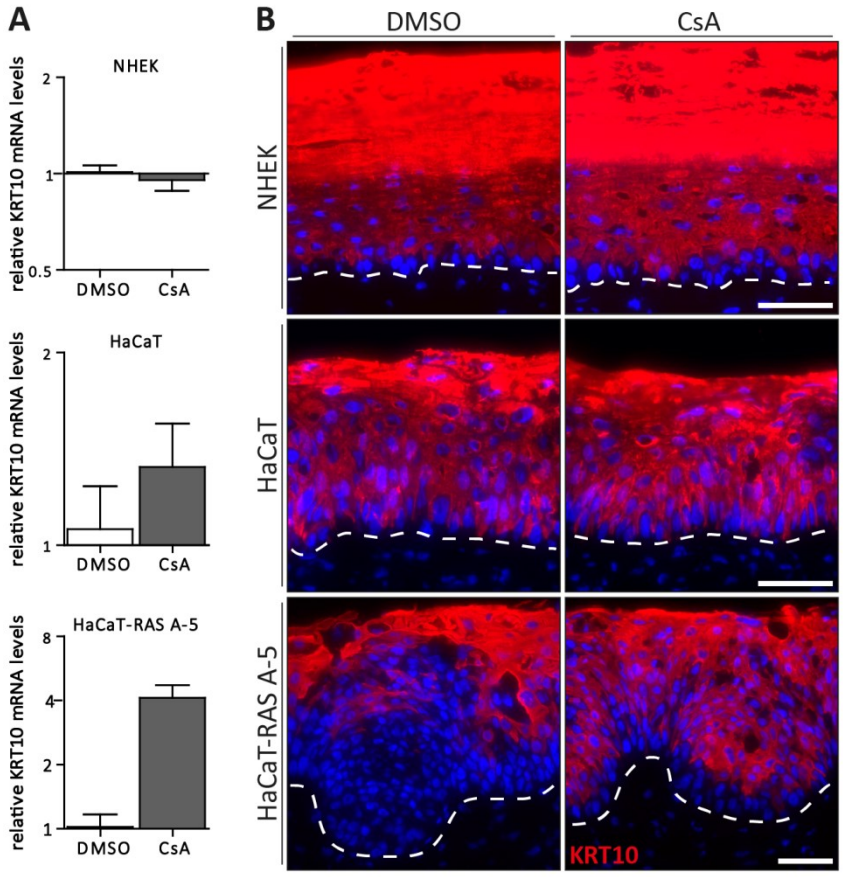

Figure 2.11 Relative gene expression and protein localization of KRT10 in NHEK, HaCaT and HaCaT-RAS A-5 epithelia treated with CsA.
(A) *Relative KRT10 RNA expression*. RNA isolated from indicated epithelia treated with DMSO (0.04%) or CsA (10 µg ml^{-1}) for 3 weeks was quantified by qRT-PCR. The graphs show the mean and the standard error of the mean. NHEK: n=9 (from 3 independent experiments), HaCaT: n=6 (from 2 independent experiments), HaCaT-RAS A-5: n=3 (1 experiment). **(B)** *Immunofluorescent staining* for KRT10 (red) on cryosections from the indicated OTCs treated with DMSO (0.04%) or CsA (10 µg ml^{-1}) for 2 (HaCaT) or 3 (NHEK and HaCaT-RAS A-5) weeks. Sections were counterstained by DAPI to stain nuclei (blue). The dotted line marks the basement membrane. Scale bars: 50 µm.

FLG is a typically used epidermal marker to demonstrate late/terminal differentiation. FLG was not detected by the array in HaCaT epithelia, but 3.7-fold up-regulated in HaCaT-RAS A-5 epithelia. qRT-PCR measurements revealed a similar pattern as for KRT10 expression: RNA levels were not critically changed (mean 1.1-fold up-regulated) by CsA in NHEK epithelia, were 2.5-fold up-regulated in HaCaT epithelia and 4.6-fold up-regulated in HaCaT-RAS A-5 epithelia (Figure 2.12A). By immunofluorescent staining FLG was detected in the stratum granulosum and the stratum corneum of control (DMSO) NHEK epithelia. As the strata granulosum and corneum are less developed in HaCaT-OTCs and HaCaT-RAS A-5 -OTCs the staining for FLG was accordingly less strong. However, in HaCaT- and HaCaT-RAS

A-5-OTCs, CsA treatment increased the amount of deposited FLG in the outermost strata; while no change could be detected in CsA-treated NHEK epithelia (Figure 2.12B).

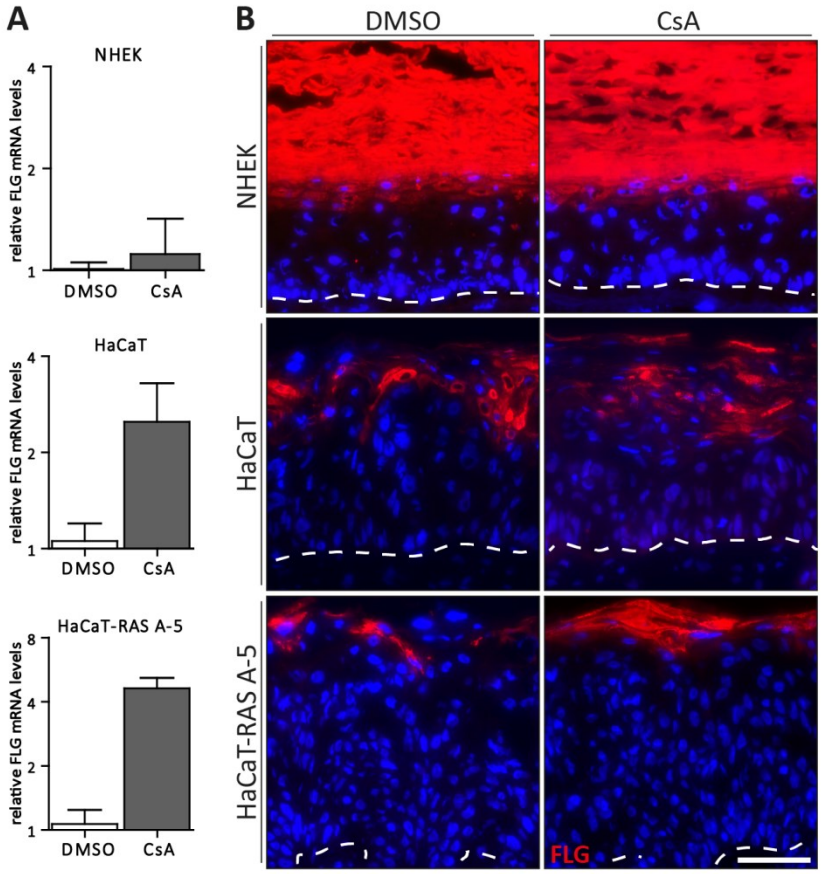

Figure 2.12 Relative gene expression and protein localization of FLG in NHEK, HaCaT and HaCaT-RAS A-5 epithelia treated with CsA.
(A) *Relative FLG RNA expression*. RNA isolated from indicated epithelia treated with DMSO (0.04%) or CsA (10 µg ml^{-1}) for 3 weeks was quantified by qRT-PCR. The graphs show the mean and the standard error of the mean. NHEK: n=9 (from 3 independent experiments), HaCaT: n=8 (from 3 independent experiments), HaCaT-RAS A-5: n=6 (2 independent experiments). **(B)** *Immunofluorescent staining* for FLG (red) on cryosections from the indicated OTCs treated with DMSO (0.04%) or CsA (10 µg ml^{-1}) for 3 weeks. Sections were counterstained by DAPI to stain nuclei (blue). The dotted line marks the basement membrane. Scale bar: 50 µm.

Small proline rich (SPRR) proteins function as cross-linking proteins within the cornified envelope. Expression of SPRR2B was slightly up-regulated in the HaCaT genome wide RNA expression array data set (1.9-fold) and strongly up-regulated in the HaCaT-RAS A-5 data set (5.9-fold). qRT-PCR measurements showed that SPRR2B was 0.7-fold down-regulated in NHEK epithelia. In contrast to the profile data no mayor SPRR2B RNA regulation was seen for HaCaT epithelia (1.1-fold up-regulation) upon CsA treatment. In CsA-treated HaCaT-RAS A-5 cells SPRR2B RNA levels were 8-fold up-regulated by qRT-PCR (Figure 2.13A). SPRR2 proteins were widely distributed in the stratum corneum and differentiating cells of control NHEK epithelia, less concentrated in HaCaT epithelia and nearly absent from control HaCaT-RAS A-5 epithelia. Concurrent to the RNA results from SPRR2B, the antibody recognized more SPRR2 within the CsA-treated HaCaT-RAS A-5 epithelium. No major

differences could be detected for SPRR2 deposition in CsA-treated NHEK and HaCaT epithelia (Figure 2.13B).

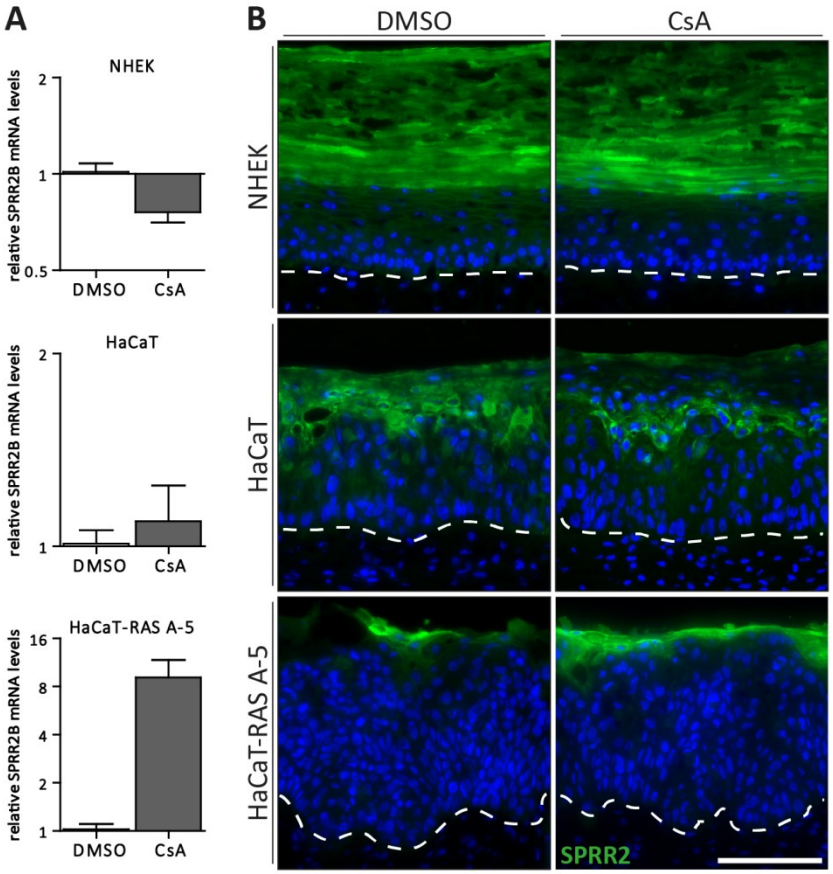

Figure 2.13 Relative gene expression and protein localization of SPRR2B/SPRR2 in NHEK, HaCaT and HaCaT-RAS A-5 epithelia treated with CsA.
(A) *Relative SPRR2B RNA expression*. RNA isolated from indicated epithelia treated with DMSO (0.04%) or CsA (10 µg ml^{-1}) for 3 weeks was quantified by qRT-PCR. The graphs show the mean and the standard error of the mean. n=9 (3 independent experiments). **(B)** *Immunofluorescent staining* for SPRR2 (red) on cryosections from the indicated OTCs treated with DMSO (0.04%) or CsA (10 µg ml-1) for 3 weeks. Sections were counterstained by DAPI to stain nuclei (blue). The dotted line marks the basement membrane. Scale bar: 100 µm.

Several genes from the GO-term 'epidermal development' were up-regulated upon CsA treatment, while some were down-regulated. Cornulin (CRNN) was 0.2-fold down-regulated in HaCaT epithelia and 0.49-fold down-regulated in HaCaT-RAS A-5 epithelia according to the expression profiles. Validation by qRT-PCR confirmed down-regulation of CRNN in HaCaT epithelia (0.2-fold) and HaCaT-RAS A-5 (0.62-fold). Different from HaCaT and HaCaT-RAS A-5 epithelia, CRNN was slightly up-regulated (1.5-fold) in NHEK-OTCs (Figure 2.14).

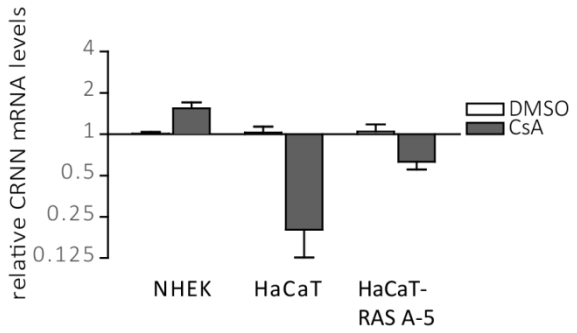

Figure 2.14 Relative CRNN gene expression in CsA-treated NHEK, HaCaT and HaCaT-RAS A-5 epithelia.
RNA isolated from indicated epithelia treated with DMSO (0.04%) or CsA (10 µg ml^{-1}) for 3 weeks was quantified by qRT-PCR. The graphs show the mean and standard error of the mean. NHEK: n=9 (from 3 independent experiments), HaCaT and HaCaT-RAS A-5: n=6 (from 2 independent experiments).

To summarize, most of the results from the RNA expression profile could be replicated by qRT-PCR. Noteworthy, fold changes were generally higher according to qRT-PCR than to the RNA expression profile. Moreover, in case of LCE3A (HaCaT-RAS A-5), KRT10 (HaCaT) and FLG (HaCaT) qRT-PCR revealed RNA up-regulation, which was not detected by expression profiling. Only in the case of SPRR2B HaCaT epithelia, which was 1.9-fold up-regulated according to the RNA expression profile, qRT-PCR did not validate the finding and qRT-PCR only detected a very weak 1.1-fold up-regulation. Noteworthy, the low mean expression value resulted from 3 different independent experiments, which individually revealed a 0.6-fold down-regulation and 1.1-fold or 1.64-fold up-regulation, respectively. These inter-experimental variations, which can be identified by the quite high standard errors of the mean, were also observed from other measurements, like for example KRT10 in HaCaT epithelia. In principal inter-experimental variations in morphology and grade of differentiation typically occur in OTCs with HaCaT and HaCaT-RAS A-5 keratinocytes. These inter-experimental different grades of differentiation could be reflected in the magnitude of fold change of CsA-induced differentially expressed genes. A general observation was: the more differentiated the control OTCs were, the less strongly was the fold change in differentiation-associated genes induced by continuous CsA treatment. In accordance to that observation, gene expression of differentiation-associated genes in NHEK epithelia, which is fully differentiated, was only very weakly affected and fold changes were in all cases below the fold changes of the less differentiated HaCaT or HaCaT-RAS A-5 epithelia. Moreover, and in line with that observation, fold changes of CsA-induced gene expression in HaCaT-RAS A-5 epithelia, which inherently are less differentiated than HaCaT epithelia, usually was affected strongest. In case of HaCaT-RAS A-5 epithelia increased RNA expression could as well nicely be demonstrated by immunofluorescent staining of LCE2, LCE3, KRT10, FLG and SPRR2. In case of HaCaT epithelia immunofluorescent staining only could reveal more deposition for LCE3 and FLG. For all other stainings a quantitative statement was impaired due to the inherent high deposition of the

corresponding proteins. Nevertheless, all immunofluorescent stainings of CsA-treated HaCaT and HaCaT-RAS A-5 epithelia revealed an improved stratification.

2.2.4. Continuous CsA treatment led to an increase in transepithelial electrical resistance in HaCaT- and HaCaT-RAS A5-OTCs

Interestingly, many of the CsA-induced regulated genes were involved in 'epidermal development' and differentiation. The epidermis has a protective function, preventing pathogens or chemicals entering the human body as well as being a barrier against UV irradiation. Epithelia with reduced differentiation most often also exhibit defects in barrier function, as it is for example the case for atopic dermatitis (Palmer *et al.* 2006; Mildner *et al.* 2010). Measurements of transepithelial electrical resistance (TEER) (Koria *et al.* 2003) was used in order to determine a potential difference in the skin barrier of OTCs treated with CsA.

Compared to NHEK epithelia, HaCaT and HaCaT-RAS A-5 epithelia, which are characterized by a parakeratotic epithelium, differentiate less (Berning *et al.* 2015). Accordingly NHEK-OTCs showed the highest TEER of about 10,000 Ω. This reflected a fully developed skin barrier, which impeded the current flow of applied voltage. In contrast, the measured resistance from HaCaT- and HaCaT-RAS A-5-OTCs displayed multi-fold lower values of 180 Ω and 50 Ω, respectively. This clearly revealed the reduced differentiation and demonstrated a non-functional skin barrier (Figure 2.15A). Next TEER was measured to quantify changes in barrier function of HaCaT- and HaCaT-RAS A-5-OTCs treated with CsA. Interestingly, resistance increased in CsA-treated HaCaT- and HaCaT-RAS A-5-OTCs to 280 Ω and 70 Ω, respectively, correlating to the increase in differentiation-associated genes (Figure 2.15B).

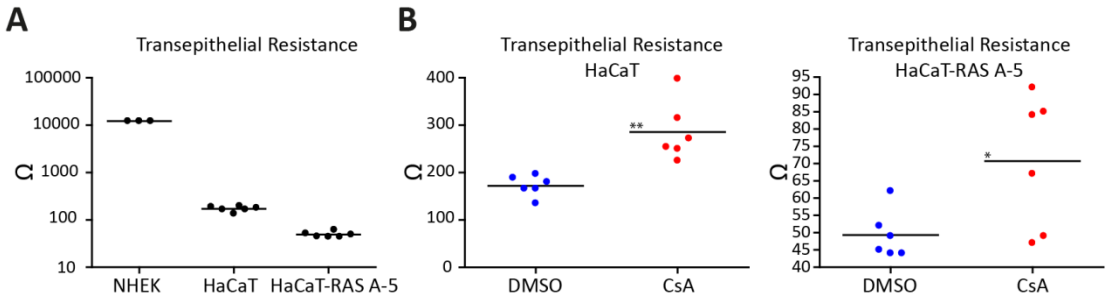

Figure 2.15 Transepithelial electrical resistance of NHEK-, HaCaT- and HaCaT-RAS A-5-OTCs and HaCaT- and HaCaT-RAS A-5-OTCs treated with CsA.
The transepithelial electrical resistance (TEER) was measured with a Volt-Ohm meter. **(A)** *TEER of control OTCs*. **(B)** *TEER of DMSO- and CsA-treated OTCs*. OTCs were treated with DMSO (0.04%) or CsA (10 µg ml^{-1}) for 3 weeks. n=6 (from two independent experiments). The line indicates the mean. p-value (two-sided unpaired t-test). *≤0.05, **≤0.01.

2.2.5. Did CXCL14, DEFB4A or IGFL1 increase differentiation in HaCaT- and HaCaT-RAS A-5-OTCs?

CsA specifically up-regulated differentiation-associated genes like LCEs and thereby improved the barrier function of HaCaT- and HaCaT-RAS A-5-OTCs. In order to identify potential factors inducing

these differentiation-associated genes, a gene list was put together which contained genes differentially expressed in HaCaT and HaCaT-RAS A-5 epithelia (Table 7.3).

Three candidates from this list were chosen for validation by qRT-PCR in independent experiments. The first factor was defensin beta 4A (DEFB4A) which was the second highest up-regulated gene in HaCaT epithelia and also was regulated in HaCaT-RAS A-5 epithelia. Defensins play an important role in bacterial defense (Ganz 2005) and are regulated during keratinocyte differentiation. Moreover, DEFB1 was also shown to induce differentiation in HaCaT keratinocytes (Frye *et al.* 2001; Abiko *et al.* 2003). The second factor was the cytokine CXCL14, whose expression is strongly increased in dense epithelial cells in parallel to differentiation markers like IVL (Ikoma *et al.* 2012). Third, the rather undescribed factor IGFL1 was chosen, which was found to be expressed in embryonic growing and differentiating epithelial tissue (Emtage *et al.* 2006) and being up-regulated in skin upon wounding and inflammation (Lobito *et al.* 2011; Nuutila *et al.* 2012). Up-regulation of all three factors could be validated by qRT-PCR in HaCaT and HaCaT-RAS A-5 epithelia (Figure 2.16).

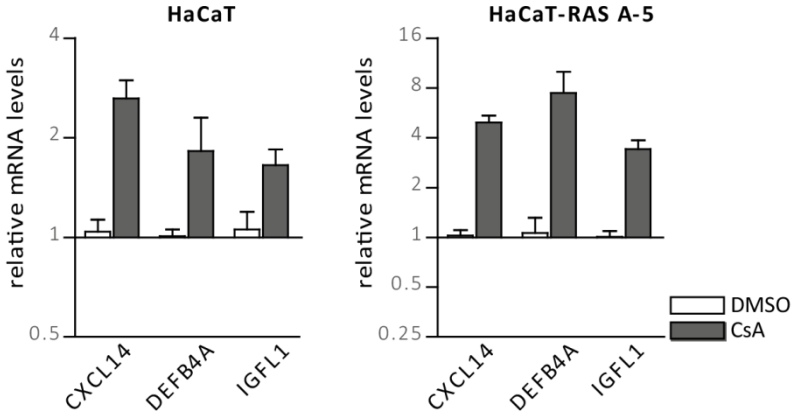

Figure 2.16 Relative gene expression of CXCL14, DEFB4A and IGFL1 in HaCaT and HaCaT-RAS A-5 epithelia treated with CsA.
RNA isolated from indicated epithelia treated with DMSO (0.04%) or CsA (10 µg ml^{-1}) for 3 weeks was quantified by qRT-PCR. The graphs show the mean and the standard error of the mean. CXCL14 (HaCaT): n=11 (from 4 independent experiments), DEFB4A and IGFL1 (HaCaT): n=8 (from 3 independent experiments), CXCL14 (HaCaT-RAS A-5): n=9 (3 independent experiments), DEFB4A and IGFL1 (HaCaT-RAS A-5): n=3 (1 experiment).

In order to determine whether one of these 3 factors could induce differentiation in HaCaT or HaCaT-RAS A-5 cells, OTCs were treated with DEFB4A (100 ng ml^{-1}), CXCL14 (100 ng ml^{-1}) or IGFL-1 (10nM). OTCs treated with CsA were run in parallel for comparison. Treatment was performed for 3 weeks before OTCs were harvested and the RNA from the epithelia was sampled. 4 genes, FLG, LCE1B, LCE2A and LCE3A were chosen to assess the state of differentiation. In case of HaCaT-RAS A-5-OTC RNA extraction was done from the whole OTC as separation of epithelia and dermal equivalent was not possible.

In CsA-treated HaCaT epithelia FLG, LCE1B, LCE2A and LCE3A were upregulated 5.9-fold, 1.6-fold, 3.1-fold and 2.6-fold, respectively (Figure 2.17A), which confirmed previous experiments. In contrast, DEFB4A treatment led to 0.9-fold, 0.7-fold and 0.95-fold down-regulation of FLG, LCE1B and LCE2A RNA, respectively, and 1.4-fold up-regulation of LCE3A. Accordingly H&E histological sections did not reveal an increase in differentiation (Figure 2.17B). A similar result was obtained with CXCL14 treatment. Histology of PBS-treated HaCaT-OTCs and CXCL14-treated HaCaT-OTCs were very similar. Moreover, FLG, LCE1B, LCE2A and LCE3A RNA expression were hardly regulated: 0.8-fold, 0.9-fold, 0.95-fold down-regulated and 1.1-fold up-regulated, respectively (Figure 2.17C). H&E histological stainings of IGFL1-treated HaCaT-OTCs did not reveal an induction of differentiation. While LCE1B and LCE2A RNA expression was hardly changed upon IGFL1 (both 0.8-fold down-regulated), FLG was 0.4-fold down-regulated and LCE3A 1.5-fold up-regulated (Figure 2.17D).

As previous experiments showed the strongest effect on HaCaT-RAS A-5 upon continuous CsA treatment, they might be more susceptible for differentiation triggers. Therefore HaCaT-RAS A-5 cells were as well treated with DEFB4A, CXCL14 and IGFL1. RNA levels of FLG, LCE1B, LCE2A and LCE3A revealed a considerable increase in CsA-treated HaCaT-RAS A-5-OTCs: 4.2-fold, 8.9-fold, 14.7-fold and 2.7-fold up-regulation, respectively. Moreover, the H&E histological staining showed improved stratification (Figure 2.18A). On the contrary, DEFB4A treatment led to a decrease in FLG, LCE1B, LCE2A and LCE3A RNA levels (0.4-fold, 0.5-fold, 0.3-fold and 0.9-fold, respectively). Consequently, stratification or differentiation did not change significantly in H&E histological stainings (Figure 2.18B). Similarly, CXCL14 did not induce obvious differentiation in HaCaT-RAS A-5-OTCs. FLG, LCE1B and LCE2A RNA levels were decreased upon CXCL14 treatment (0.6-fold, 0.9-fold and 0.5-fold, respectively), while LCE3A was 1.1-fold up-regulated (Figure 2.18C). IGFL1 treatment did not majorly influence gene expression of FLG, LCE1B and LCE3A (0.95-fold, 0.95-fold and 0.99-fold down-regulated), while LCE2A was 1.4-fold up-regulated. Accordingly, H&E histology revealed a comparable undifferentiated epithelium for control- and IGFL1-treated HaCaT-RAS A-5-OTCs (Figure 2.18D).

Summarized these factors (DEFB4A, CXCL14 and IGFL1) did not consistently enhance the expression of the tested differentiation genes and accordingly they did not change the histology appearance of the epithelia. These results suggested that these factors were not responsible for a better structured and differentiated epithelium induced by CsA treatment of HaCaT and HaCaT-RAS A-5 epithelia, but rather were up-regulated concurrent to up-regulation of differentiation-associated genes.

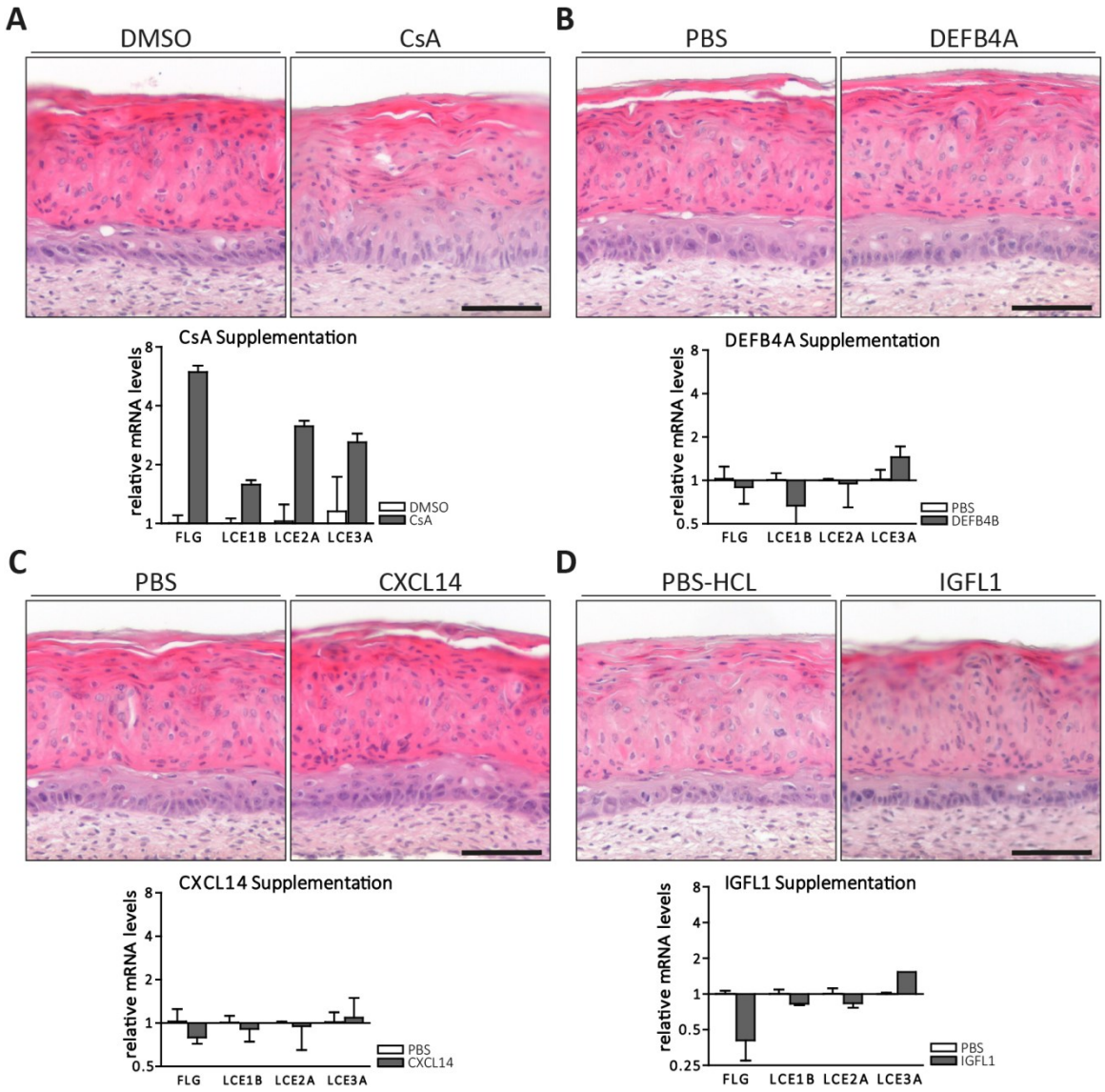

Figure 2.17 H&E histology of HaCaT-OTCs stimulated with CsA, DEFB4A, CXCL14 or IGFL1 and corresponding RNA levels of differentiation markers (FLG, LCE1B, LCE2A, LCE3A).
HaCaT-OTCs were either stimulated with **(A)** *CsA (10 µg ml^{-1})*, **(B)** *DEFB4A (100 ng ml^{-1})*, **(C)** *CXCL14 (100 ng ml^{-1})* or **(D)** *IGFL1 (10 nM)* or the corresponding indicated solvent for 3 weeks and then processed for H&E histological stainings and RNA isolation from the epithelium. Relative RNA expression was quantified by qRT-PCR. Scale bars: 100 µm. The graphs show the mean and the standard error of the mean. n=2.

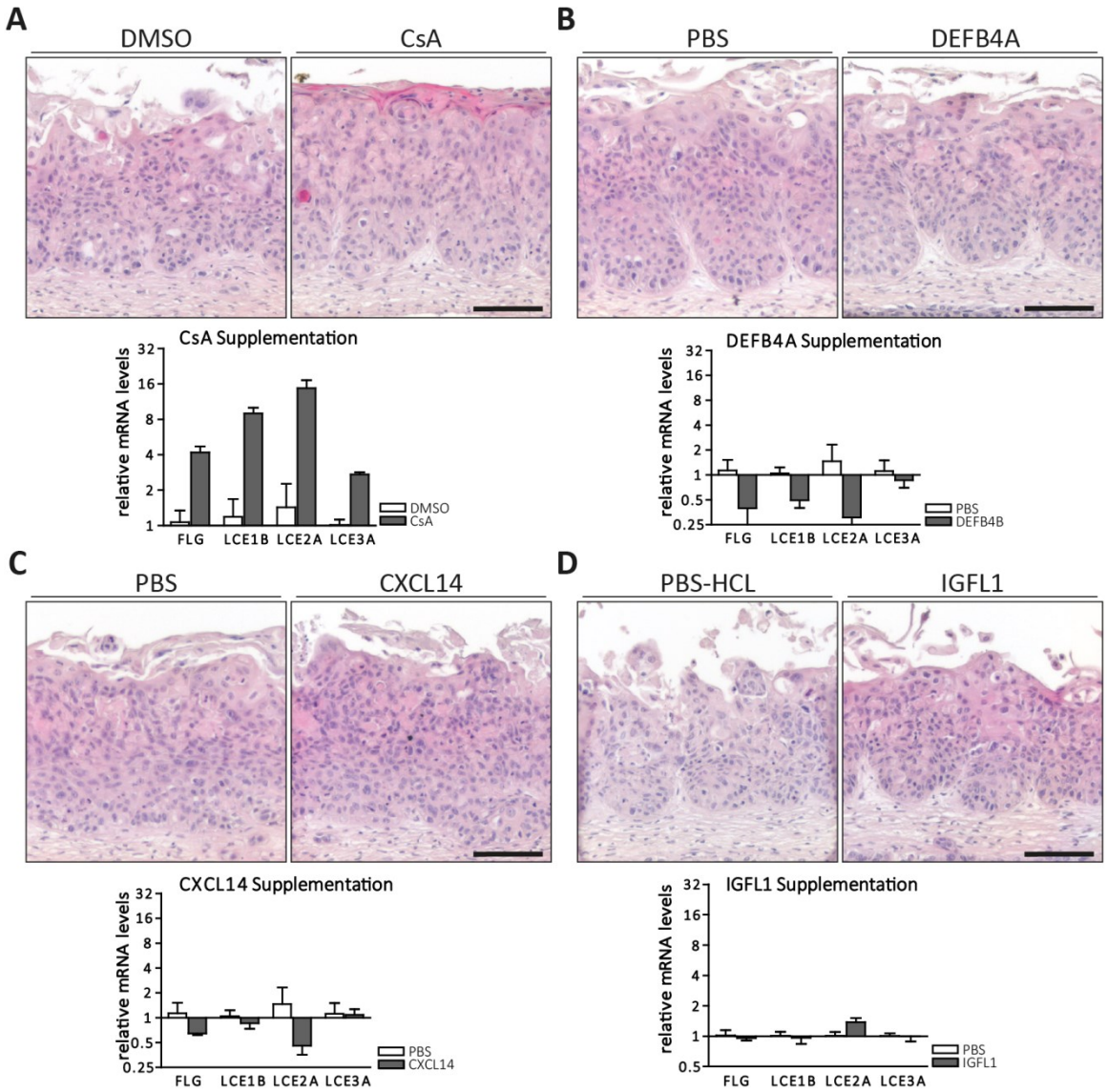

Figure 2.18 H&E histology of HaCaT-RAS A-5-OTCs stimulated with CsA, DEFB4A, CXCL14 or IGFL1 and corresponding RNA levels of differentiation markers (FLG, LCE1B, LCE2A, LCE3A).
HaCaT-RAS A-5-OTCs were either stimulated with **(A)** *CsA* (10 µg ml^{-1}), **(B)** *DEFB4A* (100 ng ml^{-1}), **(C)** *CXCL14* (100 ng ml^{-1}) or **(D)** *IGFL1* (10 nM) or the corresponding indicated solvent for 3 weeks and then processed for H&E histological stainings and RNA isolation from the epithelium. Relative RNA expression was quantified by qRT-PCR. Scale bars: 100 µm. The graphs show the mean and the standard error of the mean. n=3.

2.3. CsA treatment of HaCaT-OTCs cultivated for over 4 weeks

NHEK-OTCs can be cultivated for several months. In contrast, it is a general trait of HaCaT cells that when grown in OTCs they lose vitality after about 4-6 weeks and the epithelium renders atrophic. As the organization of the HaCaT epithelium normalized under CsA treatment we asked whether the improved organization would also favor a longer life span of the epithelium. Therefore, the previous long-term experiment was extended to 6 weeks of CsA treatment.

As expected, the control HaCaT-OTCs treated with DMSO showed the typical growth pattern with the vital cell layers, marked by intense nuclei staining, diminishing after 4 weeks. After 5 weeks the vital epithelium was reduced to 1 cell layer and after 6 weeks only few basal cells remained vital. In contrast, in the CsA-treated cultures more vital cells were present and the epithelium was nicely organized also after 4-6 weeks. Astonishingly, after cultivation for 6 weeks, CsA-treated HaCaT-OTCs still had a multi-layered vital epithelium, strongly resembling normal human epidermis. Additionally, CellTiter-Blue® assays were performed in order to measure the cell metabolism and thus vitality of the HaCaT-OTCs. These measurements validated that, while after 3 weeks of CsA or DMSO treatment the vitality of the OTCs was comparable, after 4-6 weeks of treatment the vitality of HaCaT-OTCs treated with CsA was higher than that of the DMSO-treated HaCaT-OTCs, describing the difference vital cells (Figure 2.19B).

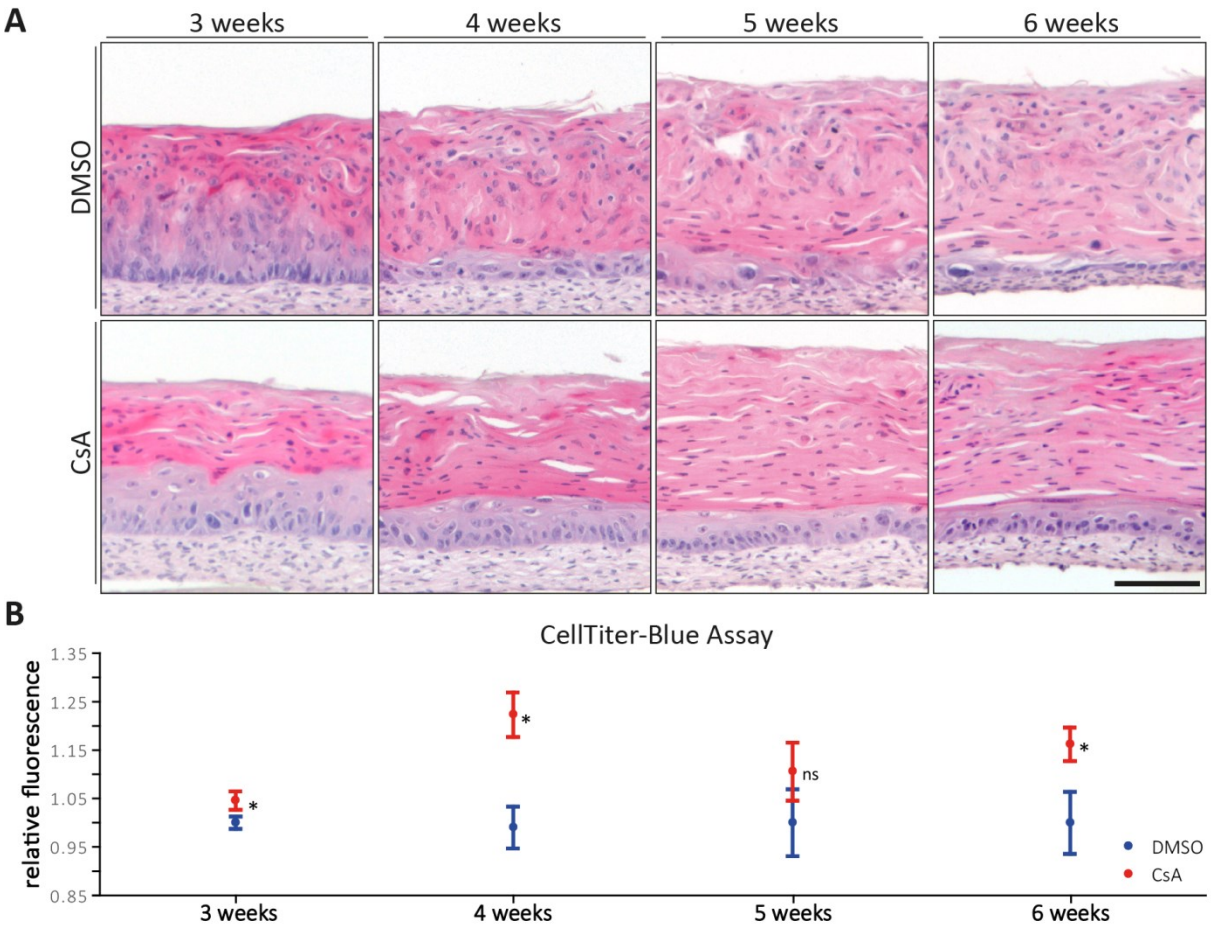

Figure 2.19 H&E histology of CsA-treated (3-6 weeks) HaCaT-OTCs and relative cell metabolism.
HaCaT-OTCs were treated with CsA (10 µg ml^{-1}) or the solvent DMSO (0.04%) for 3 – 6 weeks. **(A)** *H&E histological staining*. Scale bar: 100 µm. **(B)** *CellTiter-Blue® assay (relative metabolism)*. Relative fluorescence of metabolized resazurin (additive) was measured within the culture medium. The graph shows the mean (n=3) and the standard error of the mean. Values from one time point were normalized to the mean of all DMSO replicates from that time point. p-value (two-sided, unpaired t-test). *≤0.05; ns: not significant = p-value > 0.05.

2.3.1. Genome wide RNA expression profile from HaCaT-OTCs treated with DMSO or CsA for 4 weeks

In order to get further insights into the regulation of the HaCaT epithelium with and without CsA, a genome wide RNA expression profile was done from RNA isolated from the epithelium of HaCaT-OTCs treated for 4 weeks with DMSO or CSA, respectively. Here the 4 weeks' time point was chosen in order to still evaluate vital cells in both treatment conditions. Atrophy in control HaCaT-OTCS treated with DMSO already was too much advanced in older HaCaT-OTCs. Raw data from three biological replicates, from HaCaT-OTC epithelia treated with DMSO or CsA, respectively, were normalized. Clustering according to NMDS (Figure 2.20A) and hierarchical clustering (Figure 2.20B) demonstrated that biological replicates clustered according to their treatment group, showing a similar expression pattern. Differentially expressed genes were calculated and filtered by p-value (≤ 0.01). The 20 highest and lowest differentially expressed genes are listed in the appendix (Table 7.3).

In total 508 genes were differentially expressed. 23% (117/508) of these genes were regulated above 1.5-fold. 51% (258/508) of all differentially expressed genes and 63% (74/117) of differentially expressed genes above 1.5-fold regulation were down-regulated (Figure 2.20C).

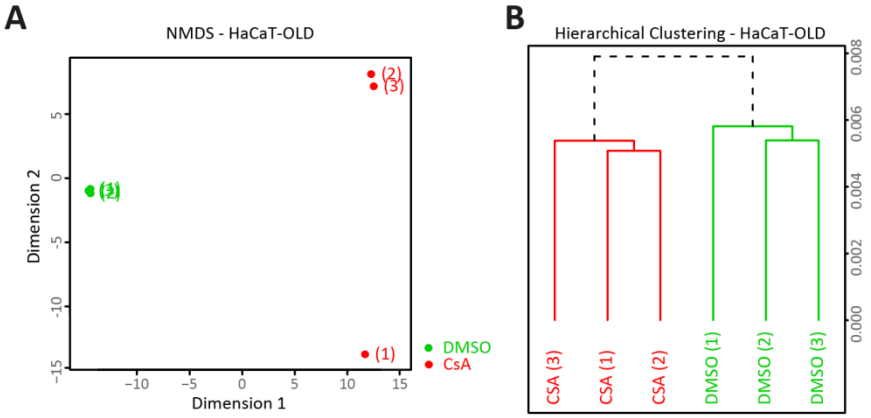

C

Numbers of differentially expressed genes

	HaCaT-OLD	
No. of genes	Total	≥ 1.5-fold
Total	508	117
Up-regulated	250	43
Down-regulated	258	74

Figure 2.20 RNA expression profile from CsA-treated (4 weeks) HaCaT epithelia.
(A) *Non-metric multidimensional scaling (NMDS)* and **(B)** *hierarchical clustering* were applied to assess the discriminability of the 3 biological replicates from both treatment groups (DMSO and CsA). Clustering and visualization was performed with Chipster from normalized data. **(C)** *Numbers of differentially expressed genes (DMSO vs. CsA).* Left column: total number of differentially expressed genes. Right column: Number of differentially expressed genes with a fold change ≥ 1.5. Differentially expressed genes were calculated with Chipster (filtered by p-value ≤ 0.01).

Differentially expressed genes were used for Ingenuity® Pathway Analysis to find molecular/cellular functions and pathways which are affected by CsA in these old HaCaT-OTCs. The TOP 3 molecular and cellular functions from this analysis were: 'cellular movement', 'cellular growth & proliferation' and 'cell death & survival' (Figure 2.21A). The activation z-scores, which describe the potential up- or down-regulation of annotated function, are depicted in Figure 2.21B. Z-scores for the function 'cellular movement' predicted a mixture of activation and inactivation for most terms, except for the terms invasion and recruitment, for which the z-scores predicted exclusively an activation in CsA-treated HaCaT epithelia. Z-scores for the function 'cellular growth & proliferation' mainly predicted activation for all terms in CsA-treated HaCaT epithelia, while for the function 'cell death & survival' predominantly an inactivation was predicted in CsA-treated HaCaT epithelia (Figure 2.21B). When looking at the most probably affected pathways, these included: HGF signaling, Integrin signaling and Oncostatin M signaling. All three were predicted to be activated in CsA-treated HaCaT epithelia (Figure 2.21C).

A

IPA Analysis: Predicted Impacted Molecular and Cellular Functions

Priority	Name	p-value	# Molecules
1	Cellular Movement	2.41E-04-1.31E-21	170
2	Cellular Growth and Proliferation	3.31E-04-8.01E-15	237
3	Cell Death and Survival	3.35E-04-2.41E-12	203

B

IPA Analysis: Predicted Activation Scores for...

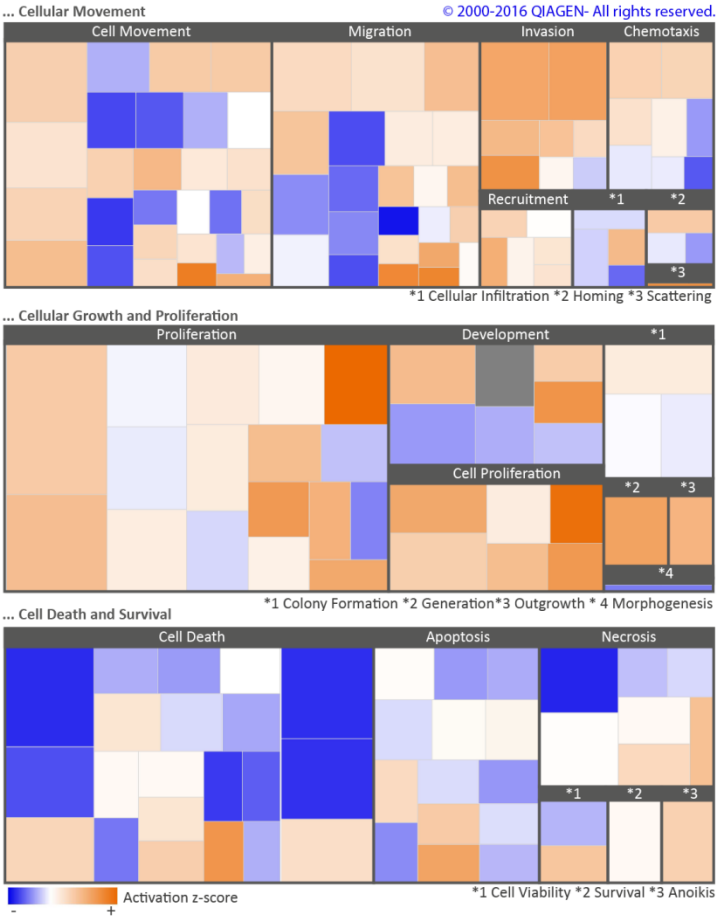

C

IPA Analysis: Predicted Canonical Pathways

Priority	Name	p-value	# Molecules	z-score
1	HGF signaling	2.35E-05	16/114	1.508
2	Integrin signaling	1.42E-02	16/212	2.496
3	Oncostatin M signaling	1.45E-02	6/34	0.816

Figure 2.21 Prediction of molecular/cellular functions and canonical pathways impacted by CsA in HaCaT-OLD epithelia using Ingenuity® Pathway Analysis.
Differentially expressed genes (filtered by p-value: 0.01) from HaCaT epithelia treated with DMSO or CsA for 4 weeks were used for Ingenuity® Pathway Analysis. **(A)** *Top 3 predicted cellular functions*. List is sorted by p-value (Benjamini-Hochberg procedure). **(B)** *Z-Score visualization of top molecular/cellular functions*. One square corresponds to one annotated molecular/cellular function within the indicated topic. The square size is calculated based on the magnitude of z-score. The activation z-score expresses the predicted positive or negative activation of a specific function. **(C)** *Top 3 canonical pathways*. List is sorted by p-value (Benjamini-Hochberg procedure). Pathways without a z-score or a z-score of 0 were neglected.

2.3.2. Comparison of RNA expression profiles from CsA-treated HaCaT epithelia (2 and 4 weeks treatment)

When comparing the complete gene set (HaCaT-OLD, DMSO vs. CsA, 4 weeks treatment) with the RNA expression profile from HaCaT epithelia, described in 2.2.2 (DMSO vs. CsA, 2 weeks treatment), the numbers of differential gene expression were comparable (Figure 2.8 and Figure 2.20). However, only 26% of both gene sets were overlapping (130/507 and 130/508) (Figure 2.22). Moreover, when looking at canonical pathways predicted by Ingenuity® Pathway Analysis in CsA-treated HaCaT-OLD epithelia (Figure 2.21), less of these genes were differentially regulated in HaCaT epithelia treated with CsA for 2 weeks in comparison to HaCaT-OLD epithelia treated with CsA for 4 weeks. In case of HGF signaling 16 genes were part of the gene set 'HGF signaling' (Ingenuity® Pathway Analysis) from HaCaT-OLD epithelia, while only 5 were present in the HaCaT epithelia (2 weeks treatment) data set. 16 genes from the HaCaT-OLD data set were part of the Ingenuity® Pathway Analysis gene set 'Integrin signaling', while it were 6 genes in the HaCaT (2 weeks treatment) data set. None of the genes of the HaCaT data set were part of the gene set 'Oncostatin M signaling' (Ingenuity® Pathway Analysis), while there were 6 from the HaCaT-OLD data set (Figure 2.22.). The higher number of genes from Ingenuity® Pathway Analysis canonical pathway gene sets (HGF, Integrin and Oncostatin M) in the HaCaT-OLD data set could indicate that these pathways were not activated after 2 weeks of CsA treatment, but might be activated after 4 weeks of continuous treatment.

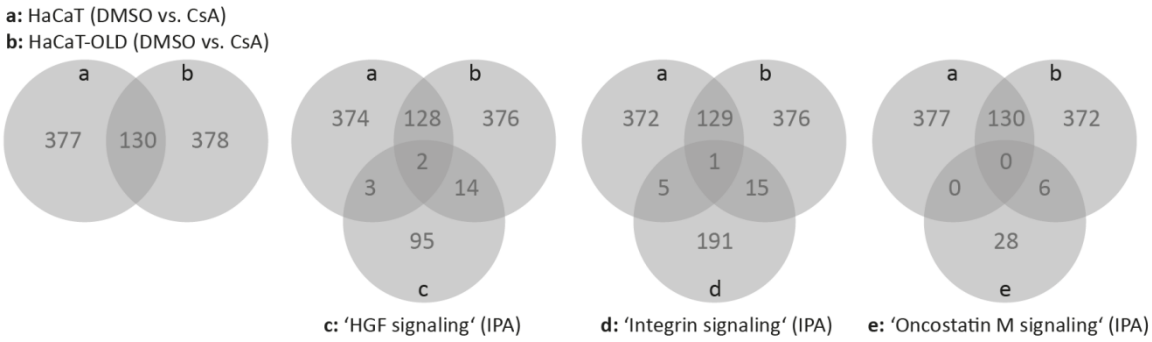

Figure 2.22 Comparison of RNA expression profiles from CsA-treated HaCaT epithelia (2 and 4 weeks of treatment).
Overlap of differential gene expression from data sets HaCaT (2 weeks CsA treatment, chapter 2.2.2) and HaCaT-OLD (4 weeks treatment) with Ingenuity® Pathway Analysis canonical pathway gene sets.

2.4. Impact of UV irradiation on CsA-treated HaCaT and HaCaT-RAS A-5 epithelia

Organ transplant patients are strongly advised to avoid extensive sun exposure (Perez *et al.* 2016) and it was shown that rigorous sunscreen use has a beneficial impact on invasive cSCCs occurrence in those patients (Ulrich *et al.* 2009). Moreover, like in immunocompetent patients, renal transplant patients have a high number of UV-specific mutations in their skin lesions (Queille *et al.* 2007) and cSCCs in organ transplant recipients appear as well primarily in sun exposed areas (Smith *et al.* 2004). Thus, additional UV irradiation may be an important co-factor for the development of cSCCs in organ transplant recipients. Therefore, an experiment was performed, which combines UV irradiation and continuous CsA treatment. HaCaT- and HaCaT-RAS A-5-OTCs were used and treated with CsA for 2 or for 3 weeks, respectively. In addition, OTCs were irradiated with UVA and UVB (5 J/cm^2 UVA, 10 mJ/cm^2 UVB) three times per week. This single dose is below the minimal erythema dose, which, depending on the skin type, lies between 23 and 51 mJ/cm^2 UVB (Perez Ferriols *et al.* 2014). For UVA no abnormal skin reaction could be determined by Perez *et al.* for doses as high as 20 J/cm^2.

2.4.1. Assessment by H&E histology and Ki67 staining of CsA-treated HaCaT and HaCaT-RAS A-5 epithelia irradiated with UV

Histological H&E stainings were assessed to potentiate morphological changes of HaCaT- and HaCaT-RAS A-5-OTCs after CsA or UV or UV+CsA treatment. Similar to the previous experiments CsA enhanced the tissue organization and also increased differentiation, as indicated by more intense eosin staining in the upper parts HaCaT-RAS A-5 epithelia. HaCaT epithelia were not so much improved by CsA, based on H&E histological staining, as seen in previous experiments. Interestingly, UV irradiation resulted in a similar phenotype as CsA treatment, enhancing tissue organization and differentiation in HaCaT- and HaCaT-RAS A-5-OTCs. The combination of UV+CsA did not further change that phenotype. Also in combination tissue organization and differentiation was improved. Importantly, neither for HaCaT nor for HaCaT-RAS A-5 cells did a combinatory treatment induce invasion (Figure 2.23A).

Cryosections from treated HaCaT- and HaCaT-RAS A-5-OTCs were stained for Ki67 to measure the proliferation index. As also shown in Figure 2.6, CsA decreased the proliferation index of HaCaT and HaCaT-RAS A-5 keratinocytes grown in OTCs. UV irradiation and the combination of UV irradiation with CsA caused as well a reduction in mean proliferation. However, in contrast to CsA treatment this trend was not significant (Figure 2.23B). In detail the proliferation indices of HaCaT epithelia were as follows: the CsA proliferation index being the lowest (19.5), UV a bit higher (20.7) and the combination of UV +CsA a bit higher than CsA or UV alone (23.5), but still less than the control (26.2). In HaCaT-RAS A-5 epithelia the mean proliferation indices had a similar trend to the results from the HaCaT epithelia: the index was lowest for CsA treatment (27.3), higher in UV irradiated samples

(42.5), and even higher in the combination of UV+CsA (48.2), which was similar to the control samples (50.9) (Figure 2.23B).

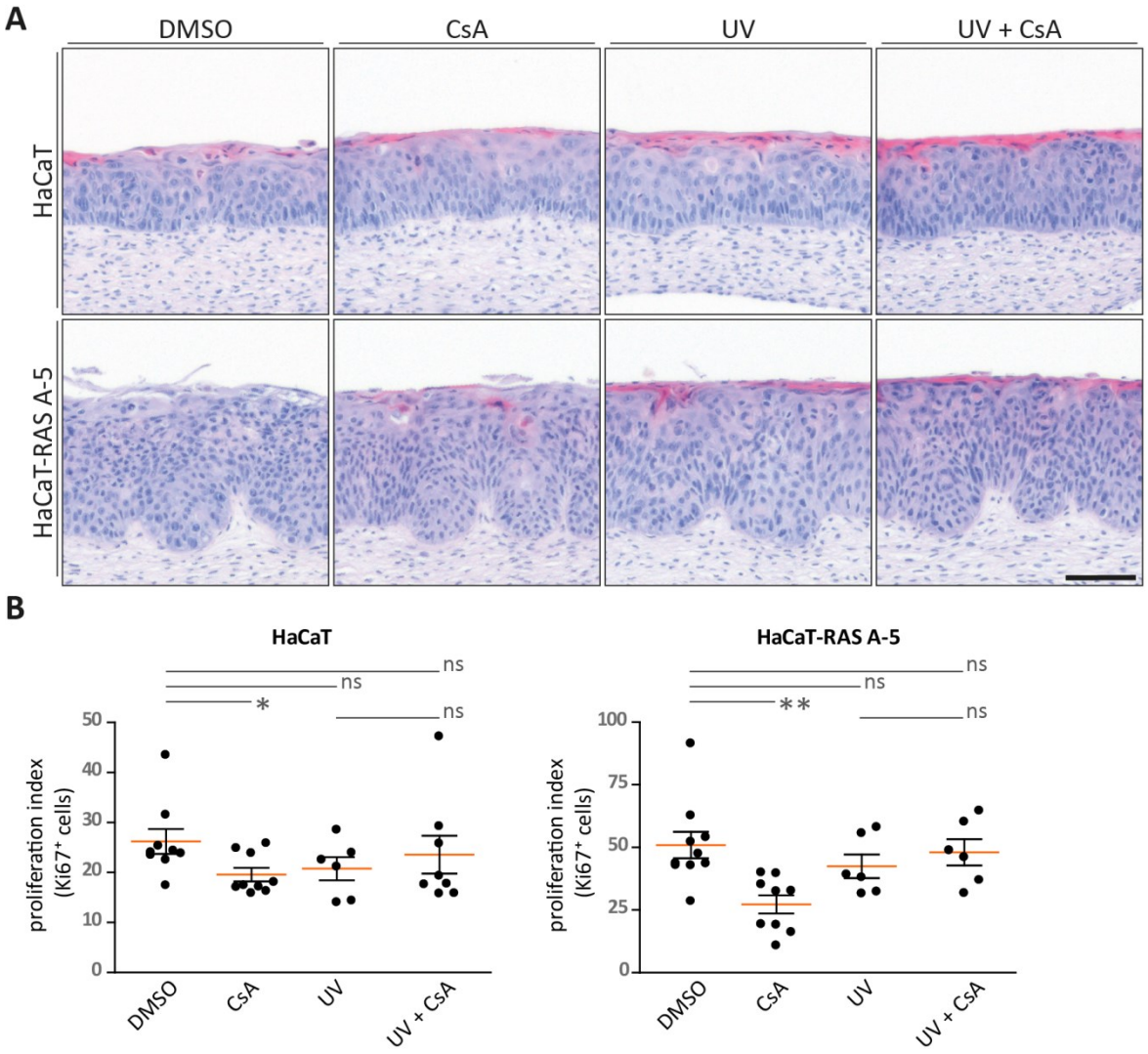

Figure 2.23 Impact of UV irradiation on CsA-treated HaCaT and HaCaT-RAS A-5 epithelia.
(A) *H&E histological staining of* HaCaT- and HaCaT-RAS A-5-OTCs after 2 weeks (HaCaT) or 3 weeks (HaCaT-RAS A-5) of treatment. Treatment conditions (three time per week): DMSO (0.04%), CsA (10 µg ml^{-1}), UV (5 J/cm^2 UVA + 10 mJ cm^2 UVB; OTCs were as well treated with 0.04% DMSO) or UV+CsA. Scale bar: 100 µm. **(B)** *Proliferation index (Ki67$^+$ cells)*. Each data point represents the number of Ki67$^+$ cells per length of basement membrane. Data from OTCs treated with DMSO or CsA alone were also shown in Figure 2.6. The orange bar marks the mean. DMSO, CsA: n=9 (from 3 biological replicates), UV (HaCaT): n=6 (from 3 biological replicates), UV+CsA (HaCaT): n=8 (from 3 biological replicates), UV, UV+CsA (HaCaT-RAS A-5): n=6 (from 2 biological replicates). The error bars are the standard error of the mean. *: p-value of 0.03, **: p-value of 0.002, ns: not significant = p-value > 0.05 (two-sided, unpaired t-test).

2.4.2. Genome wide RNA expression profiles of HaCaT and HaCaT-RAS A-5 epithelia treated with UV or UV+CsA

In order to reveal changes on a transcriptional level, genome wide expression profiles were made. Raw data from all treatment groups (DMSO, CsA, UV, UV+CsA) were normalized together. Raw data from DMSO and CsA were already used for the analysis described in section 2.2.2. Replicates from

HaCaT epithelia separated by NMDS into four groups (Figure 2.24A) and hierarchical clustering divided both UV groups from non-UV, as depicted in the dendrogram (Figure 2.24B). In contrast, biological replicates from HaCaT-RAS A-5 epithelia were not as strictly separated by NMDS (Figure 2.24C). Accordingly, hierarchical clustering could not separate UV groups from non-UV groups and also located 1 UV replicate within the UV+CsA group, as depicted in the dendrogram (Figure 2.24D). However, histology did not reveal any abnormalities for this one sample (data not shown), which did cluster to the wrong treatment group. Moreover, the histology of both treatment groups, UV and UV+CsA very much resembled, which might be reflected in the expression profile. Thus, all replicates were included in the differential gene expression analysis. The lists of the 20 highest and lowest differentially expressed genes (p-value ≤ 0.01) for DMSO vs. UV and DMSO vs. UV+CsA can be found in the appendix (Tables 7.5 - 7.8). Moreover, a list with differentially expressed genes, which are regulated in both cell types, HaCaT and HaCaT-RAS A-5, as well as in all treatment options (CsA, UV and UV+CsA) can be found in the appendix (Table 7.9).

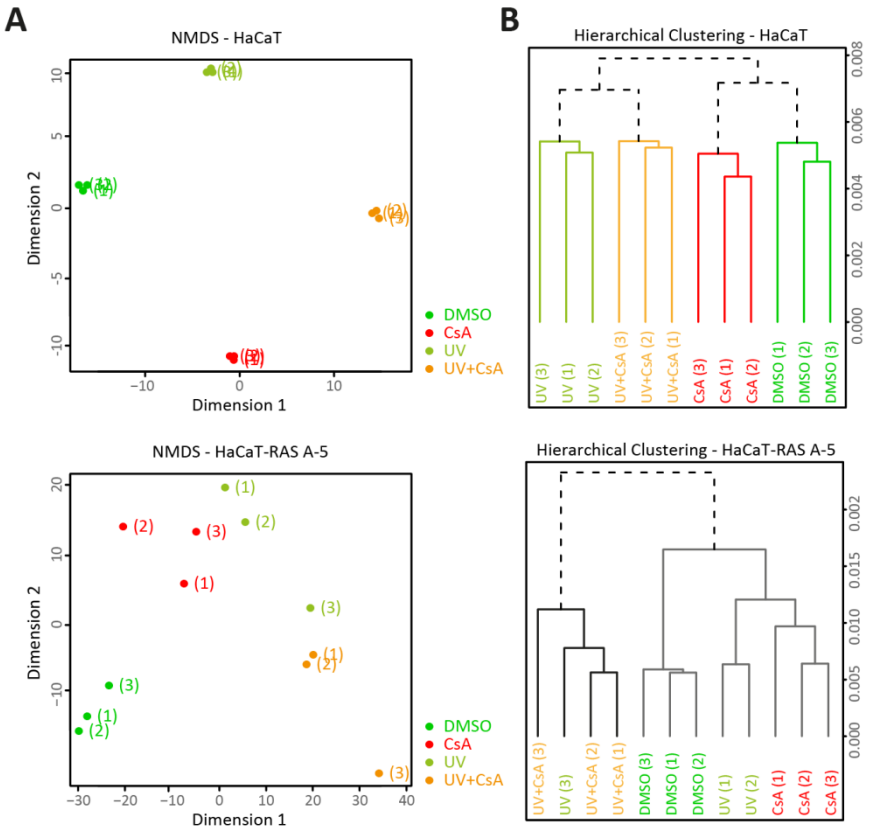

Figure 2.24 Visualizations of biological replicates from genome wide RNA expression profiles from HaCaT and HaCaT-RAS A-5 epithelia treated with DMSO, CsA, UV or UV+CsA by NMDS and hierarchical clustering.
(A) *Non-metric multidimensional scaling (NMDS)* and **(B)** *hierarchical clustering* were applied to assess the discriminability of the 3 biological replicates from 4 treatment groups (DMSO, CsA, UV and UV+CsA). Clustering and visualization was performed with Chipster from normalized data.

2.4.2.1. Overlap of RNA expression profiles from epithelia treated with CsA, UV or UV+CsA

904 genes were differentially expressed in HaCaT epithelia treated with the combination UV+CsA. More than half of these genes (67%) were regulated below 1.5-fold and only 218 were regulated above 1.5-fold. From these 218 differentially expressed genes 63% (138/218) were down-regulated, while from the total number of differentially expressed genes 53% were down-regulated (475/904). In HaCaT epithelia, which were irradiated with UV without CsA treatment, much less genes were differentially expressed. In total 346 genes were differentially expressed, with 31% of these genes being regulated above 1.5-fold. 62% (222/346) of total differentially expressed genes and 76% (82/108) of differentially expressed genes above 1.5-fold regulation were down-regulated (Figure 2.25A). H&E histology revealed that phenotypes of CsA, UV and UV+CsA resembled. When comparing the expression profiles with each other, 25% (125/509) of the CsA expression profile, 36% (125/346) of the UV expression profile and 14% (125/904) of the UV+CsA expression profile overlapped with all three gene sets (CsA, UV and UV+CsA) (Figure 2.25B). When filtering the expression profiles according to the GO-term 'epidermal development', these percentages of overlap increased to 37% (14/38, CsA), 54% (14/26, UV) and 24% (14/58, UV+CsA) (Figure 2.25B). The heat map, visualizing differentially expressed genes filtered by the GO-term 'epidermal development', revealed that those genes, which were regulated in all three gene sets, were either all up- or all down-regulated (Figure 2.25C).

A

	CsA		UV		UV + CsA	
No. of genes	Total	≥ 1.5-fold	Total	≥ 1.5-fold	Total	≥ 1.5-fold
Total	507	128	346	108	904	218
Up-regulated	229	53	124	26	429	80
Down-regulated	278	75	222	82	475	138

B

C

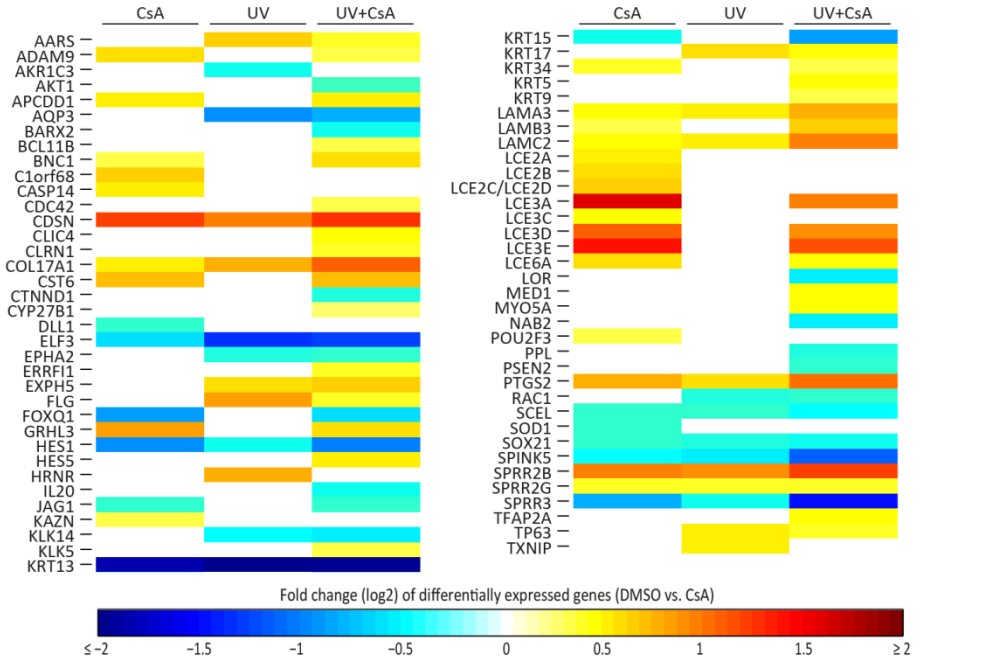

Figure 2.25 Numbers and overlap of differentially expressed genes (DMSO vs. CsA, DMSO vs. UV or DMSO vs. UV+CsA) from HaCaT epithelia.
(A) *Numbers of differentially expressed genes (DMSO vs. CsA, DMSO vs. UV and DMSO vs. UV+CsA).* Whole genome RNA expression profiles from HaCaT epithelia treated with DMSO, CsA, UV or UV+CsA. The table shows the total number of differentially expressed genes and the number of differentially expressed genes with a fold change ≥ 1.5. Differentially expressed genes were calculated with Chipster (filtered by p-value ≤ 0.01). **(B)** *Overlap of differential gene expression* from complete data sets (DMSO vs. CsA, DMSO vs. UV and DMSO vs. UV+CsA) or those data sets filtered for the GO-term 'epidermal development' (GO-0008544). **(C)** *Heatmap* of differentially expressed genes (DMSO vs. CsA, *DMSO vs. UV and DMSO vs. UV+CsA*) filtered by the GO-term 'epidermal development' (GO-0008544) from HaCaT epithelia. Fold changes (log2) are depicted by the indicated color. The rows are sorted alphabetically. Data from DMSO vs. CsA was also shown in Figure 2.9.

2594 genes were differentially expressed in HaCaT-RAS A-5 epithelia after the combinatorial treatment of UV+CsA. 46% (1188/2594) were regulated above 1.5-fold, of which 61% (724/1188) were down-regulated. From the total number of differentially expressed genes 48% (1239/2594) were down-regulated. UV irradiation without CsA treatment resulted in 962 differentially expressed genes, which is less than half of that regulated in the combination of UV+CsA. Of these 962 genes

62% (597/962) were above 1.5-fold regulated. 55% (331/597) of these genes were down-regulated and from the total number of differentially expressed genes 58% (557/962) were down-regulated (Figure 2.26A). As for HaCaT-OTCs, the histology of HaCaT-RAS A-5-OTCs of all treatment groups (CsA, UV and UV+CsA) resembled. When comparing the expression profiles, 70% (365/521) of all genes from the CsA expression profile, 38% (365/962) from the UV expression profile and 14% (365/2594) from the UV+CsA expression profile were overlapping with all three gene sets (CsA, UV, UV+CsA). When comparing expression profiles filtered according to the GO-term 'epidermal development', these percentages increased to 78% (36/46, CsA), 47% (36/76, UV) and 37% (36/97, UV+CsA) (Figure 2.26B). The heat map, visualizing differentially expressed genes filtered by the GO-term 'epidermal development', revealed those genes, which were regulated in all three gene sets, were either all up- or all down-regulated (Figure 2.26C).

In summary the comparison of the data sets showed that there was quite a high overlap of gene expression altered by CsA, UV and UV+CsA treatment in HaCaT epithelia and even more in HaCaT-RAS A-5 epithelia. Moreover, as for CsA treatment, UV irradiation led to increased regulation of 'epidermal development' genes, which was as well true for the combination treatment UV+CsA. Especially in the case of HaCaT-RAS A-5 epithelia, which in general were more affected by CsA, UV or UV+CsA treatment than HaCaT epithelia, a similar regulation pattern for the 'epidermal development' genes for all three treatments (CsA, UV and UV+CsA) was detected, suggesting a common regulation pattern of the differentiation program for CsA treatment and UV irradiation.

A

	CsA		UV		UV + CsA	
No. of genes	Total	≥ 1.5-fold	Total	≥ 1.5-fold	Total	≥ 1.5-fold
Total	521	327	962	597	2594	1188
Up-regulated	199	139	405	266	1355	464
Down-regulated	322	188	557	331	1239	724

B

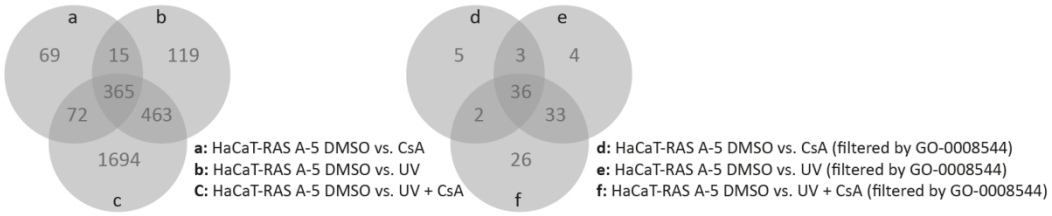

C

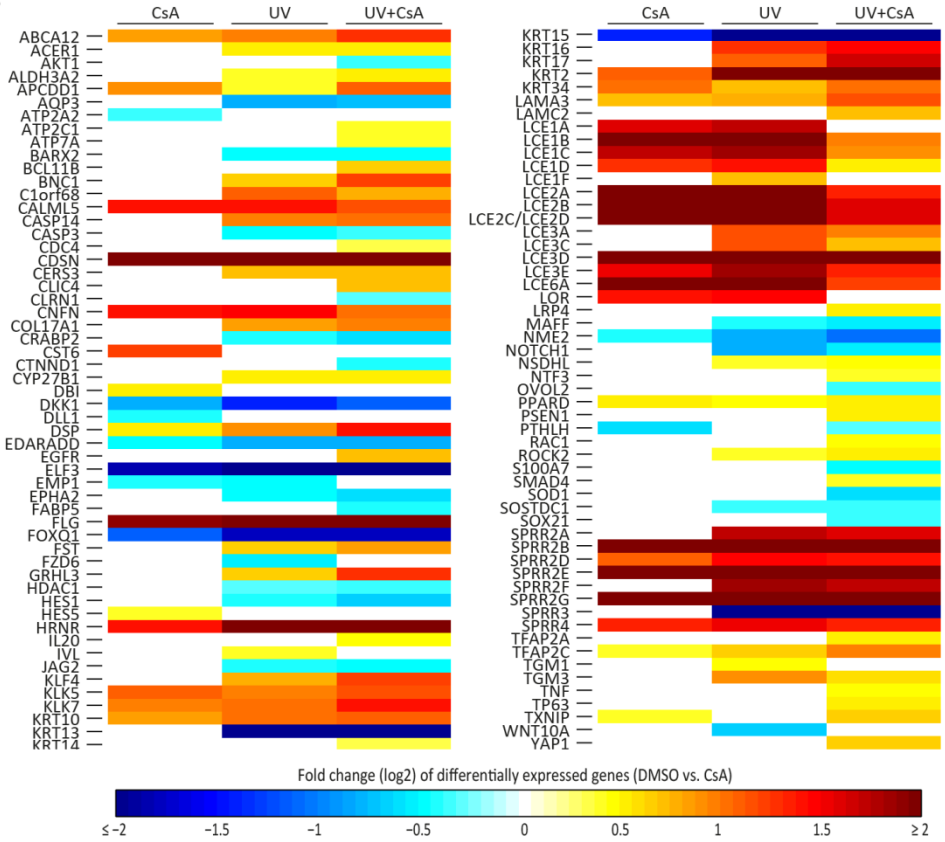

Figure 2.26 Numbers and overlap of differentially expressed genes (DMSO vs. CsA, DMSO vs. UV or DMSO vs. UV+CsA) from HaCaT-RAS A-5 epithelia.

(A) *Numbers of differentially expressed genes (DMSO vs. CsA, DMSO vs. UV and DMSO vs. UV+CsA).* Whole genome RNA expression profiles from HaCaT-RAS A-5 epithelia treated with DMSO, CsA, UV or UV+CsA. The table shows the total number of differentially expressed genes and the number of differentially expressed genes with a fold change ≥ 1.5. Differentially expressed genes were calculated with Chipster (filtered by p-value ≤ 0.01). **(B)** *Overlap of differential gene expression* from complete data sets (DMSO vs. CsA, DMSO vs. UV and DMSO vs. UV+CsA) or those data sets filtered for the GO-term 'epidermal development' (GO-0008544). **(C)** *Heatmap* of differentially expressed genes (DMSO vs. CsA, *DMSO vs. UV and DMSO vs. UV+CsA*) filtered by the GO-term 'epidermal development' (GO-0008544) from HaCaT-RAS A-5 epithelia. Fold changes (log2) are depicted by the indicated color. The rows are sorted alphabetically. Data from DMSO vs. CsA was also shown in Figure 2.9.

2.4.3. Comparison analysis of RNA expression data sets from CsA and UV+CsA treatment by Ingenuity® Pathway Analysis

Most of the genes regulated by CsA treatment were also regulated by UV and or UV+CsA, 65% (328/507) in the case of HaCaT and 87% (452/521) in the case of HaCaT-RAS A-5. However, 49% (441/904) in the case of HaCaT and 65% (1694/2594) in the case of HaCaT-RAS A-5 of the genes regulated by the combination UV+CsA were unique to that combination treatment and were not regulated by CsA or UV (Figure 2.25B and Figure 2.26B). In order to get an idea of different molecular regulation in CsA and UV+CsA samples, the data sets were used for a comparison analysis with Ingenuity® Pathway Analysis. While some canonical pathways, like interferon signaling and G2/M DNA damage checkpoint regulation, were regulated likewise in CsA- and UV+CsA-treated epithelia, others like thrombin and Rho family GTPases signaling, were down-regulated in CsA-treated epithelia, but up-regulated in UV+CsA-treated epithelia.

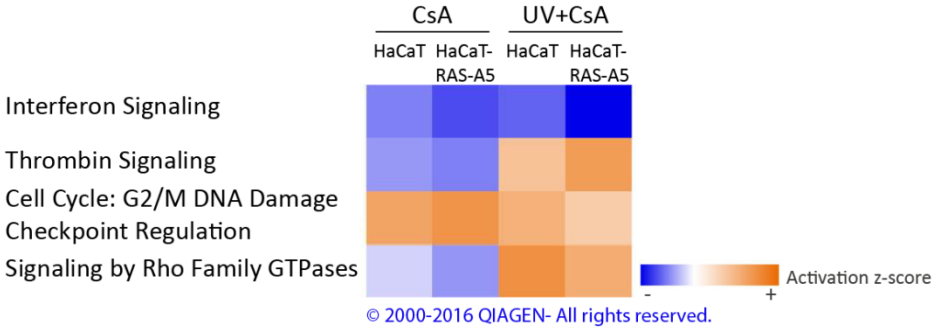

Figure 2.27 Prediction of canonical pathways impacted by CsA and UV+CsA in HaCaT and HaCaT-RAS A-5 epithelia using Ingenuity® Pathway Analysis.
Differentially expressed genes (filtered by p-value: 0.01) from HaCaT and HaCaT-RAS A-5 epithelia (DMSO vs. CsA and DMSO vs. UV+CsA) were used for a comparison analysis with Ingenuity® Pathway Analysis. The list is sorted by z-scores from all 4 data sets. The activation z-score expresses the predicted positive or negative activation of the specific pathway.

2.4.4. Validation of differential gene expression by qRT-PCR

Several genes from the RNA expression profile were chosen for validation by qRT-PCR. In case of HaCaT, ELF3, FLG, LCE1B and LCE2A were analyzed. ELF3 is a transcription factor, which was down-regulated in CsA, UV and UV+CsA-treated HaCaT epithelia (0.64-fold, 0.39-fold and 0.41-fold, respectively). In all three cases down-regulation could be validated by qRT-PCR (CsA: 0.45-fold, UV: 0.37-fold and UV+CsA: 0.25-fold). FLG was not regulated in the CsA RNA expression profile, while it was 1.76-fold and 1.34-fold up-regulated in the UV and UV+CsA RNA expression profile. Validation by qRT-PCR from one experiment could not detect regulation of FLG in CsA and UV+CsA-treated HaCaT epithelia, while it revealed a 1.75-fold up-regulation in UV irradiated HaCaT epithelia. Next, two LCE genes, which stood out at previous experiments, were examined by qRT-PCR. LCE1B was not detected in the CsA, UV or UV+CsA RNA expression profile, while LCE2A was 1.43-fold up-regulated in

the CsA RNA expression profile, while it was not detected in the UV or UV+CsA expression profile. In contrast to the expression profile, LCE1B RNA up-regulation could be measured in CsA-, UV- and UV+CsA-treated HaCaT epithelia by qRT-PCR (2.54-fold, 3.34-fold and 2.46-fold, respectively). LCE2A RNA expression was 1.94-fold up-regulated in case of CsA-treatment, not regulated in case of UV irradiation and 1.51-fold up-regulated in the combinatorial treatment UV+CsA (Figure 2.28).

For validation with HaCaT-RAS A-5 epithelia following genes were chosen: ELF3, FLG, KRT10, KRT15, LCE1b and LCE2A. ELF3 was down-regulated in the RNA expression profile from HaCaT-RAS A-5 epithelia treated with CsA (0.28-fold), UV (0.12-fold) or UV+CsA (0.09-fold). All three results could be replicated by qRT-PCR (CsA: 0.26-fold, UV: 0.08-fold and UV+CsA: 0.06-fold). FLG was up-regulated in HaCaT-RAS A-5 epithelia treated with CsA (3.78-fold), UV (5.94-fold) or UV+CsA (5.59-fold), according to the RNA expression profile. Using qRT-PCR these findings were replicated (CsA: 5.07-fold, UV: 4.8-fold, UV+CsA: 3.55-fold). KRT10 was as well up-regulated in CsA- (1.74-fold), UV- (2-fold) and UV+CsA- (2.2-fold) treated HaCaT-RAS A-5 epithelia according to the RNA expression profiles. Validation was successful by qRT-PCR: CsA (4.12-fold), UV (4.33-fold) and UV+CsA (4.59-fold). In contrast to KRT10, KRT15 was down-regulated in all three treatment conditions in HaCaT-RAS A-5 epithelia according to the RNA expression profile (CsA: 0.38-fold, UV: 0.12-fold and UV+CsA 0.11-fold). These down-regulations could be validated by qRT-PCR: CsA (0.36-fold), UV (0.06-fold) and UV+CsA (0.06-fold). Last, LCE1B and LCE2A were up-regulated in all treatment options in the RNA expression profiles in HaCaT-RAS A-5 epithelia. LCE1B: CsA (4.08-fold), UV (4.21-fold) and UV+CsA (1.92-fold). LCE2A: CsA (4.41-fold), UV (6.71-fold) and UV+CsA (2.58-fold). Measurements by qRT-PCR validated all results. However, the up-regulation was stronger affected than in the RNA expression profile. LCE1B: CsA (12.4-fold), UV (14.77-fold) and UV+CsA (10.9-fold). LCE2A: CsA (13.75-fold), UV (23.36-fold) and UV+CsA (15.56-fold).

To summarize, qRT-PCR measurements from HaCaT-RAS A-5 epithelia could be validated in all examples, while for HaCaT epithelia some measurements deviated from the RNA expression profile. Differential gene expression was in general much stronger in HaCaT-RAS A-5 epithelia than in HaCaT epithelia, which might explain why low regulation in some cases (for example 1.34-fold up-regulation in UV+CsA-treated HaCaT epithelia) could not be replicated by qRT-PCR. In contrast in case of LCE1B and LCE2A gene regulation could be detected by qRT-PCR, which was not evident in the RNA expression profile. In general replication of qRT-PCR with RNA from HaCaT epithelia might need replication with further experiments, which could strengthen the results in case of weak differential gene expression.

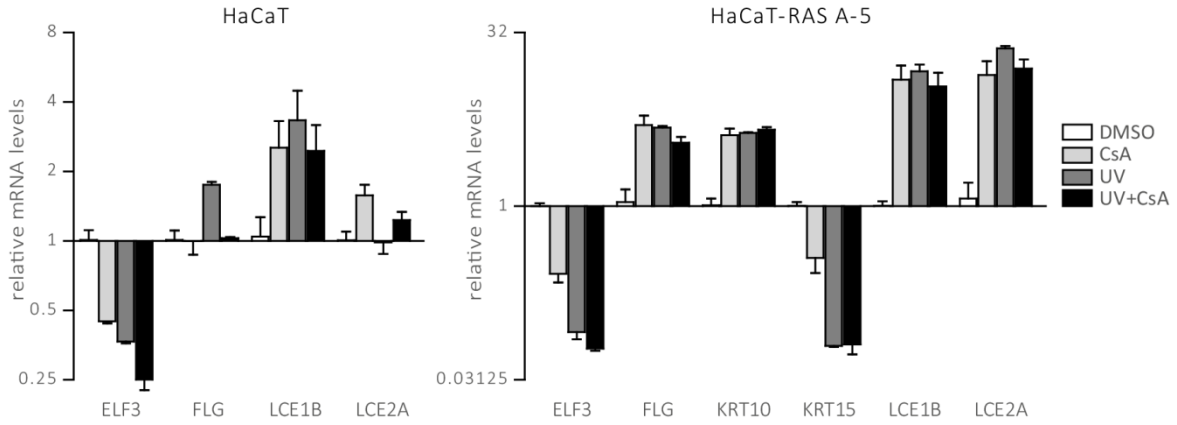

Figure 2.28 Relative RNA expression of HaCaT and HaCaT-RAS A-5 epithelia treated with CsA, UV or UV+CsA. RNA isolated from indicated epithelia treated with DMSO (0.04%), CsA (10 µg ml^{-1}), UV (5 J/cm^2 UVA + 10 mJ/cm^2 UVB; OTCs were as well treated with 0.04% DMSO) or the combination UV+CsA, was quantified by qRT-PCR. The graphs show the mean and the standard error of the mean. n=3.

2.5. Continuous CsA treatment of HaCaT-OTCs in GOLD serum

Experiments described so far were replicated several times in order to exclude experimental variation. Results, like morphology and regulation of differentiation-associated gene expression could be replicated in several independent experiments. Due to logistical reasons the serum had to be replaced making it necessary to perform further experiments with a different serum (GOLD serum). OTCs will be stated HaCaT-GOLD-OTCs in contrast to the previous experiment in another serum. Experiments in GOLD serum comprised continuous treatment of HaCaT-GOLD-OTCs with CsA for 1, 2 and 3 weeks.

2.5.1. Morphology of CsA-treated HaCaT-GOLD-OTCs

Histology examination of control HaCaT-GOLD-OTCs treated with DMSO demonstrated that HaCaT cells established a multi-layered well organized epidermis with a parakeratotic stratum corneum increasing over time. These results were comparable to previous experiments. Upon CsA treatment tissue organization was disturbed and already after 1 week of treatment the HaCaT cells invaded the dermal equivalent. Moreover, an increase in differentiated cell layers when compared with the corresponding control OTC was shown (Figure 2.29A). Staining for the proliferation marker Ki67 revealed that the invasion was not associated with increased proliferation (Figure 2.29B). Moreover, the metabolic activity of HaCaT-GOLD-OTCs remained unchanged by CsA treatment for the first two weeks and after 3 weeks it even slightly decreased (Figure 2.29C). In order to visualize the invasion and the disruption of the basement membrane, two components from the basement membrane were stained: Collagen IV (ColIV) and Collagen VII (ColVII). The epidermal dermal junction in control HaCaT-GOLD-OTCs treated with DMSO showed strong reactivity with the ColIV antibody, demonstrating the presence of a continuous basement membrane. In CsA-treated HaCaT-GOLD-OTCs ColIV staining at the dermal-epidermal junction was distinct to the control HaCaT-GOLD-OTCs. While it was clustered underneath non-invading epithelial cells, intense staining was absent at sites of invasion in CsA-treated HaCaT-GOLD-OTCs (Figure 2.29D). In contrast to the ColIV staining ColVII deposition was not demonstrating a continuous basement membrane staining in the control HaCaT-GOLD-OTCs treated with DMSO. Different to the normal skin distribution of ColVII, ColVII in HaCaT-GOLD-OTCs was only scattered in some areas of the epidermal dermal junction. This distribution of ColVII was not further changed by CsA treatment and ColVII disposition at the epidermal dermal junction could be detected only very sparsely (Figure 2.29E). Summarized, histology revealed that the experiment using the GOLD serum validated the differentiation phenotype, but in addition resulted in invasion of the HaCaT keratinocytes.

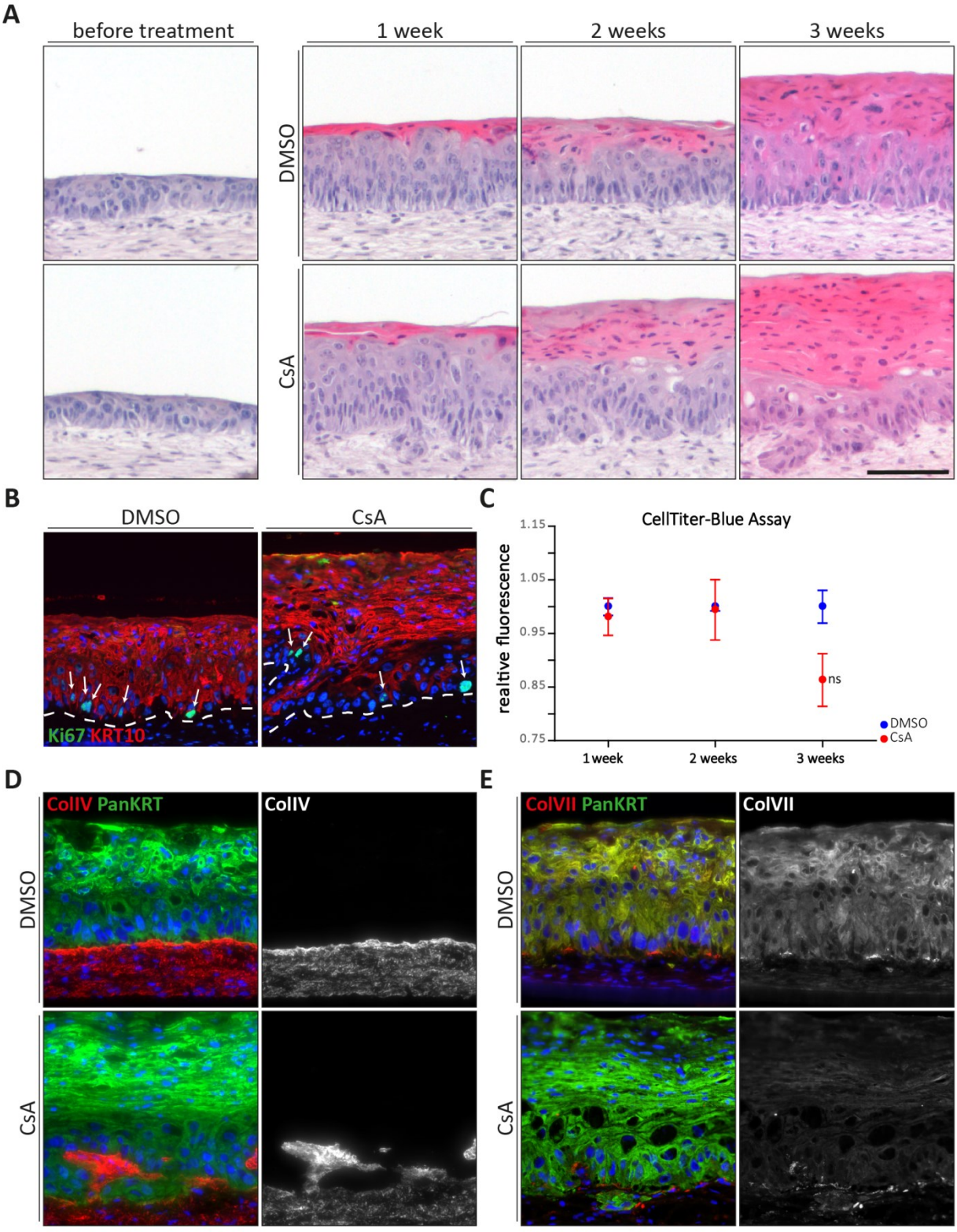

Figure 2.29 HaCaT-GOLD-OTCs after 1-3 weeks of continuous CsA treatment.
(A) *Histology H&E staining* of HaCaT-GOLD-OTCs 1 week after epithelia seeding and after 1, 2 or 3 weeks of treatment with CsA (10 µg ml^{-1}) or the solvent DMSO (0.04%). Scale bar: 100 µm. **(B)** I*mmunofluorescent staining for Ki67* (green) and KRT1O (red). Cryosections of HaCaT-GOLD-OTCs, treated with CsA (10 µg ml^{-1}) or DMSO (0.04%) for 3 weeks were counterstained with DAPI to visualize nuclei (blue). Arrows indicate $Ki67^{+}$ cells. Scale bar: 100 µm. **(C)** *CellTiter-Blue® assay (relative metabolism).* Relative fluorescence of metabolized resazurin (additive) was measured within the culture medium. The graph shows the mean (n=3) and the standard error of the mean. Values from one time point were normalized to the mean of all DMSO replicates from that time point. ns: not significant = p-value > 0.05 (two-sided unpaired t-test). *Immunofluorescence*

staining for **(D)** *ColIV* (red) and PanKRT (green) or **(E)** *ColVII* (red) and PanKRT (green) on cryosections from HaCaT-GOLD-OTCs treated with DMSO (0.04%) or CsA (10 µg ml^{-1}) for 3 weeks. Sections were counterstained by DAPI to stain nuclei (blue). Scale bars: 50 µm.

2.5.2. Proteolytic activity was increased in HaCaT-GOLD-OTCs treated with CsA

In order to reveal enzymatic activity enabling this penetration an *in situ* gelatinase assay was performed. The assay could demonstrate the presence of gelatinase activity within the basal keratinocyte cell layer and the dermis from CsA-treated HaCaT-GOLD-OTCs (Figure 2.30A). A general gelatinase activity was also measured within the differentiated cell layers of DMSO and CsA-treated epithelia. This activity occurs because of the assembly and crosslinking of the cornified envelope (Candi *et al.* 2005). Genome wide RNA expression profiles showed up-regulation of MMP10, MMP3 and MMP1 in the epithelium of CsA-treated HaCaT-GOLD-OTCs. This could be validated by qRT-PCR (Figure 2.30A). Interestingly, expression of these genes in the fibroblast in the dermal equivalent was down-regulated after CsA treatment (Figure 2.30B). Protein levels of pro-MMP1, total MMP3 and pro-MMP10 were measured by ELISA in the culture medium. Interestingly and despite the RNA regulation, only MMP10 was slightly upregulated and pro-MMP1 and total MMP3 were clearly down-regulated after continuous CsA treatment (Figure 2.30C).

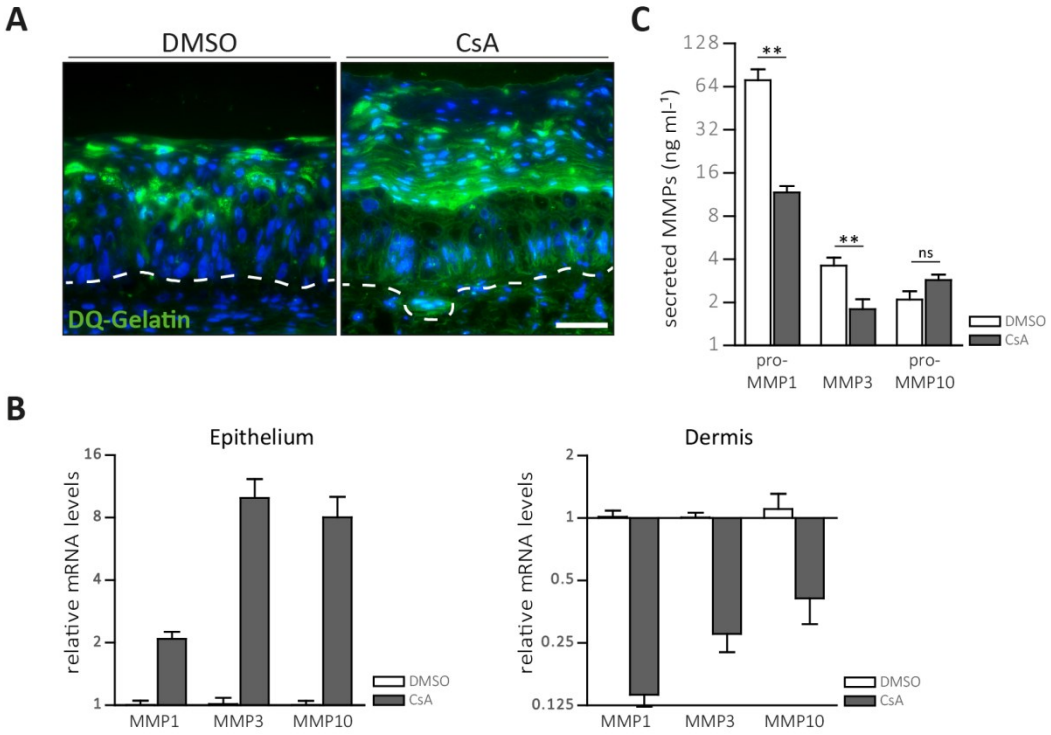

Figure 2.30 Proteolytic activity and MMP1, MMP3 and MMP10 protein and RNA levels in HaCaT-GOLD-OTCs treated with CsA.

(A) *Gelatin in situ zymography* with unfixed cryosections from HaCaT-GOLD-OTCs treated with DMSO (0.04%) or CsA (10 µg ml^{-1}) for 3 weeks. The dotted line marks the basement membrane. Scale bar: 50 µm. **(B)** *Relative RNA expression.* RNA isolated from HaCaT-GOLD epithelia treated with DMSO (0.04%) or CsA (10 µg ml^{-1}) was quantified by qRT-PCR. The graphs show the mean and the standard error of the mean. n=6 (from 2 and 3 weeks of treatment). **(C)** P*rotein levels* of pro-MMP1, MMP3 and pro-MM10 within the culture medium were

measured by ELISA. The graph shows the mean and the standard error of the mean. n=6 (from 2 and 3 weeks of treatment). **: p-value ≤0.01, ns: not significant = p-value > 0.05 (two-sided, unpaired t-test).

2.5.3. Genome-wide RNA expression profile from HaCaT-GOLD epithelia treated with CsA

For a deeper insight into the regulation induced by CsA in the GOLD serum a genome-wide RNA expression profile was conducted. RNA from control (DMSO) and CsA-treated HaCaT-GOLD-OTCs were analyzed in biological triplicates. These triplicates clearly separated along the first dimension using NMDS (Figure 2.31A) and also could be divided in two different groups by hierarchical clustering as depicted by a dendrogram (Figure 2.31B). The 20 highest and lowest differentially expressed genes (p-value ≤ 0.01) are listed in the appendix (Table 7.10). In total 1915 genes were differentially regulated, of which 26% (490/1915) were regulated above 1.5-fold. Of these differentially expressed genes 40% (194/490) were down-regulated; while from the total number of differentially expressed genes 49% (929/1915) were down-regulated (Figure 2.31C). Histology of the GOLD experiment suggested an induction of differentiation. Moreover, differentiation-associated genes, like LCE3E and LCE3D were within the TOP 20 regulated genes from HaCaT-GOLD epithelia treated with CsA. To get a complete list of all genes involved in differentiation, the gene set was filtered for the GO-term ‘epidermal development’ (GO-0008544). In total 81 genes were involved in ‘epidermal development’ (Figure 2.31D).

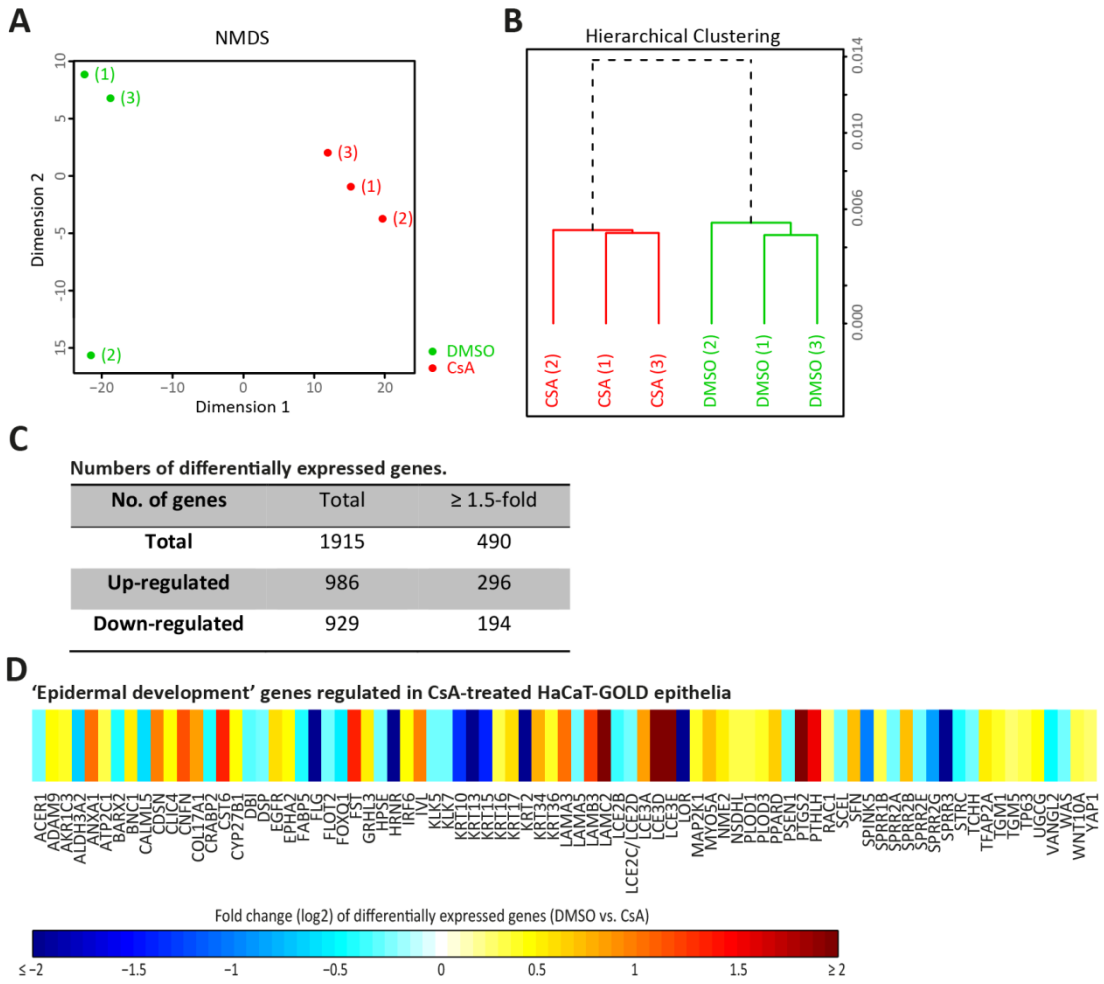

Figure 2.31 RNA expression profile from CsA-treated HaCaT-GOLD epithelia.
(A) *Non-metric multidimensional scaling (NMDS)* and **(B)** *hierarchical clustering* were applied to assess the discriminability of the 3 biological replicates from 2 treatment groups (DMSO and CsA). Clustering and visualization was performed with Chipster from normalized data. **(C)** Numbers of d*ifferentially expressed genes (DMSO vs. CsA).* The table shows the total number of differentially expressed genes and the number of differentially expressed genes with a fold change ≥ 1.5. Differentially expressed genes were calculated with Chipster (filtered by p-value ≤ 0.01). **(D)** *Heatmap* of differentially expressed genes (DMSO vs. CsA) filtered by the GO-term 'epidermal development' (GO-0008544) from the CsA-treated HaCaT-GOLD RNA expression profile. Fold changes (log2) are depicted by the indicated color. The rows are sorted alphabetically.

2.5.4. Validation of RNA expression profile by qRT-PCR and immunofluorescent staining

Following genes were chosen for validation by qRT-PCR: LCE3A, SPRR2B, KRT10, FLG, GRHL3 and HRNR. Except for GRHL3 and HRNR protein immunofluorescent staining for these proteins was performed on cryosections from DMSO- and CsA-treated HaCaT-GOLD-OTCs. LCE3A was up-regulated 1.8-fold according to the RNA expression array, while LCE2A was not within the differentially expressed genes. qRT-PCR measurements of LCE3A RNA revealed a clear increase of about 3.9-fold, while RNA levels of LCE2A were only slightly up-regulated (1.3-fold) (Figure 2.32A). Localization of LCE2 and LCE3 proteins was not changed by CsA treatment. Moreover, regulation of LCE2 or LCE3 could not be detected by immunofluorescent staining (Figure 2.32B). SPRR2B RNA was 1.7-fold up-regulated according to the RNA expression array. Using qRT-PCR it was revealed that it was 0.7-fold

down-regulated (Figure 2.32A). Signal intensity of the corresponding IF staining was similar between DMSO- and CsA-treated HaCaT-GOLD-OTC. However, basal cells in CsA-treated HaCaT-GOLD-OTCs were less stained by the anti-SPRR2B antibody (Figure 2.32B). The RNA expression profile showed that KRT10 is down-regulated (0.39-fold), which was validated by qRT-PCR (0.1-fold down-regulated) (Figure 2.32A). Immunofluorescence hardly showed a difference in the amount of KRT10 deposition in HaCaT-GOLD-OTCs treated with DMSO or CsA. In both epithelia KRT10 was present in the differentiated cell layers. However, while in DMSO-treated epithelia KRT10 deposition started quite early and some basal cells were as well KRT10 positive, in CsA-treated HaCaT-GOLD epithelia KRT10 occurred later, in the second suprabasal cell layer. Moreover, KRT10 was absent from keratinocytes which invaded into the dermal equivalent (Figure 2.32B). FLG expression was down-regulated (0.2-fold) by CsA in GOLD serum according to the expression array. qRT-PCR could validate this finding and demonstrated a downregulation of 0.29-fold (Figure 2.32A). Despite the clear down-regulation in RNA, immunofluorescence showed no clear difference in the amount of FLG protein in DMSO- and CsA-treated HaCaT-GOLD epithelia. FLG was deposited in the late differentiated cell layers of HaCaT-GOLD-OTCs treated with DMSO. In CsA-treated HaCaT-GOLD epithelia FLG was also deposited in the late differentiating cells (Figure 2.32B). GRHL3 RNA expression was hardly up-regulated in the expression array (1.4-fold), in qRT-PCR the up-regulation even diminished to 1.1-fold. Like FLG, HRNR was downregulated (0.14-fold) in the expression profile. This finding could as well be validated by qRT-PCR, which even showed a stronger down-regulation (0.015-fold) (Figure 2.32A).

To summarize, the results from the RNA expression array for LCE3A, KRT10, FLG and HRNR could be replicated by qRT-PCR, while for SPRR2B RNA contrary results were revealed with qRT-PCR (1.7-fold up-regulation according to the array and 0.7-fold down-regulation according to qRT-PCR). For GRHL3 regulation was only very weakly measureable according to qRT-PCR (1.1-fold up-regulation), in contrast to 1.4-fold up-regulation in the array. Moreover, qRT-PCR revealed weak up-regulation (1.3-fold) of LCE2A, which was not detected by the RNA expression profile. Finally, immunofluorescent stainings nicely demonstrated the improved structure of the HaCaT-GOLD epithelium induced by CsA treatment.

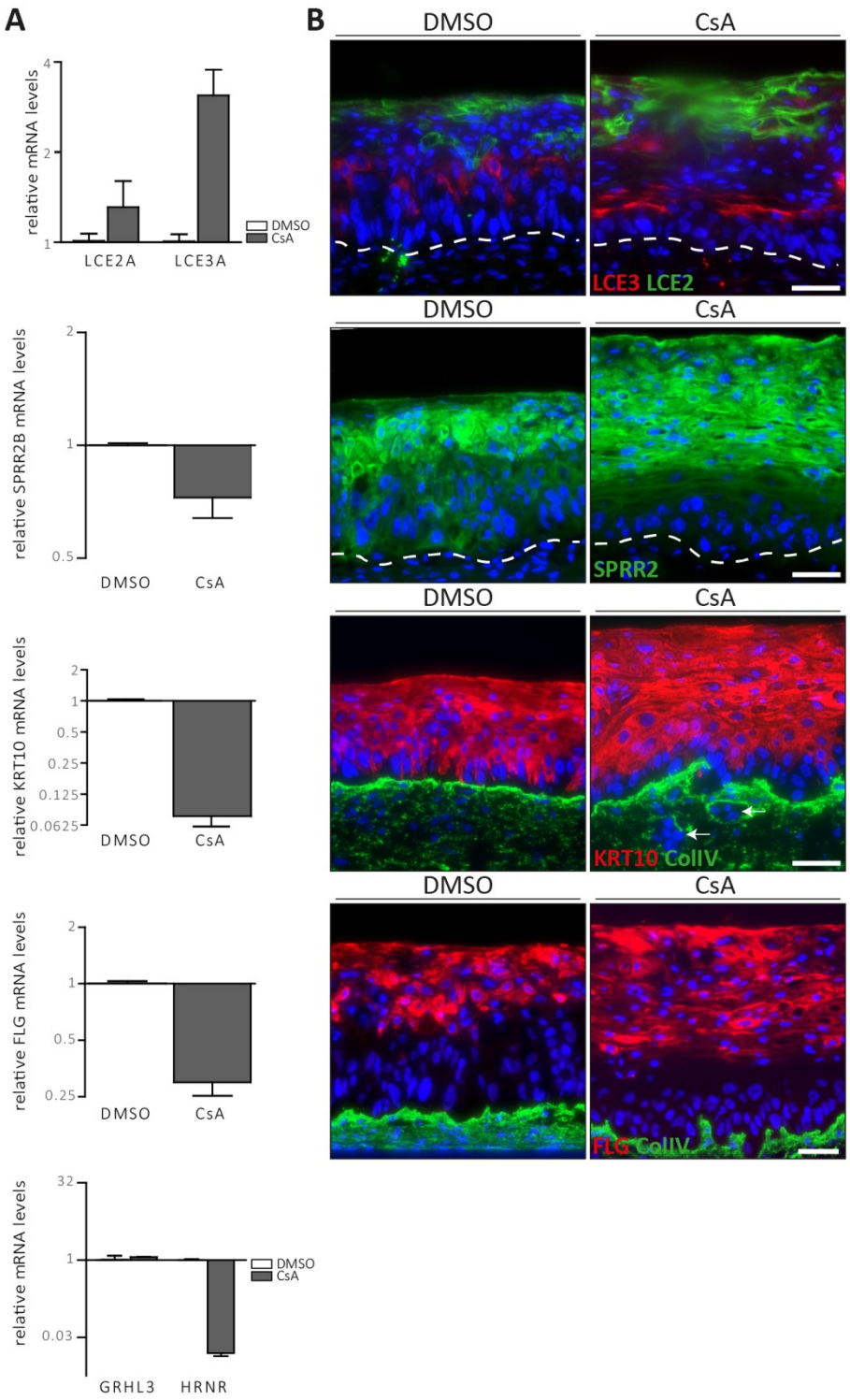

Figure 2.32 Relative RNA expression/protein localization of selected genes in CsA-treated HaCaT-GOLD epithelia.

(A) *Relative RNA expression* of indicated genes. RNA isolated from HaCaT-GOLD epithelia treated with DMSO (0.04%) or CsA (10 µg ml^{-1}) was quantified by qRT-PCR. The graphs show the mean and standard error of the mean. n=6 (from 2 and 3 weeks of treatment). **(B)** *Immunofluorescent staining* for indicated proteins on cryosections from HaCaT-GOLD-OTCs treated with DMSO (0.04%) or CsA (10 µg ml^{-1}) for 2 weeks (LCE2, LCE3, and KRT10) or 3 weeks (SPRR2B, FLG). Sections were counterstained by DAPI to stain nuclei (blue). The dotted line marks the basement membrane. Arrows indicate KRT10 negative keratinocytes within the dermal equivalent. Scale bars: 50 µm.

2.5.5. IL-1α and CSF2 are up-regulated in CsA-treated HaCaT-GOLD-OTCs

One of the TOP 20 up-regulated genes of the expression profile of CsA-treated HaCaT-GOLD epithelia was interleukin-1α (IL-1α), which were 5.4-fold up-regulated. Using ELISA, it was demonstrated that secreted Il-1α protein was up-regulated in CsA-treated HaCaT-GOLD-OTCs (58 pg ml^{-1}) in comparison to the DMSO-treated control OTCs (10 pg ml^{-1}) (Figure 2.33A). IL-1α, secreted by keratinocytes, contributes to proper growth and differentiation of keratinocytes by inducing granulocyte-macrophage colony-stimulating factor (GM-CSF; gene: CSF2) and fibroblast growth factor 7 (FGF7) expression in fibroblasts (Maas-Szabowski *et al.* 2000). Accordingly RNA levels of CSF2 and FGF7 were measured in fibroblasts from CsA-treated HaCaT-GOLD-OTCs and also in the epithelial part. In addition, RNA levels of two other known growth factors, epidermal growth factor (EGF) and hepatocyte growth factor (HGF) were analyzed. HGF expression in fibroblast was also shown to be regulated by IL-1α (Maas-Szabowski & Fusenig 1996), while EGF is known to improve epithelization (Bhora *et al.* 1995; El Ghalbzouri *et al.* 2004). Mean CSF2 RNA expression was very slightly up-regulated (1.35-fold) in fibroblasts, while FGF7 did not appear to be regulated. Interestingly CSF2 expression in keratinocytes was strongly up-regulated (4.89-fold). However, this was not the case for FGF7, which was down-regulated (0.6-fold) in keratinocytes. Levels of RNA of EGF and HGF were down-regulated in both samples; from CsA-treated dermis and epithelium (Figure 2.33B). In order to demonstrate whether the increase in CSF2 RNA expression in keratinocytes is leading to an increase in GM-CSF an ELISA was performed. However, despite the high increase in CSF2 RNA, the protein level was only increased very slightly from about 4 pg ml^{-1} to about 5.3 pg ml^{-1}. This increase was not significant and the standard error of the mean was quite high. This could be correlated to the general low abundance of GM-CSF in the culture medium and hence measurements of the protein around the detection minimum of the ELISA kit (Figure 2.33C).

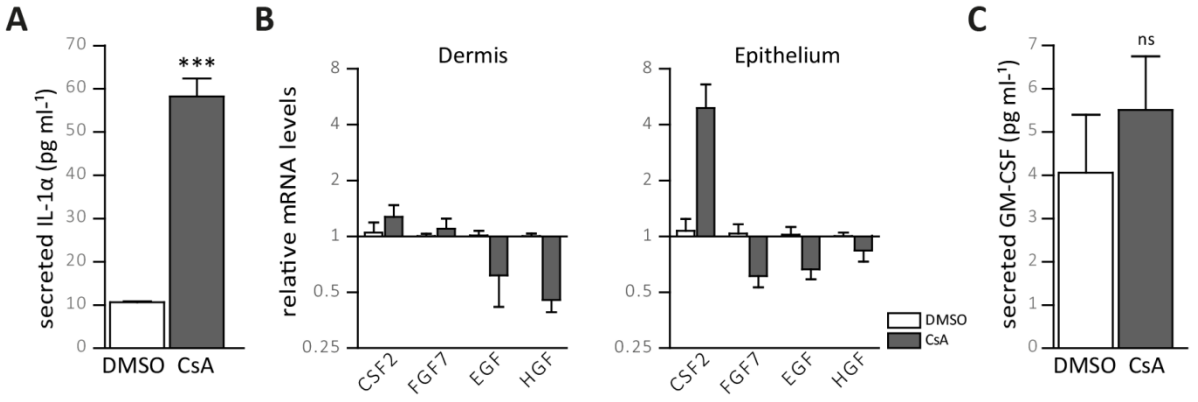

Figure 2.33 IL-1α and GM-CSF protein levels and CSF2, FGF7, EGF and HGF RNA expression levels in CsA-treated HaCaT-GOLD-OTCs.
(A) *Protein levels* of IL-1α within the culture medium from HaCaT-GOLD-OTCs treated with DMSO (0.04%) or CsA (10 µg ml^{-1}) was measured by ELISA. The graphs show the mean and the standard error of the mean. n=6 (from 2 and 3 weeks of treatment). ***: p-value < 0.0001 (two-sided, unpaired t-test). **(B)** *Relative RNA expression in the dermis* or *the epithelia* from HaCaT-GOLD-OTCs treated with DMSO (0.04%) or CsA (10 µg ml^{-1})

quantified by qRT-PCR. The graph shows the mean and the standard error of the mean. n=6 (from 2 and 3 weeks of treatment). **(C)** *Protein levels* of GM-CSF within the culture medium of HaCaT-GOLD-OTCs treated with DMSO (0.04%) or CsA (10 µg ml^{-1}) measured by ELISA. The graph shows the mean and the standard error of the mean. n=6 (from 2 and 3 weeks of treatment). ns: not significant = p-value > 0.05 (two-sided, unpaired t-test).

2.5.6. Ingenuity® Pathway Analysis of CsA-treated HaCaT-GOLD epithelia expression profile

In order to further analyze the RNA expression profile from CsA-treated HaCaT-GOLD epithelia the data was used for Ingenuity® Pathway Analysis. The analysis for molecular and cellular functions revealed the following three functions most likely affected by CsA treatment: 'cellular movement', 'cell death & survival' and 'cellular growth & proliferation' (Figure 2.34A). In accordance with the invasive phenotype, nearly all functions from the top term 'cellular movement' were predicted to be activated; amongst others these are invasion and migration. The only function within the term 'cellular movement', which was predicted to be down-regulated, is related to cellular infiltration of inflammatory cells. In contrast, most functions from the term 'cell death & survival' were predicted to be down-regulated. Interestingly, and despite our finding that CsA is not increasing proliferation of HaCaT cells, the functions from the term 'cellular growth and proliferation' were all predicted to be up-regulated.

Next the pathway mostly likely affected by CsA was determined by Ingenuity® Pathway Analysis. It was revealed that this was Integrin signaling. Interestingly, none of the genes related to Integrin signaling (Figure 2.35A) were among the top regulated genes. Upon this finding two Integrins, namely Integrin α-6 (ITGA6) and Integrin β-1 (ITGB1) were visualized by immunofluorescent staining in DMSO- and CsA-treated HaCaT-GOLD epithelia (Figure 2.35B). Both, ITGA6 and ITGB1, were deposited at the epidermal dermal junction in DMSO-treated HaCaT-GOLD-OTCs. Interestingly, in CsA-treated HaCaT-GOLD-OTCs, ITGA6 and ITGB1 clustered below non-invading basal cells, while only little ITGA6 or ITGB1 was present at the invasive front.

A

IPA Analysis: Predicted Impacted Molecular and Cellular Functions

Priority	Name	p-value	# Molecules
1	Cellular Movement	7.52E-05-5.04E-27	499
2	Cell Death and Survival	7.81E-05-3.33E-23	694
3	Cellular Growth and Proliferation	7.90E-05-3.99E-20	786

B

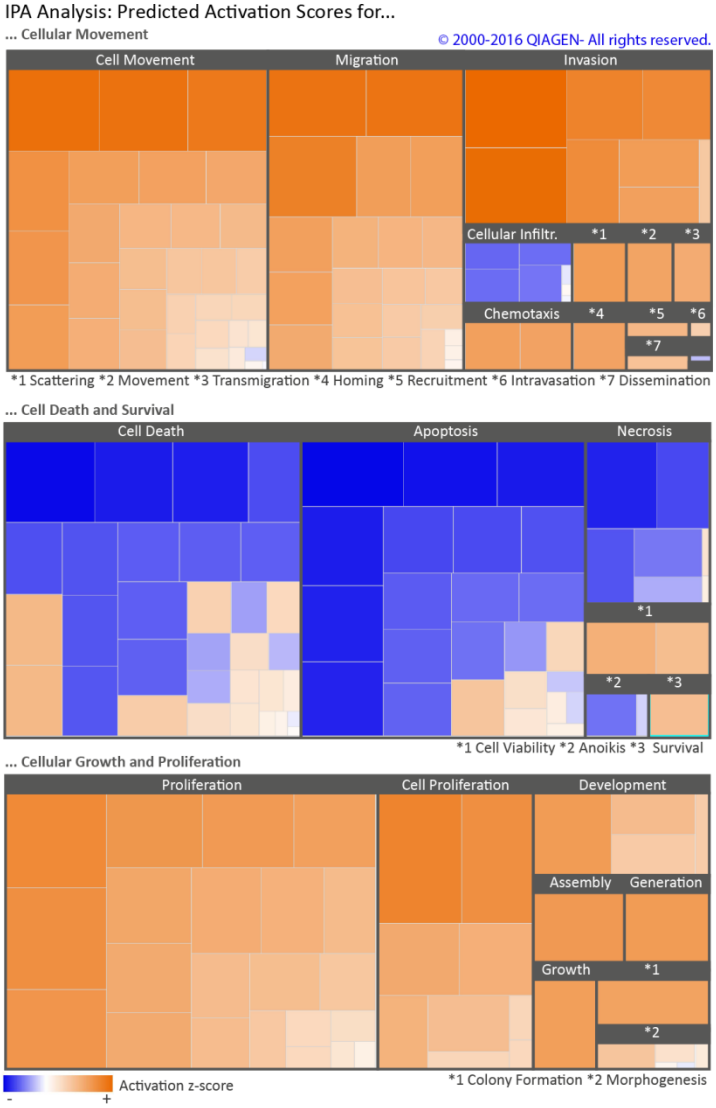

Figure 2.34 Prediction of molecular/cellular functions impacted by CsA in GOLD serum using Ingenuity® Pathway Analysis.

Differentially expressed genes (filtered by p-value ≤ 0.01) from HaCaT-GOLD epithelia (DMSO vs. CsA, 2 weeks treatment) were used for Ingenuity® Pathway Analysis. **(A)** *Top 3 predicted cellular functions*. List is sorted by p-value (Benjamini-Hochberg procedure). **(B)** *Z-Score visualization of top molecular/cellular functions*. One square corresponds to one annotated molecular/cellular function within the indicated topic. The square size is calculated based on the magnitude of z-score. The activation z-score expresses the predicted positive or negative activation of a specific function.

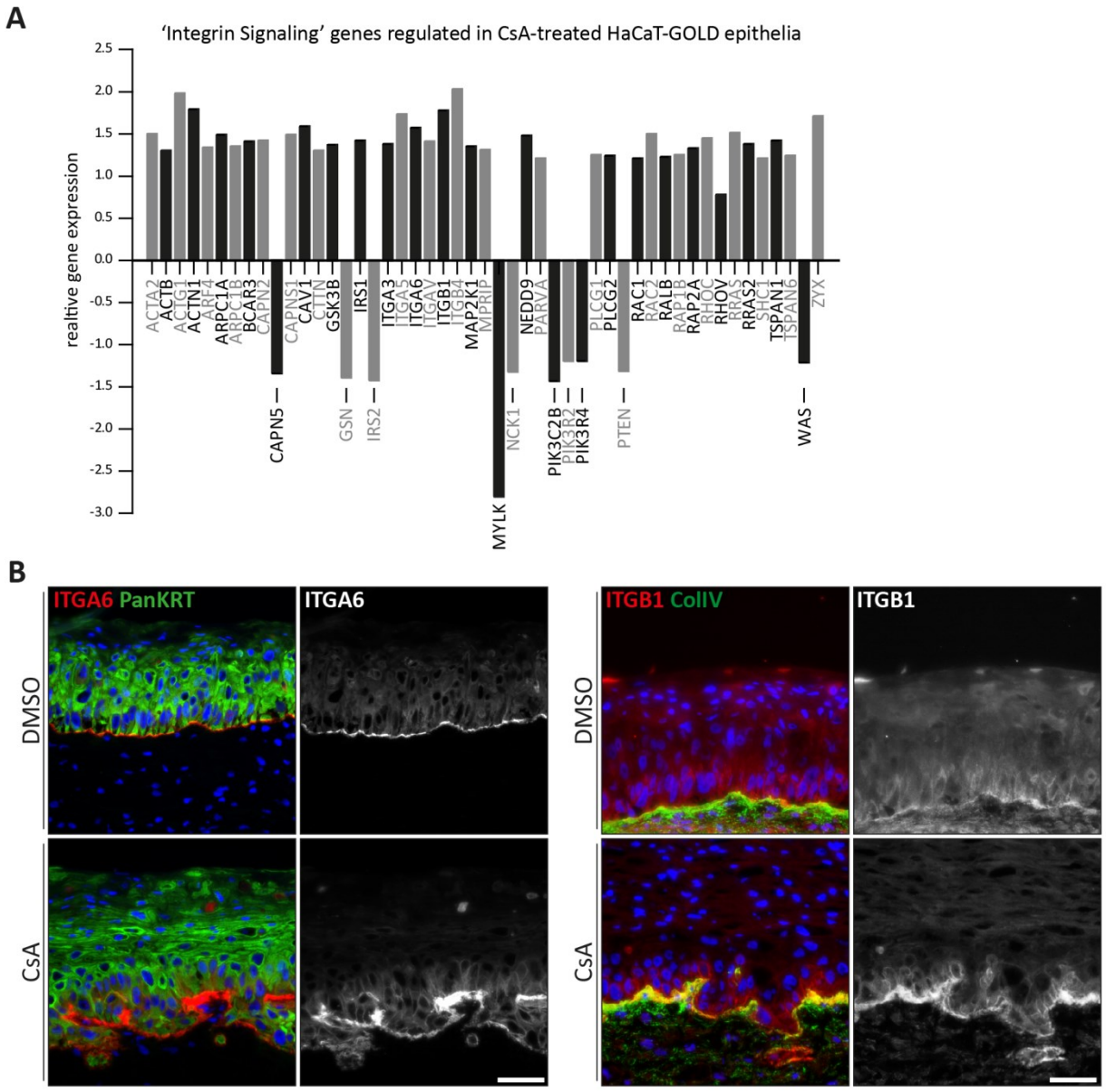

Figure 2.35 'Integrin signaling' genes and ITGA6 and ITGB1 localization in CsA-treated HaCaT-GOLD epithelia. **(A)** *Differentially expressed genes 'Integrin Signaling'* from CsA-treated HaCaT-GOLD epithelia. Genes were taken from the expression profile and sorted for association with 'Integrin Signaling' according to Ingenuity® Pathway Analysis. Fold changes were recalculated from $\log_2$. Values below 1 (negative fold changes) were converted by the following formula: fold change= –(1/x). **(B)** *Immunofluorescent staining for* (left) *ITGA6* (red) and PanKRT (green) or (right) *ITGB1* (red) and ColIV (green) on cryosections from HaCaT-GOLD-OTCs treated with DMSO (0.04%) or CsA (10 µg ml^{-1}) for 3 weeks. Sections were counterstained by DAPI to stain nuclei (blue). Scale bars: 50 µm.

2.6. ColVII deposition, MMP levels, IL-1α and CSF2/GM-CSF in CsA-treated HaCaT epithelia

The results described in previous passages showed that in some parts the results from CsA-treated HaCaT and HaCaT-GOLD epithelia differed. While in both experiments the epithelial structure was improved, only in GOLD serum the HaCaT keratinocytes invaded into the dermal equivalent. Accordingly, different aspects were analyzed in the HaCaT-GOLD experiment in comparison to the HaCaT experiment. In the next paragraph aspects which emerged during the analysis of the HaCaT-GOLD experiment were analyzed as well in the HaCaT experiment: ColVII deposition, MMP expression and secretion and IL-1α/GM-CSF expression and secretion.

ColVII staining of HaCaT-OTCs revealed a deposition at the epidermal/dermal junction indicating for a continuous basement membrane. Moreover, the deposition resembled human skin (Martins *et al.* 2009). Deposition of ColVII was not affected by CsA treatment in HaCaT-OTCs, which as well showed a continuous basement membrane staining (Figure 2.36).

Secretion of pro-MMP1, MMP3 and pro-MMP10 were measured by ELISA. Culture medium from CsA-treated HaCaT-OTCs had in average a lower amount of pro-MMP1 (8.9 ng ml^{-1}) and MMP3 (3.3 ng ml^{-1}) in comparison to the DMSO-treated control OTCs, which had 30.3 ng ml^{-1} pro-MMP1 and 13.3 ng ml^{-1} MMP3. Secreted pro-MMP10 deviated only very slightly in CsA-treated HaCaT-OTCs (5.6 ng ml^{-1}) from DMSO-treated HaCaT-OTCs (6.4 ng ml^{-1}) (Figure 2.37A). While all RNAs from MMP1, MMP3 and MMP10 were downregulated (0.6-fold, 0.6-fold and 0.7-fold, respectively) in CsA-treated HaCaT epithelia, RNA expression of MMP1 and MMP10 were slightly up-regulated (1.2-fold and 1.5-fold, respectively) and MMP3 down-regulated (0.6-fold) in the dermal part (Figure 2.37B).

The expression profile from CsA-treated HaCaT epithelia did not reveal a change in IL-1α. In line with the expression profile no significant difference in IL-1α protein was detected in the culture medium of CsA-treated (32.6 pg ml^{-1}) or control HaCaT-OTCs (22.6 pg ml^{-1}) (Figure 2.38A). Moreover, CSF2 RNA measured by qRT-PCR was down-regulated in the dermis and the epithelium (0.52-fold and 0.4-fold, respectively) (Figure 2.38B). Moreover, the GM-CSF protein level in CsA-treated HaCaT-OTCs (6.2 pg ml^{-1}) was slightly lower than in the control HaCaT-OTCs (10.6 pg ml^{-1}) (Figure 2.38C).

To summarize, the findings concerning ColVII deposition in DMSO-treated HaCaT-GOLD epithelia and MMP, IL-1α and CSF2/GM-CSF expression or secretion in CsA-treated HaCaT-GOLD epithelia, could not be replicated in CsA-treated HaCaT epithelia. This could indicate that some of these findings might play a role in the additional invasive phenotype in CsA-treated HaCaT-GOLD epithelia.

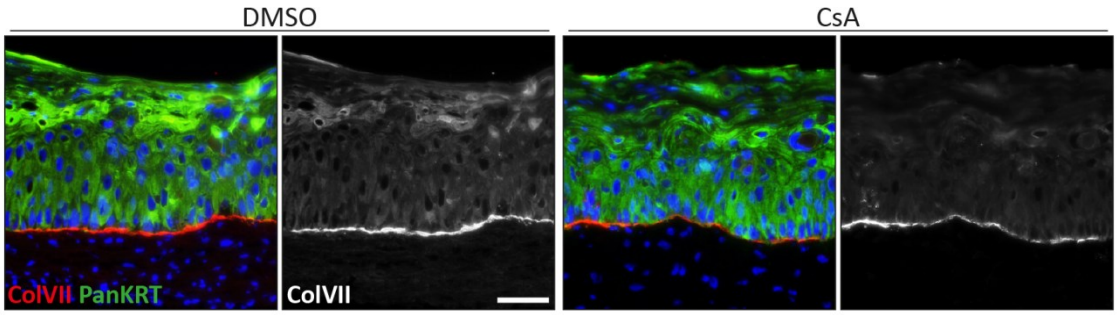

Figure 2.36 ColVII deposition in HaCaT-OTCs treated with DMSO or CsA.
Immunofluorescent staining for ColVII (red) and PanKRT (green) on cryosections from HaCaT-OTCs treated with DMSO (0.04%) or CsA (10 µg ml^{-1}) for 3 weeks. Sections were counterstained by DAPI to stain nuclei (blue). Scale bar: 50 µm.

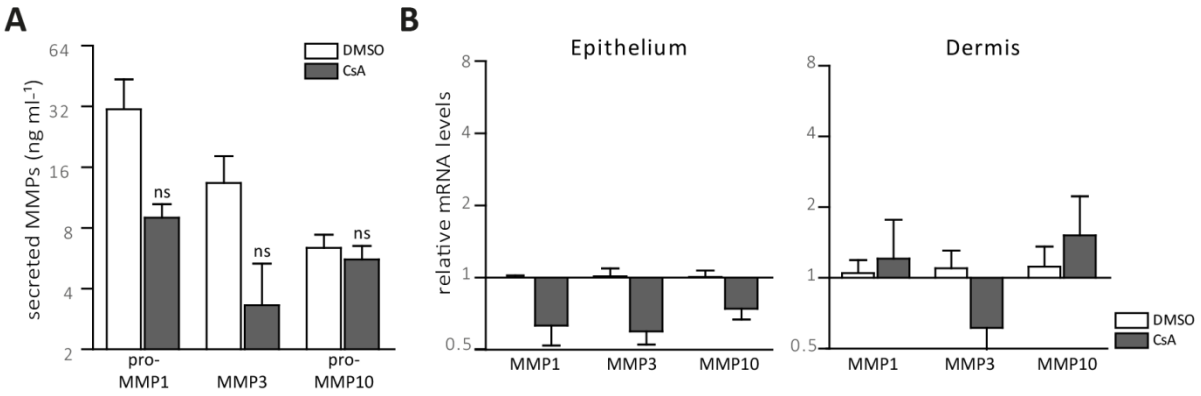

Figure 2.37 Protein and RNA levels of MMP1, MMP3 and MMP10 in CsA-treated HaCaT-OTCs.
(A) *Protein levels* of pro-MMP1, MMP3 and pro-MM10 within the culture medium of HaCaT-OTCs treated with DMSO (0.04%) or CsA (10 µg ml-1) were measured by ELISA. The graph shows the mean and the standard error of the mean. n=6 (from 2 and 3 weeks of treatment). ns: not significant = p-value > 0.05 (two-sided, unpaired t-test). **(B)** *Relative RNA expression*. RNA isolated from HaCaT-GOLD epithelia treated with DMSO (0.04%) or CsA (10 µg ml^{-1}) was quantified by qRT-PCR. The graphs show the mean and the standard error of the mean. n=6 (from 2 and 3 weeks of treatment).

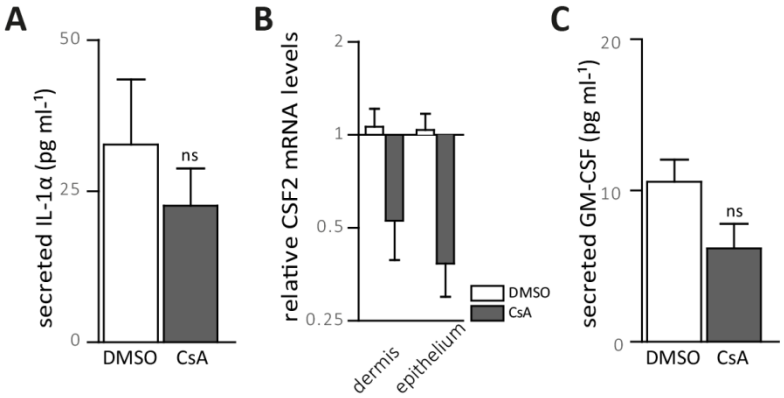

Figure 2.38 IL-1α and GM-CSF protein levels and CSF2 RNA expression levels in CsA-treated HaCaT-OTCs.
(A) *Protein levels* of IL-1α within the culture medium of HaCaT-OTCs treated with DMSO (0.04%) or CsA (10 µg ml^{-1}) were measured by ELISA. n=6 (from 2 and 3 weeks of treatment). ns: not significant = p-value > 0.05 (two-sided, unpaired t-test). **(B)** *Relative CSF2 RNA expression* in the dermis or in the epithelium from HaCaT-OTCs treated with DMSO (0.04%) or CsA (10 µg ml^{-1}) quantified by qRT-PCR. The graph shows the mean and the standard error of the mean. n=6 (from 2 and 3 weeks of treatment). **(C)** *Protein levels* of GM-CSF within the culture medium of HaCaT-OTCs treated with DMSO (0.04%) or CsA (10 µg ml^{-1}) were measured by ELISA. The

graph shows the mean and the standard error of the mean. n=6 (from 2 and 3 weeks of treatment). ns: not significant = p-value > 0.05 (two-sided, unpaired t-test).

2.7. Comparison of the HaCaT and HaCaT-GOLD epithelial RNA expression profiles (DMSO vs. CsA)

In order to get an idea of the molecular differences between the CsA-treated HaCaT and the CsA-treated HaCaT-GOLD experiment, both RNA expression profiles (each DMSO vs. CsA) were compared with each other.

The number of differentially expressed genes (DMSO vs. CsA) in HaCaT-GOLD epithelia (invasive) was nearly 4-fold higher in comparison to the HaCaT epithelia (non-invasive). Interestingly, the number of down-regulated genes was lower in GOLD than in the other experiment (48% vs. 55%). For genes differentially expressed above 1.5-fold, this difference even increased, with 39% of down-regulated genes in CsA-treated HaCaT-GOLD epithelia in comparison to 59% in CsA-treated HaCaT epithelia (Figure 2.8A and Figure 2.31C). The higher number of differentially expressed genes could also be seen in the scatterplot, which as well showed the higher magnitude of fold changes in CsA-treated HaCaT-GOLD epithelia in comparison to the CsA-treated HaCaT epithelia (Figure 2.39A). Looking at the overlap of differential gene expression from both data sets it was revealed, that 54% (272/507) of the HaCaT data set were overlapping with HaCaT-GOLD, while only 14% (272/1915) of the HaCaT-GOLD data set were overlapping with the HaCaT data set. When filtering the data sets for the GO-term 'epidermal development' the percentages of overlap increased for both data sets; 63% (24/38) in the case of HaCaT and 29% (24/81) in the case of HaCaT-GOLD (Figure 2.39B). In total 38 (HaCaT) and 81 (HaCaT-GOLD) differentially expressed genes belonged to the GO-term 'epidermal development. The heatmap of these genes showed that the majority (21) of the 24 overlapping genes, regulated in HaCaT and HaCaT-GOLD, were both likewise either up- or down-regulated (Figure 2.39C).

Making a comparison analysis with HaCaT and HaCaT-GOLD epithelial RNA expression profiles using Ingenuity® Pathway Analysis, it became apparent that functions related to cell migration, movement and invasion had a positive z-score, meaning a predicted activation of that function, for CsA-treated HaCaT-GOLD (invasive phenotype). These results were in line with the Ingenuity® Pathway Analysis of the individual CsA-treated HaCaT-GOLD analysis in Figure 2.34. However, the same functions had a negative z-score and with that a predicted inactivation in CsA-treated HaCaT epithelia (non-invasive phenotype). One function which was likewise activated in both data sets was 'synthesis of lipids' (Figure 2.40A). The comparison also revealed that while 49 genes of the HaCaT-GOLD data set were part of the Ingenuity® Pathway Analysis 'Integrin signaling' gene set, only 6 genes of the HaCaT data set were part of that gene set (Figure 2.40B).

Summarized, the high number of genes uniquely differentially expressed (DMSO vs. CsA) in the HaCaT-GOLD experiment might play a role in the additional invasive phenotype of CsA-treated HaCaT-GOLD keratinocytes. It was shown that the HaCaT and HaCaT-GOLD data sets both manifested regulation of 'epidermal development' genes, but differed in respect to Ingenuity® Pathway Analysis and prediction of cell functions related to invasion and activation of the integrin pathway.

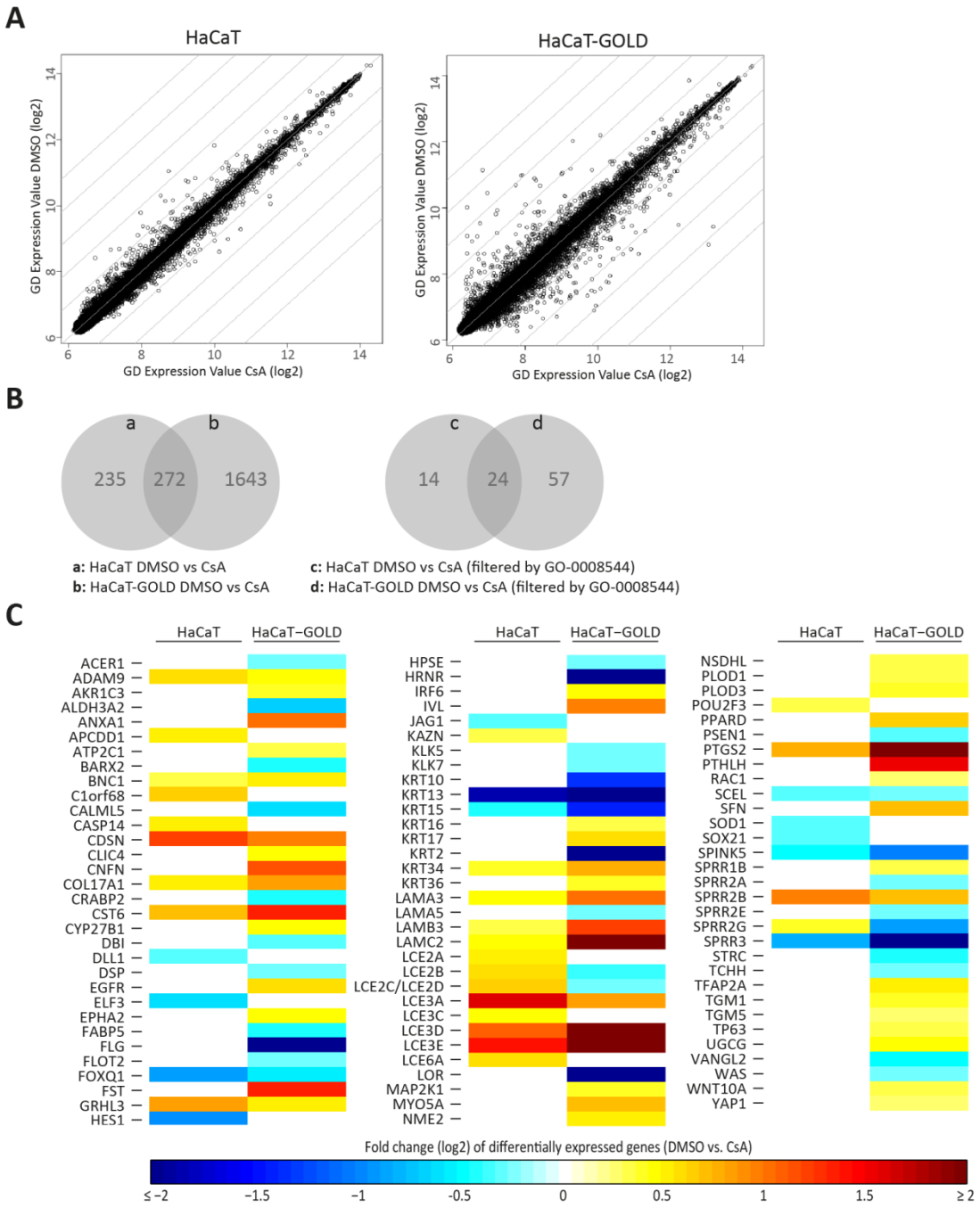

Figure 2.39 Comparison of whole genome RNA expression profiles (DMSO vs. CsA) from HaCaT and HaCaT-GOLD epithelia.
(A) *Scatterplots of relative gene expression.* Each dot shows the mean of the relative expression value from 3 biological replicates for one gene (log2). Y-axis (DMSO), x-axis (CsA). Dots on line of origin = no differential gene expression. Data for the scatterplot were neither normalized nor filtered. The HaCaT scatterplot was also shown in Figure 2.8. **(B)** *Overlap of differential gene expression* (DMSO vs. CsA) from both data sets (HaCaT and

HaCaT-GOLD epithelia). Left: whole data sets. Right: Data sets filtered by the GO-term 'epidermal development' (GO-0008544). **(C)** *Heatmap* of differentially expressed genes (DMSO vs. CsA) filtered by the GO-term 'epidermal development' (GO-0008544) from HaCaT and HaCaT-GOLD RNA expression profiles. Fold changes (log2) are depicted by the indicated color. The rows are sorted alphabetically. Data from HaCaT was also shown in Figure 2.9 and Figure 2.25.

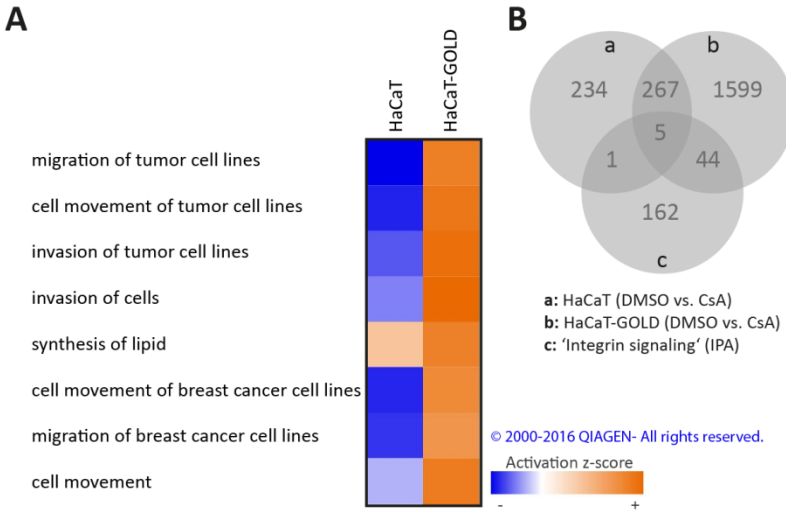

Figure 2.40 Ingenuity® Pathway Analysis comparison of RNA expression profiles (DMSO vs. CsA) from HaCaT and HaCaT-GOLD epithelia.
(A) *Predicted cellular/molecular functions (*Ingenuity® Pathway Analysis*)* induced by CsA in HaCaT and HaCaT-GOLD epithelia. Indicated are the activation z-scores, which express the predicted positive or negative activation of the function. The list is sorted by the magnitude of z-scores of both data sets. **(B)** *Overlap of differentially expressed genes* from the expression profiles (DMSO vs. CsA) from HaCaT and HaCaT-GOLD epithelia with the Ingenuity® Pathway Analysis gene set 'Integrin signaling'.

2.8. ATF expression in OTCs treated with CsA

Previously it was suggested that ATF3 is playing a role in CsA-induced tumorigenesis (Wu *et al.* 2010). In our RNA expression profiles ATF3 regulation was not apparent. However, in order to examine a possible association of ATF3 expression and CsA treatment in our experiments, RNA expression of ATF3 and also of ATF4 and ATF5 was analyzed in CsA-treated NHEK-, HaCaT-, HaCaT-GOLD- and HaCaT-RAS A-5-OTCs.

RNA expression of ATF3 was 1.31-fold up-regulated upon CsA treatment in NHEK epithelia, while the expression of ATF4 and ATF5 was not regulated on average. ATF3 RNA expression in CsA-treated HaCaT epithelia was 1.35-fold up-regulated and expression of ATF4 (0.64-fold) and ATF5 (0.65-fold) were down-regulated. In HaCaT-GOLD epithelia treated with CsA ATF3 expression was minorly up-regulated (1.06-fold), ATF4 down-regulated (0.84-fold) and ATF5 expression was not changed. Last, in CsA-treated HaCaT-RAS A-5 epithelia ATF3 was 1.26-fold up-regulated, ATF4 1.22-fold up-regulated and ATF5 minorly (1.06-fold) up-regulated (Figure 2.41).

Summarized CsA might have an impact on ATF3 expression in NHEK, HaCaT and HaCaT-RAS A-5 epithelia. Noteworthy, the changes measured in our experiments were very low, below a fold change of 2. Nevertheless, further experiments were not performed, due to the reason that the proposed CsA-induced and ATF3-driven senescence inhibitory mechanism (Wu *et al.* 2010) relies on $p53^{wt}$ and H-ras^{V12} cells, which are not present in our HaCaT system, nor common in human cSCCs (Boukamp 2005a).

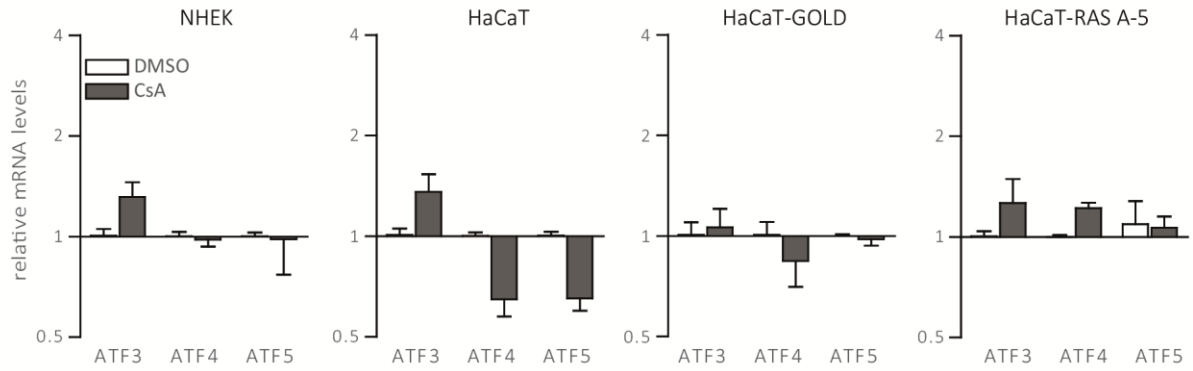

Figure 2.41 Relative ATF3, ATF4 and ATF5 RNA expression in NHEK, HaCaT-, HaCaT-GOLD-, and HaCaT-RAS A-5 epithelia treated with CsA.
RNA isolated from indicated epithelia treated with DMSO (0.04%) or CsA (10 µg ml^{-1}) for 3 weeks was quantified by qRT-PCR. The graphs show the mean and the standard error of the mean. NHEK, HaCaT and HaCaT-RAS A-5: n=9 (from 3 independent experiments), HaCaT-GOLD: n=3.

3. DISCUSSION

Raising incidence of cSCCs in organ transplant patients are a huge challenge in immunosuppression therapy. Yet the direct impact of CsA on human keratinocytes remains elusive. While studies in cultured cells can give valuable insight into the biology of CsA, it might not be necessarily relevant for keratinocytes, as it was shown that calcineurin/NFAT signaling is in fact ubiquitously present in various cell types, but depends on different co-signaling pathways in different cell types (Crabtree 1999; Aramburu *et al.* 2004). Besides, effects seen in cultured cells can be tremendously different to the effects within a tissue context. In order to prevent species-dependent differences, a human *in-vivo*-like 3D organotypic skin culture system was used to unravel the direct impact of CsA on human keratinocytes in a homeostatic and physiologically relevant environment.

3.1. Improvement of differentiation of HaCaT and HaCaT-RAS A-5 cells by CsA

One constant characteristic of CsA treatment in our experiments was the normalization of epidermal differentiation. HaCaT- and HaCaT-RAS A-5-OTCs regenerate an epithelium with reduced differentiation. After CsA treatment the epithelial strata were better distinguishable and developed much more like skin *in-vivo*. Importantly, this was consistent also when different sera were used for performing the OTCs. While another phenotype, invasion of HaCaT cells into the dermis, was only seen in one particular serum (discussed in section 3.2). In line with the better structured epithelium seen in H&E histology, improved distribution of differentiation markers, as demonstrated by immunofluorescent stainings could be demonstrated. This was also confirmed by gene expression analysis: As defined by GO-terms, CsA caused regulation of ‘epidermal development’ genes. Moreover, we could show that CsA-treated HaCaT and HaCaT-RAS A-5 epithelia had a higher transepithelial electric resistance, reflecting an improved skin barrier. Interestingly regulation of gene expression was dependent on the basic differentiation status of the cell type. HaCaT cells, which still have maintained a better differentiation potential in comparison to HaCaT-RAS A-5 cells under standard conditions, showed less regulation than the poorly differentiating HaCaT-RAS A-5 cells. Moreover, in NHEK epithelia, which form a perfect epidermis, i.e. optimally differentiate under standard conditions, CsA did not seem to be able to further potentiate differentiation: CsA-dependent differential gene expression of ‘epidermal development’ genes was not apparent in NHEK cells grown in OTCs. We thus hypothesize that CsA is inducing a normalization of epithelia leading to an improvement of differentiation (Figure 3.1), by contributing to the regulation of the differentiation program. However, it remains open whether normalization is induced in all epithelia with reduced differentiation or whether only in p53 mutant epithelia. HaCaT and HaCaT-RAS A-5 cells are p53 mutant cells and it was shown that p53 mutant cells are more easily pushed into terminal

differentiation (Freije *et al.* 2014). Additional experiments, with different p53 mutant and wild type keratinocytes would be needed to validate whether a p53 mutation is necessary for the phenotype we have described.

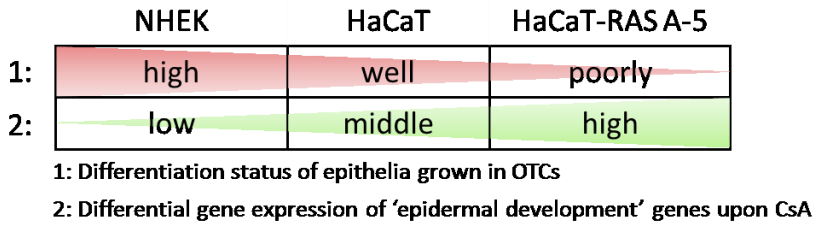

Figure 3.1 Hypothesis: CsA-induced normalization of differentiation.
NHEK (normal human epidermal keratinocytes). The more differentiated the epithelium of the corresponding cell type in OTCs is, the less are 'epidermal development' genes affected by CsA.

3.1.1. The role of Calcineurin and CsA in epidermal differentiation and improvement of the skin barrier

In-vitro studies with murine keratinocytes suggested that calcineurin inhibition by CsA leads to a decrease in the expression of some calcium-induced differentiation markers (KRT1, LOR and FLG) (Santini *et al.* 2001). A closer look into calcineurin and NFAT mice models challenges this assumption. Neither a knockdown of calcineurin A nor of calcineurin B reduces epidermal differentiation in mice. While knockouts of epidermal calcineurin B1 exhibit a cyclic alopecia phenotype (Mammucari *et al.* 2005), mice with a calcineurin A-α knockout had a decreased stratum spinosum and thickened stratum corneum. While the authors discussed whether a parallel increase in Tunnel positive cells within the suprabasal cells could argue for an increase in apoptosis or argues for an increase in premature differentiation (Pena *et al.* 2010), our results would argue for the latter. Similar to the calcineurin B knockout, a knockdown in NFATc1 caused an increase in follicular cell cycling and follicular growth (Horsley *et al.* 2008). However, neither did the knockdown affect the interfollicular epidermis, nor did overexpression of NFATc1 impact terminal differentiation. This suggested that NFATc1 is primarily playing a role in follicular cells (Horsley *et al.* 2008). In contrast to the NFATc1 knockdown, an NFATc2 knockdown did not cause alopecia, nor did the mice show any other obvious abnormality (Hodge *et al.* 1996). Additionally, as discussed by Wu *et al.*, no skin phenotypes were described for other NFAT mutants, including NFATc3 and NFATc4 (Wu *et al.* 2007).

Taking together, the literature shows that calcineurin signaling plays a role in the epidermis, however, little information is available on the mechanism of calcineurin within the epidermal context and its exact role in differentiation. Our data clearly demonstrated that continuous CsA treatment led to 'normalization' of stratification and thus improvement of differentiation of HaCaT and HaCaT-RAS A-5 cells when grown in OTCs. However, further experiments would be needed to link this phenotype

with a decrease in calcineurin signaling or to exclude calcineurin signaling responsible for this phenotype. Evidence could be provided by the usage of different inhibitors, like for example the peptide VIVIT, which was shown to inhibit NFAT activity, but not general calcineurin activity (Aramburu *et al.* 1999) or by molecular inhibition, overexpressing the endogenous RCAN1, which binds calcineurin and thereby inhibits NFAT activity (Fuentes *et al.* 2000).

Calcineurin or NFAT knockout models can provide information about the role of calcineurin signaling in epidermal differentiation. However, while we did not see changes in differentiation in the epidermis of NHEK, we saw an improvement/normalization of differentiation in HaCaT and HaCaT-RAS A-5 epithelia. Both epithelia show a reduced state of differentiation under standard culture condition. Hence mice models with initial defective skin epithelia would reflect our results better. Interestingly, in NC/Nga mice, a model for atopic dermatitis (Suto *et al.* 1999), in which sodium dodecyl sulfate treatment disrupted the skin barrier, CsA improved the clinical phenotype and enhanced KRT10 expression (Kim *et al.* 2013). Moreover, up-regulation of KRT10 after combined CsA and Rapamycin treatment was also described in a humanized mouse model of inflamed human skin grafts (huPBL-SCID-huSkin) (de Oliveira *et al.* 2012). In that study, the CsA-induced reduction of inflammation was discussed to be the major decisive cause for the improved phenotype. In light of our own results, the improvement of skin barrier and the up-regulation of KRT10 might also be due to a direct impact of CsA on the keratinocytes. In addition, *in-vivo* data from atopic dermatitis showed that topical treatment with pimecrolimus, another calcineurin inhibitor, led to an improvement of barrier function and also restoration (up-regulation) of FLG after three weeks (Jensen *et al.* 2009). CsA treatment has been reported to be also beneficial for severe cases of psoriasis (Ho 2004). In psoriasis, an inflammatory disease, which is as well characterized by a defective skin barrier (Bergboer *et al.* 2012), several LCE genes are reduced in lesioned skin as compared to uninvolved skin (Bergboer *et al.* 2011). Interestingly, LCE genes were among the genes, which in our results were consistently up-regulated by CsA in HaCaT and HaCaT-RAS A-5 cells. Hence, while CsA most certainly has a beneficial impact on psoriatic lesions by reducing the inflammation, our results suggest that improvement of psoriatic lesions by CsA is also caused by up-regulation of LCE genes in the keratinocytes and thereby improving the skin barrier.

3.1.2. Similarities between CsA and UV irradiation on epidermal differentiation and improved skin barrier

We found that in HaCaT and HaCaT-RAS A-5 epithelia long-term UV irradiation caused an increase in epidermal differentiation. Especially in HaCaT-RAS A-5 epithelia, which only poorly differentiate under standard conditions, a strong increase in differentiation could already be seen in histological stainings. Interestingly morphology in histological stainings of UV-irradiated OTCs resembled the

morphology of CsA-treated OTCs. Moreover, comparison of gene expression profiles revealed a considerable overlap of genes regulated by long-term UV irradiation and continuous CsA treatment. The combination UV+CsA induced a much higher number of differentially expressed genes than UV-irradiation and CsA-treatment alone. Nevertheless this did not further strengthen the phenotype of improved differentiation based on histological stainings. Noteworthy, comparing the 'epidermal development' gene expression profiles of CsA, UV and UV+CsA demonstrated that those genes, which were regulated in all three conditions, were either all up- or all down-regulated, arguing for a common regulatory mechanism induced by UV irradiation and CsA treatment.

Single UV irradiation was shown to decrease barrier function (Haratake *et al.* 1997; Biniek *et al.* 2012). However, there is also evidence that the epithelia can restore barrier function (Johnson *et al.* 2014) and increase the stratum corneum upon continuous UV irradiation in the sense of a protective shield against UV (Cabral *et al.* 2001). Interestingly, the study from Haratake *et al.* showed that CsA, administered directly after the UV irradiation, prevented the short-term UV-induced barrier defects. The authors argued that CsA reduced inflammation and T cell infiltration and thereby restored the barrier function. However, considering our results, this might have at least in part been a direct effect of CsA on gene expression in the keratinocytes. Also in line with our findings that CsA did not augment differentiation in NHEK, the authors did not find an impact of CsA on the skin barrier of healthy unaffected skin (Haratake *et al.* 1997).

Within the 'epidermal development' gene sets several genes from two specific gene groups were affected by CsA, UV and UV+CsA. These two gene groups were LCE and SPRR. Both were previously shown to be induced by UV irradiation and suggested to be part of a long term protective adaption of skin towards UV irradiation (Kartasova & van de Putte 1988; Cabral *et al.* 2001; Jackson *et al.* 2005). Especially SPRR4, which is differentially expressed also in our HaCaT-RAS A-5 epithelia in all treatment options (CsA, UV and UV+CsA), seems to play a central role in the adaption to UV irradiation (Cabral *et al.* 2001). As CsA regulated a similar set of 'epidermal development' genes as UV, it might be hypothesized that a CsA-sensitive signaling pathway is taking a part in the above mentioned UV adaption mechanism. While it might be a CsA-sensitive signaling pathway, it might be asked, whether this adaption mechanism is a NFAT- or even calcineurin-independent mechanism, as it was shown that UV activates NFAT (Huang *et al.* 2000), which is commonly inhibited by CsA (Hermann-Kleiter & Baier 2010).

3.1.3. Differentiation status of cSCCs and high-risk cSCCs in organ transplant recipients

We showed that CsA improved differentiation of poorly or moderately differentiated epithelia. In agreement, in organ transplant recipients, as it is the case in immunocompetent patients, the

majority of cSCCs is well differentiated (Smith *et al.* 2004; Lindelöf *et al.* 2006). On the other hand, patients treated with CsA are more prone to cutaneous catastrophic carcinomas (Abikhair *et al.* 2016) and also CsA enhanced metastasis in mice models (Hojo *et al.* 1999; Guba *et al.* 2002). Although the probability for poorly differentiated cSCCs is higher to develop into high risk cSCCs (Brougham *et al.* 2012), differentiation status per se does not exclude advanced disease (Cherpelis *et al.* 2002) and some studies even showed that the majority of metastatic cSCCs are well differentiated (Dinehart *et al.* 1997).

3.2. CsA-induced invasion

Using GOLD serum in the OTC experiments, continuous CsA treatment caused extensive invasion of the HaCaT keratinocytes. Invasion into the dermal equivalent and especially penetration through the basement membrane were nicely demonstrated by immunofluorescent staining for the basement membrane marker ColIV. In contrast, experiments using a different serum, could not replicate the CsA-induced invasive growth of HaCaT keratinocytes. Noteworthy, the improvement of stratification and differentiation was consistent in both sera.

3.2.1. The role of MMPs in CsA-induced invasion

While enhanced proliferation could be excluded as causative origin for the invasion, we measured enhanced gelatinase activity, arguing for an enzymatic assisted invasion. One interesting factor, MMP26, was found more often in tumor cells from cSCCs from organ transplant recipients than in cSCCs from immunocompetent patients and could be one factor responsible for the more aggressive cSCCs in organ transplant recipients (Kuivanen *et al.* 2009). However, we did not find MMP26 within our expression data. In contrast, gene expression analysis showed a massive up-regulation of MMP3 and MMP10, as well a 2-fold up-regulation of MMP1 within the epithelial cells. MMP expression levels were as well measured in the corresponding CsA-treated fibroblast from the dermal equivalent. However, in contrast to the epithelial cells, all three MMPs, MMP1, MMP3 and MMP10 were down-regulated in CsA-treated fibroblasts. Moreover, despite massive RNA expression in the epithelial cells, there was only a weak up-regulation of pro-MMP10 proteins, while pro-MMP1 and MMP3 proteins were clearly down-regulated by CsA.

Interestingly, ITGA6, which we showed is reduced at the basement membrane at invasion sites in CsA-treated HaCaT-GOLD-OTCs, is a direct substrate of MMP10 (Schlage *et al.* 2015). Furthermore, MMP10 RNA transcripts were shown to be up-regulated in cSCCs in comparison to skin and to actinic keratosis (Haider *et al.* 2006; Lambert *et al.* 2014). Moreover, Mitsui *et al.* demonstrated that MMP10 is especially up-regulated at the leading edge of cSCCs (Mitsui *et al.* 2014). In line with our expression data, MMP10 proteins were shown to be more expressed by cancer cells than from

stroma cells in cSCCs (Boyd *et al.* 2009). Interestingly, it was previously shown that CsA is inducing MMP10 expression in another tissue context. Tiu *et al.* presented gene expression data of CsA-treated SCC-15 oral epithelial cells indicating up-regulation of MMP10 (Tiu *et al.* 2006). In addition Dannewitz *et al.* revealed enhanced MMP10 expression in oral epithelial cells from CsA-induced gingival overgrowth, a common side effect of CsA therapy in organ transplant recipients (Dannewitz *et al.* 2006). While we miss the proof that the slight increase in MMP10 by CsA seen in our experiments is sufficient for the invasive growth of HaCaT keratinocytes, MMP10 was also shown to activate pro-MMP9 (Schlage *et al.* 2015). MMP9 proteins are as well commonly up-regulated in cSCCs (Verdolini *et al.* 2001; Roh *et al.* 2012) and activation of pro-MMP9 by MMP10 might explain why we did not see enhanced MMP9 RNA expression in the CsA-treated HaCaT-GOLD epithelia.

3.2.2. The role of integrins in CsA-induced invasion

Analysis of the RNA expression profile of CsA-treated HaCaT-GOLD epithelia with Ingenuity® Pathway Analysis revealed that several genes from the integrin signaling pathway were regulated. Among these were ITGA6 and ITGB1, which are expressed in basal keratinocytes (Janes & Watt 2006). In agreement with the RNA expression results, Immunofluorescent staining of CsA-treated HaCaT-GOLD epithelia demonstrated enhanced ITGA6 and ITGB1 deposition in basal keratinocytes, especially at the basement membrane underneath non-invading basal cells, in comparison to the control HaCaT-OTCs.

Increased expression of Integrins is associated with head and neck cancer (Bornstein *et al.* 2016), where they participate in the invasion process. However, dysregulation of Integrin are as well found in cSCCs (Savoia *et al.* 1993; Janes & Watt 2006). Moreover, knockdown of ITGB1 in vulvar SCC cells diminished their invasive capacity (Brockbank *et al.* 2005), while overexpression of active ITGB1 in basal keratinocytes favored chemical induced malignant skin tumor formation (Ferreira *et al.* 2009). Moreover, gene expression profiling from actinic keratosis and cSCCs revealed a set of genes involved in migration, including ITGA5 (Lambert *et al.* 2014). When comparing cSCCs to normal epidermis it was shown that ITGA3, ITGA5, and ITGA6 were up-regulated, especially at the leading edge of the invasive cSCCs (Mitsui *et al.* 2014). Moreover, CsA was shown to up-regulate ITGB3 in trophoblast cells (Huang *et al.* 2014). In contrast, CsA caused downregulation of ITGB1 and ITGA5 in oral epithelial cells (Sardarian *et al.* 2015). In the epithelia of the HaCaT-GOLD cells we found up-regulation of ITGB1 and ITGA6 upon CsA treatment and this correlated with invasive growth. The final proof for their role in the invasive process by e.g. blocking antibodies or knockdown of the integrins, however, still needs to be undertaken.

3.2.3. The role of IL-1α and GM-CSF

While CsA induced invasion of HaCaT keratinocytes grown in GOLD serum, CsA did not induce invasion in a different serum. Lists of differentially expressed genes from both experiments, CsA-treated HaCaT epithelia (versus the corresponding DMSO control) and CsA-treated HaCaT-GOLD epithelia grown in GOLD serum (versus the corresponding DMSO control grown as well in GOLD serum), were both screened and compared. One gene which was strongly up-regulated in the CsA-treated invasive HaCaT-GOLD cells, which was not regulated in the non-invasive CsA-treated HaCaT cells, was IL-1α. Moreover, not only RNA levels were increased, IL-1α proteins were also strongly up-regulated in CsA-treated HaCaT-GOLD-OTCs. IL-1α is typically expressed in skin and is playing a role in keratinocyte growth regulation via a paracrine loop with fibroblasts (Maas-Szabowski *et al.* 2000). While in that regulatory loop IL-1α and IL-1β from keratinocytes stimulate CSF2/GM-CSF expression in fibroblasts, we could not find CSF2 up-regulation in CsA-treated fibroblasts. However, it was already suggested earlier that IL-1α is also up-regulating CSF2 in keratinocytes (Kupper *et al.* 1988). In agreement with that publication we demonstrated elevated CSF2 levels in CsA-treated HaCaT-GOLD epithelia. Concerning the involvement of IL-1α and CSF2/GM-CSF with the invasive phenotype, it was previously shown *in-vitro* that excess IL-1α enhanced migration of keratinocytes (Chen *et al.* 1995). Moreover, forced expression of GM-CSF enhanced infiltration of HaCaT-RAS A-5 keratinocytes into the underlying collagen, when grown in collagen-based organotypic cultures (Obermueller *et al.* 2004). Moreover the same group showed that stimulation of head and neck SCC cells with GM-CSF enhanced migration of these cells and that blocking GM-CSF antibodies reduced invasive growth of these head and neck SCC cells grown in organotypic cultures (Gutschalk *et al.* 2006). In our CsA-treated HaCaT-GOLD-OTCs the levels of GM-CSF protein was, however, comparably low. Thus without further proof, for example using blocking antibodies against GM-CSF, it has to remain open whether GM-CSF was at least in part responsible for the invasive phenotype.

3.2.4. The difference between CsA-treated HaCaT and HaCaT-GOLD epithelia

While CsA enhanced *in-vitro* invasion of trophoblast cells (Tang *et al.* 2012) and A-549 adenocarcinoma cells (Hojo *et al.* 1999), it also was found to reduce *in-vitro* invasion, namely of prostate cancer cells (Kawahara *et al.* 2015), glioblastoma cells (Sliwa *et al.* 2007) and liver cells (Sakai *et al.* 2004). These different publications nicely demonstrated that CsA is not inducing invasion in every cell context, but rather requires the right conditions. Our experiments proved that not only different cell types respond differently, but that the same HaCaT keratinocytes when grown in different sera responded to CsA with invasion in only one of the sera. Although improved differentiation could be seen in all tested sera. Thus the external influence can have profound influence and obviously is able to sensitize or desensitize a cell for CsA-induced invasion. One

difference between HaCaT- and HaCaT-GOLD-OTCs, which were grown in the standard and the GOLD serum, was the deposition of ColVII. ColVII is part of the basement membrane (Leigh *et al.* 1988). While in the standard serum HaCaT-OTCs were stained positive for ColVII at the dermal epidermal junction, HaCaT-GOLD OTCs were almost negative for ColVII. ColVII RNA expression could be measured in these OTCs (data not shown), suggesting that the GOLD serum is not supporting ColVII maturation and deposition at the basement membrane of HaCaT-GOLD-OTCs. Loss of ColVII by a mutation in patients with dystrophic epidermolysis bullosa causes severe blistering of the skin (Brummer *et al.* 1993). Moreover, these patients are also much more susceptible to cSCCs. While it is still discussed why these patients are more susceptible for cSCCs (Kim & Murrell 2015), it was shown that re-expression of ColVII in dystrophic epidermolysis bullosa-derived fibroblasts, prevents invasion of dystrophic epidermolysis bullosa-derived SCC cells in organotypic cultures (Ng *et al.* 2012). However, the loss of ColVII in our system was not enough to induce invasive growth of non-tumorigenic HaCaT-GOLD keratinocytes, but needed additional CsA treatment. The absence of ColVII at the basement membrane probably facilitated invasion, but was not the exclusive cause. In addition, we saw that differential gene expression induced by CsA was much stronger affected in GOLD serum. Those additional regulated genes most likely were necessary for the invasive growth of HaCaT keratinocytes in the GOLD serum. Furthermore, more genes were downregulated (59%) in the case of the standard serum, in comparison to the GOLD serum (40%). It was shown that in splenocytes of CsA-treated rats the RNA synthesis rate was decreased by 63% (Eun *et al.* 1987). It might be that this inhibition of RNA synthesis is overcome in the GOLD serum, leading to a much greater differential gene expression.

While it remains elusive what the exact difference between the sera is, extensive mass spectrometry could give a hint. For example Zheng *at al.* compared the protein composition of three different sera by mass spectrometry. These sera promoted different growth properties of cultured retinal epithelial pigment cells and they found that in those sera, which did not promote growth as good as the other serum, several growth factors, like TGFβ1 or bFGF, were less or not present (Zheng *et al.* 2006). Another promising approach is the comparison of the differential gene expression between the epithelia of control HaCaT-OTCs from both sera. This analysis is currently ongoing in cooperation with the bioinformatics group by Jörg Galle at the Interdisciplinary Centre for Bioinformatics in Leipzig. Results could show which pathways are activated or inactivated in one or the other serum and which might sensitize the HaCaT keratinocytes to CsA-induced invasion.

3.3. CsA-induced maintenance of vital cell layers in HaCaT epithelia

Control HaCaT-OTCs lose vitality and become atrophic when cultured for more than 4 weeks. Interestingly, continuous CsA treatment for 4 weeks decelerated this process. First of all this was

demonstrated by histological staining, showing that CsA-treated HaCaT-OTCs maintained more vital cell layers after 4 weeks than the control HaCaT-OTCs. Moreover, we could demonstrate that these CsA-treated HaCaT-OTCs with more vital cell layers were metabolically more active than the time matched control HaCaT-OTCs. Furthermore, Ingenuity® Pathway Analysis predicted that CsA-treated OTCs underwent less cell death, apoptosis or necrosis after 4 weeks of treatment than the controls. In addition to less cell death, Ingenuity® Pathway Analysis also predicted that HGF and Integrin signaling were activated in the HaCaT epithelia treated for 4 weeks with CsA. Interestingly, both factors are associated with cell survival.

HGF in epithelial cells is an important growth factor and mice lacking HGF or its receptor Met, exhibit severe defects in liver or placenta development (Schmidt *et al.* 1995; Uehara *et al.* 1995). Moreover, in conditional skin knockout mice it was shown that HGF is essential for skin regeneration (Chmielowiec *et al.* 2007). Finally, it was demonstrated that HGF protects corneal epithelial cells from Staurosporine-induced cell death (Kakazu *et al.* 2004) and primary keratinocytes from UVB-induced apoptosis (Mildner *et al.* 2002). However, it has also to be mentioned that Mildner *et al.* showed that HGF is not inhibiting apoptosis in cultured HaCaT cells.

The adhesion proteins Integrins are expressed in basal, vital keratinocytes (Watt 2002). With regard to cell survival, it was shown that α3β1 integrin is necessary for keratinocyte survival (Manohar *et al.* 2004) and that loss of β4 Integrin protects epithelial cells from apoptosis (Weaver *et al.* 2002). Moreover, it was shown that adhesion of small cell lung cancer cells to extracellular matrix reduced cell death induced by chemotherapeutics and that this reduction was dependent on ITGB1 (Sethi *et al.* 1999).

Altogether, we saw that CsA maintained vital cell layers after long-term cultivation, while control OTCs lost their vital cell layers. Ingenuity® Pathway Analysis anticipated that HGF and Integrin signaling is activated in 4 weeks CsA-treated HaCaT-OTCs, but is less likely affected in 2 weeks CsA-treated HaCaT-OTCs. Accordingly, we believe that activation of these pathways is not a general trait of CsA treatment, but rather we suppose that they are down-regulated in control HaCaT-OTCs after prolonged cultivation and that this down-regulation is prevented by CsA. Hence, by maintenance of HGF and Integrin signaling CsA might prevent atrophy and the reduction in vital keratinocytes in HaCaT-OTCs older than 4 weeks.

3.4. Conclusion

In summary, our results suggest that an overall normalization of epithelia and enhanced endurance of vital keratinocytes is induced by CsA. We showed that CsA in all tested conditions restored differentiation in HaCaT and HaCaT-RAS A-5 epithelia. Furthermore, while HaCaT keratinocytes after

4 weeks cultivation in OTCs became atrophic, we demonstrated that CsA preserved the vitality of HaCaT keratinocytes grown in OTCs. This was possibly due to a reduction of cell death, triggered in HaCaT-OTCs cultured for over 4 weeks, as predicted by Ingenuity® Pathway Analysis. Our results agree with *in-vivo* data showing that CsA is not directly transforming keratinocytes into cancer cells under all conditions. Instead our results suggest that CsA could support cSCCs emergence by a potential impact on keratinocyte viability. *In-vivo* CsA may lead to preservation of basal keratinocytes, which upon genomic or external stress might get lost via differentiation or cell death. These could remain in place with CsA and may finally develop into 'defective' cell clones, further developing into cSCCs. We further showed, that under certain conditions, using a specific serum, CsA is able to induce invasion of pre-malignant HaCaT keratinocytes. Changed parameters necessary for CsA-induced invasion in our experiments might as well correlate to a subgroup of transplant patients, who develop cutaneous catastrophic carcinomas. This subgroup of patients rapidly develops, within 10 month of transplantation, up to 100 cSCCs per year (Abikhair *et al.* 2016). Our data is now suited for in depth analysis to identify pathways, which might sensitize keratinocytes for CsA-induced invasion. Finding these targets might as well help identifying patients in danger of developing cutaneous catastrophic carcinomas and to counteract this devastating CsA-induced side effect.

4. MATERIALS AND METHODS

4.1. Cell culture methods

4.1.1. Cells

Normal human dermal fibroblasts (NHDF) and normal human epidermal keratinocytes (NHEK) used in this study were derived from one healthy donor (female, 23 years, abdomen). Isolation was done by Iris Martin (DKFZ) according to the guidelines of the Institutional Commission of Ethics of the University of Freiburg (42/2005). In short, skin samples were cut into pieces and incubated in thermolysin (0.5 mg ml^{-1}) overnight at 4°C. Afterwards dermal and epidermal compartments were separated. For NHDF isolation dermal fragments were submersed in D20 medium (Table 4.1) and incubated (37°C, 5% CO_2, 5% O_2, 95% humidity) on standard cell culture plates. NHDF grew out after around 3 weeks and dermal fragments were removed. When cells reached confluency, NHDF were trypsinized and propagated or frozen in liquid nitrogen for later usage as passage 1. For NHEK isolation epidermal fragments were incubated in 0.4% Trypsin/0.05% EDTA for 10 min at 37°C. Afterwards keratinocytes were separated by vigorous tapping and filtering (70 µm). 5000 NHEKs per cm^2 were seeded on standard cell culture plates with a feeder layer. For the feeder layer 6000 irradiated NHDFs (5 Mio NHDF per ml in suspension irradiated with 70 gray) per cm^2 were seeded in $FAD_{complete}$ medium (Table 4.1) 24h prior to keratinocyte seeding in order to precondition the medium. When NHEK reached 80-90% confluency cells were trypsinized and propagated or frozen in liquid nitrogen as passage 1.

HaCaT keratinocytes (Boukamp *et al.* 1988) were used in passages 32-39 and HaCaT-RAS A-5 keratinocytes (Boukamp *et al.* 1990), HaCaT keratinocytes transfected with $H\text{-}Ras^{G12V}$, were used in passages 25-29.

Table 4.1 Cell culture media

Medium name	Application	Formula
D10	NHDF, HaCaT, HaCaT-RAS A-5 cultivation	DMEM[1], 10% (v/v) FBS[2], 1% (v/v) P/S[3]
D20	NHDF isolation	DMEM[1], 20% (v/v) FBS[2], 1% (v/v) P/S[3]
Freezing	Freezing of all cell types	DMEM, 20% (v/v) FBS, 1% (v/v) P/S, 10% DMSO[4]
rFAD	OTC cultivation	DMEM and DMEM-F12[5] (1:1), 10% (v/v) FBS, 1% (v/v) P/S, 200 µg/ml 2-phospho-L-ascorbic acid, 0.1mM cholera toxin, 0.4 µg/ml hydrocortisone
$FAD_{complete}$	NHEK isolation	DMEM and DMEM-F12 (1:1), 5% (v/v) FBS, 1% (v/v) P/S, 24 ng/ml adenine, 0.1 nM cholera toxin, 2 ng/ml EGF[6], 0.4 µg/ml hydrocortisone, 5 µg/ml insulin
FDM	Dermal equivalent cultivation	DMEM and DMEM-F12 (1:1), 10% (v/v) FBS, 1% (v/v) P/S, 200 µg/ml 2-Phospho-L-Ascorbic Acid, 2.5 ng/ml EGF, 5 ng/ml FGF[7]-basic, 5 µg/ml insulin, 1 ng/ml TGF-β1[8]
DermaLife K[9]	NHEK cultivation	As described by manufacturer.

[1] Dulbecco's Modiefied Eagle's Medium (Lonza), [2] fetal bovine serum (GOOD, GE Healthcare, Lot.: P132307 or GOLD, PAN-Biotech, Lot: A15112-1936), [3] penicillin/streptomycin (10,000 U/ml), [4] dimethyl sulfoxide, [5] 1:1 mixture DMEM and F12 (Lonza), [6] epidermal growth factor, [7] fibroblast growth factor, [8] transforming growth factor β1, [9] Lifeline Cell Technology

4.1.2. Maintenance of cultured cells

Frozen cells (stored in cryotubes in liquid N_2) were thawed at 37°C and transferred to cell type specific culture medium (Table 4.1). Cultivation was done at 37°C, 95% humidity and 5% CO_2 for NHEK, HaCaT and HaCaT-RAS A-5. NHDF were kept at 37°C, 95% humidity, 5% CO_2 and 5% O_2. Medium was exchanged every 2nd or 3rd day. HaCaT keratinocytes were split every 10th day at a ration 1:10 or at a density of 0.5 Mio cells per 10 cm dish. HaCaT-RAS A-5 cells were split every 7th day a ration of 1:15 or at a density of 0.5 Mio cells per 10 cm dish. NHDF were split after reaching confluency and seeded at a density of 1 Mio per 15 cm dish. NHEK were split at 80% confluency and seeded at a density of 1.5 Mio cells per 15 cm dish. Splitting procedure was done according to Table 4.2. In short, cells were washed with PBS, incubated with EDTA, which was removed and cells were incubated with Trypsin. The enzymatic reaction was stopped with serum containing culture medium.

Cell stocks of HaCaT and HaCaT-RAS A-5 cells were tested for cell contaminations (Multiplexion GmbH, Heidelberg, Germany). All cells, including NHEK and NHDF and media from OTCs prior to harvest, were regularly tested for mycoplasmas (Venor® GeM Classic Mycoplasma PCR Detection Kit, Minerva Biolabs; Berlin, Germany). Tests were performed according to manufacturer's protocol by Hermann Stammer. All samples from this thesis were mycoplasma negative.

For storage, cells were frozen in cryo tubes and stored at liquid N_2. 2 Mio cells of the corresponding type were centrifuged (1000 rpm) and resuspended in 1ml freezing medium (Table 4.1). For controlled and gentle freezing cryo tubes were transferred to cryo-safe freezing boxes (neoLab, Germany) and kept at -80°C for 24h before transferring to liquid nitrogen.

Table 4.2 Incubation times for cell passaging

Cell Type	1. Rinse with PBS	2. EDTA Treatment	3. Trypsin Treatment
NHDF	yes	no	3-5 min (0.05% in 0.05% EDTA)
NHEK	yes	Rinsed (0.05%)	1-3 min (0.4% in 0.05% EDTA)
HaCaT	yes	10 min (0.05%)	3-5 min (0.05% in 0.05% EDTA)
HaCaT-RAS A-5	yes	10 min (0.05%)	3-5 min (0.05% in 0.05% EDTA)

4.1.3. Preparation of organotypic skin cultures (OTCs)

OTCs were prepared as described by Berning *et al.* except for the number of fibroblasts and time of pre-cultivation of the dermal equivalents (Berning *et al.* 2015). In short, preparation was performed as follows: ThinCerts (0.4 µm, translucent, Greiner Bio-One) were kept in deep-well ThinCert 12-well cell culture plates (Greiner Bio-One) containing 5 ml FDM medium (Table 4.1). 0.33 Mio NHDFs in 0.5 ml FDM medium were seeded dropwise into the culture inserts. This seeding step was repeated two times together with an overall exchange of FDM medium within the insert and the deep-well plate on the 2nd and 4th day after the 1st seeding. Dermal equivalents were allowed to mature for 3 weeks with an exchange of FDM medium (within deep-well plate and insert) every 2nd or 3rd day. Prior seeding of keratinocytes (NHEK, HaCaT or HaCaT-RAS A-5) medium was exchanged to rFAD medium (Table 4.1). 0.25 Mio singularized (cell strainer 70 µm) keratinocytes within 0.5 ml rFAD medium were seeded dropwise on top of the dermal equivalents. After 4-5 days of submersed cultivation the medium on top of the OTCs was removed to allow air-exposed growth and regeneration of the epidermis. Harvest and processing of OTCs is described in the section of the corresponding analysis methods.

4.1.4. Stimulation of cultured keratinocytes and OTCs

CsA (239835, Calbiochem) was dissolved in sterile DMSO at a stock concentration of 25 mg ml^{-1}. Aliquots were prepared at room temperature and stored at -20°C. Thawed aliquots were used once and then discarded. Recombinant human CXCL14 (TP723048, OriGene) was dissolved in 20mM phosphate buffer, 100 mM NaCl, pH 7.2. Aliquots were stored at -20°C. Recombinant human DEFB4A (TP723032, OriGene) was dissolved in 20mM phosphate buffer, 100 mM NaCl, pH 7.2. Aliquots were stored at -20°C. Recombinant human IGFL1 (TP315281, Origene) was dissolved in 25mM Tris.HCL, pH 7.3, 100mM glycine, 10% glycerol. Aliquots were stored at -20°C.

Cells were stimulated with the stimulant or the corresponding amount of solvent. Stimulants and solvents were added to fresh culture medium and added to the cells (2D cultured cells) or to the well underneath the insert (OTCs). For long-term stimulation supplements were added with every culture medium exchange 3 times per week (Monday, Wednesday and Friday). As a standard treatment 10 µg ml^{-1} CsA or as control 0.04% DMSO was used, if not stated differently. In case of OTCs, stimulation was started 1 week after the epithelial seeding.

4.1.5. UV irradiation of OTCs

OTCs were irradiated prior to culture medium exchange 3 times per week (Monday, Wednesday and Friday). Old culture medium was removed and replaced by sterile PBS to prevent desiccation. OTCs were irradiated without cell culture lid for 3 min and 30 sec, corresponding to 5 J/cm^2 UVA and 10 mJ/cm^2 UVB. Meanwhile control plates were kept in PBS outside the incubator. Afterwards PBS was removed and replaced by fresh culture medium containing respective stimulants. UV irradiation started together with the CsA treatment 1 week after epithelial seeding. The light source was a tanning lamp (HB 404, Philipps) with UV emission between 296nm and 380nm with a maximum at 374nm.

4.2. 2D cell culture analyses

4.2.1. CellTiter-Blue® assay with cultured cells

HaCaT keratinocytes were treated with CsA in conventional cultures (2D) and analyzed using the CellTiter-Blue® assay (Promega), which measures the metabolic activity of cells. HaCaT keratinocytes (35,000 per 100 µl per well, n=8) were seeded in flat-bottomed 96-well plates. Treatment started the next day. Cells were treated with increasing amounts of CsA (50 ng ml^{-1} - 100 µg ml^{-1}) or the corresponding amount of its solvent DMSO for 72h. 20 µl resazurin (Promega) were added to the conditioned medium (100 µl) in each well and fluorescence resulting from resazurin metabolized into resorufin was measured after 1h in a standard cell culture incubator. Fluorescence was acquired using the fluorescence microplate reader infinite F200 PRO (Tecan). The fluorescence signal was detected by the following filter set (Ex = 550 nm, Em = 610nm) at 5 positions within each well. Results are presented as mean and the standard error of the mean. Data points were normalized to the mean of the lowest DMSO or CsA concentration, respectively.

4.2.2. FACS-assisted apoptosis assay

Cultured and stimulated cells were trypsinized and washed once with PBS (4°C) before transferal to the binding buffer (1 Mio cells per ml). Subsequent steps were performed according to manufacturer's protocol (FITC Annexin V Apoptosis Detection Kit I, BD Pharmingen). Samples were acquired using the flow cytometer FACSCanto TT (BD). Compensation was performed with the BD FACSDiva Software and the data was analyzed using the software FlowJo. Data was presented as mean percentage of positive cells per total cell number. Per sample 3800 – 6000 single cells were analysed.

4.2.3. Multiplex fluorescent *in situ* hybridization (M-FISH)

M-FISH analyses were performed by Brigitte Schoell from Professor Anna Jauch's group (Human Genetics, Heidelberg University Hospital). Highly proliferating cultured HaCaT cells were arrested

using colcemid (0.27 µg ml^{-1}) for 4h at 37°C. Metaphase spreads were prepared and labeled according to (Speicher *et al.* 1996; Geigl *et al.* 2006). 30 metaphases were imaged and analyzed per treatment group. New chromosomal aberrations (translocations, deletions or insertions), which occurred only once and were not present in the control (DMSO-treated) cells, were counted.

4.2.4. SYBR Green assay

Cells (10,000 per well, n=4) were seeded in 24-well plates. Treatment with 0.25, 2.5 or 10 µg ml^{-1} CsA or the solvent DMSO (0.04%) was performed starting the following day. After 24h, 48h or 72h the medium was removed and sealed plates were stored at -20°C. Thawed plates were incubated with SYBR Green (1:2500 in 0.1% Triton/PBS) for 1h at room temperature protected from light. The readout was performed using a Fluoroskan Ascent (Thermo Fisher Scientific) at 485 nm. Cell numbers were determined with the help of a standard plate with defined numbers of cells, which was measured in parallel. Results are presented as mean and the standard error of the mean. Values from each CsA concentration or DMSO were normalized to the mean of the 24h value of CsA or of the corresponding DMSO concentration, respectively.

4.3. 3D OTC analyses

4.3.1. CsA quantification within OTCs

OTCs were harvested 24h after the last treatment. OTCs were removed from the filter and washed with PBS to remove excess medium. The OTC was cut and one quarter was immersed in Dispase II (1 mg ml^{-1} in PBS) for 1h at 37°C. Afterwards the dermal and epidermal parts were separated and separately frozen in liquid nitrogen. Prior to measurements samples were weighed and submersed in cell lysis solution (Promega). For lysis the samples were agitated (85 rpm) at 30°C for several hours and sonicated (2x 15 sec, 50% amplitude). Measurements were performed by Evelyn Jäger from Professor Peter Findeisen's group (Institute for clinical chemistry, Mannheim). Samples were separated by high performance liquid chromatography (UltiMate3000, HPG-3200 RS, Dionex, Thermo Scientific) and analyzed by mass spectrometry using a ion trap (amaZonSpeed, Bruker). Quantification was done with the help of serial dilutions of CsA as a calibrator. Results were determined as µg per mg of tissue. Conversion into µg ml^{-1} was calculated according to Fisher *et al.* (Fisher *et al.* 1988).

4.3.2. CellTiter-Blue® assay

For the measurement of the metabolic activity of OTCs the CellTiter-Blue® (Promega) assay was used. Inserts containing the OTCs or OTCs removed from the insert and cut in halve were transferred to standard multi-well plates containing 840 µl conditioned medium and 160 µl resazurin (Promega). Fluorescence resulting from resazurin metabolized into resorufin was measured after 1h in a

standard cell culture incubator. For fluorescence measurements 100 µl of conditioned medium was transferred to a flat-bottomed 96-well plate. Fluorescence was acquired using the fluorescence microplate reader infinite F200 PRO (Tecan). The fluorescence signal was detected by the following filter set (Ex = 550 nm, Em = 610nm) at 5 positions within each well. Results are presented as mean and the standard error of the mean. Data points were normalized to the mean of the DMSO values from each time point. OTCs or parts of OTCs which were used for the CellTiter-Blue® assay were not used for subsequent RNA analysis. If further used for paraffin embedding, OTCs were washed in PBS for 1h.

4.3.3. Measurement of transepithelial electrical resistance (TEER)

TEER measurements were performed prior to harvest at non-sterile conditions. Inserts containing OTCs were shortly dipped in sterile PBS to remove excess medium and transferred to an Endohm chamber (World Precision Instruments, Sarasota, United States), filled with 4 ml sterile PBS. Care was taken that no air bubbles developed underneath the insert and the electrode in the bottom panel of the chamber. A sterile Teflon ring was put onto the middle of the OTC and sealed with sterile Vaseline. 200 µl sterile PBS was filled into the ring and the Endohm chamber lid was attached in a way that the top electrode within the lid contacted the PBS within the Teflon ring. The electrodes were then attached to an epithelial Voltohmmeter (Millicell ERS-2, Merck Millipore, Germany), which was set to Ohms. Power was applied and resistance was read off after 120 sec of measurement, to avoid early oscillation. The measurements were performed in collaboration with Dr Sabine Rosenberger (DKFZ).

4.3.4. ELISA

Conditioned media from DMSO- and CsA-treated OTCs was removed 24h after the last treatment and directly stored at -20°C until further usage. Samples were thawed on ice before ELISA measurements and then centrifuged (1 min, 3200 rpm) to remove particles. ELISAs were performed according to manufacturer's protocol. Media was measured from three biological replicates in technical duplicates. Following ELISA kits (R&D Systems, Germany) were used: GM-CSF (DGM00), IL-1α (DLA50), pro-MMP1 (DMP100), MMP3 (DMP300) and pro-MMP10 (DM1000). Readouts were performed using the Multiskan FC Microplate Photometer (Thermo-Scientific) at 450 nm with background subtraction at 620 nm. Statistical significance was calculated by an unpaired, two-sided t-test.

4.3.5. H&E histological staining

Sampling: OTCs were removed from the inserts, cut in halve or in one-third and transferred to stabilized formaldehyde-containing fixative (12004, Morphisto). Samples were kept in fixative for at least 24h.

All succeeding steps were performed by Angelika Krischke (DKFZ) or Iris Martin (DKFZ): Samples were dehydrated by increasing ethanol solutions and transferred to xylene before paraffin embedding. Sections (7 µm) were cut with a microtome, placed onto microscope slides and dried for 48 h at 37°C. Slides were passed through deparaffinization, rehydration, H&E staining solution and dehydration steps according to manufacturer's protocol (H&E kit, 12156, Morphisto). Ensuing sections were mounted in Eukitt (Sigma-Aldrich).

4.3.6. Indirect immunofluorescent staining

Sampling: OTCs were removed from the inserts, cut in halve or in one-third, mounted in Tissue Tek (Sakura Finetek) within a cryomold (Sakura Finetek), frozen at the gas phase of liquid nitrogen and stored at -80°C. Embedded samples were cut (6 µm) with a cryotome at -25°C (+/-1°C). Sections on microscope slides (Histobond, Marienfeld) were dried for 15 min at room temperature before storing at -80°C until further usage. Prior to IIF sections were fixed in methanol (5 min, 4°C) and consecutive acetone treatment (2 min, -20°C). Subsequently slides were immersed in 1% Triton/PBS+ (Serva Electrophoresis), followed by immersion in PBS+ and ddH_2O and then slides were dried. Blocking of unspecific binding sites was done with 5% BSA/PBS+ for 30 min at room temperature. Primary antibodies (Table 4.3) were incubated in blocking solution overnight at 4°C. Before and after secondary antibody incubation, 1h at room temperature in blocking solution containing 2 µg ml^{-1} DAPI (Sigma-Aldrich), slides were washed in 1% Triton/PBS+ (1x 5 min) and PBS+ (2x 5 min) and immersed in ddH_2O. Sections were embedded in fluorescent mounting medium (DAKO).

Modification from standard protocol: For LCE2 and LCE3 IIF stainings paraffin-embedded sections (6 µm) on microscope slides (Histobond, Marienfeld) were used. After 24 h of drying at 37°C sections were deparaffinized (2x 3 min xylene, 3 min each 90%, 70% and 60% EtOH), rehydrated in ddH_2O and then dried. All succeeding staining steps were performed as described in the previous passage starting with immersion into 1% Triton/PBS+.

Table 4.3 Primary antibodies

Specificity	Species	Dilution	Cat.-No.
ColIV	rabbit	1:100	10760 (Progen)[1]
ColIV (1042.0)	mouse	1:100	10710 (Progen)[1]
ColVII (C805)	mouse	1:500	077K4780 (Sigma-Aldrich)[2]
FLG (FLG01)	mouse	1:100	AM00245P (Acris)[3]
ITGA6 (4F10)	mouse	1:100	CBL458 (Merck Millipore)[4]
ITGB1 (P4G11)	mouse	1:100	MAB1951Z (Merck Millipore)[4]
Ki67	rabbit	1:100	15580 (Abcam)[5]
KRT10 (DE-K10)	mouse	1:30	11414 (Progen)[1]
LCE2	rabbit	1:1000	(Bergboer *et al.* 2011)
LCE3	mouse	1:5000	(Niehues *et al.* 2015)
PanKRT	guinea pig	1:100	GP14 (Progen)[1]
SPRR2	rabbit	1:100	AG-25B-0002 (AdipoGen)[6]

[1]Heidelberg, Germany; [2]Steinheim, Germany; [3]Herford, Germany; [4]Darmstadt, Germany; [5]Cambridge, United Kingdom; [6]Liestal, Switzerland

Table 4.4 Secondary antibodies

Specificity	Fluorophore	Species	Dilution	Cat.-No.
guinea pig IgG	Cy2	donkey	1:200	706-225-148 (Dianova)[1]
mouse IgG	Cy3	donkey	1:200	715-166-151 (Dianova)[1]
rabbit IgG	Alexa488	donkey	1:200	711-546-152 (Dianova)[1]
rabbit IgG	Cy3	donkey	1:200	711-166-152 (Dianova)[1]

[1] Hamburg, Germany

4.3.7. Determination of the proliferation (Ki67) index

For the proliferation index 2-3 sections from 2-3 OTC each were stained for Ki67 and ColIV as described in 4.3.6. Sections from one OTC were at least 70 µm apart. Pictures covering the full length were taken and merged using the ZEN2012 software (Zeiss). Ki67 positive cells throughout the epidermis were automatically counted using a macro in ImageJ (Table 4.5). The length of the basement membrane was as well measured in ImageJ according to the ColIV staining. Results are presented as $Ki67^+$ cells per basement length. Significance was calculated with a two-sided, unpaired t-test.

Table 4.5 ImageJ macro for proliferation index

```
roiManager ("Reset");
waitForUser ("Please select, when you finish click OK");
run ("Select None");
run ("Set Scale...", "distance=0 known=0 pixel=1 unit=pixel global");
setSlice (1);
run ("Gaussian Blur...", "sigma=2 slice");
roiManager ("Deselect");
roiManager ("Combine");
roiManager ("Reset");
roiManager ("Add");
setAutoThreshold ("Triangle dark");
run ("Threshold...");
waitForUser ("Please check the Thresh. and Process - Find Max, when you finish
click OK");
run ("Find Maxima...", "noise=(fill in) output=[Segmented Particles] above");
roiManager ("Select", 0);
run ("Analyze Particles...", "size=50-Infinity summarize add");
close ();
resetThreshold ();
roiManager ("Show None");
roiManager ("Show All");
```

4.3.8. Gelatinase assay

Unfixed cryo sections (6 µm, stored at -80°C) were incubated with the gelatinase buffer (50 µg ml^{-1} DG-gelatin and 2 µg ml^{-1} DAPI) for 1h at room temperature protected from light. The buffer was prepared as described in the manufacturer's protocol (EnzChek Gelatinase/Collagenase Assay Kit, Life Technologies). Afterwards, sections (not washed, nor fixed) were covered with a standard microscope cover slip and directly examined. For control and CsA-treated sections equal exposure times were set at the microscope.

4.4. Gene expression analyses

4.4.1. RNA Isolation

For RNA isolation, OTCs were harvested 24h after the last medium exchange including DMSO or CsA treatment. 12 OTCs were harvested in one run. During harvesting OTCs remained in conditioned medium outside the incubator. OTCs were removed from the insert and cut into halve, one-third or one-quarter; edges were as well removed (Figure 4.1).

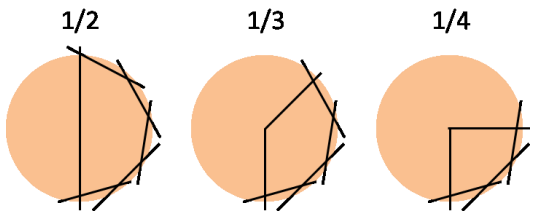

Figure 4.1 OTC cut template for RNA isolation.
Top view of an OTC, which was cut into halve (1/2), one-third (1/3) or one-quarter (1/4). Black lines: cutting edge.

The cut OTC sample was put back into conditioned medium until all OTCs were cut into appropriate samples. Afterwards all samples were transferred to 1 mg ml^{-1} Dispase II (Roche) in conditioned medium. After 1h at 37°C samples were all transferred back to conditioned medium without Dispase II. One after the other sample was separated into the dermal and epidermal compartment and transferred to 1 ml TRIzol Reagent (Life Technologies), frozen in liquid nitrogen and stored at -80°C. Alternatively samples were frozen without TRIzol reagent. TRIzol was then added to the sample after thawing prior to subsequent steps. In case separation of dermal and epidermal compartment was not necessary, samples were directly transferred to TRIzol without Dispase II treatment.

Samples in TRIzol were homogenized with the help of the FastPrep (MP Biomedicals) and the addition of ceramic beads (1.4/2.8 mm, Precellys). Samples were mixed twice (30 sec at speed 6.0) and kept on ice in between. Afterwards samples were kept at room temperature and 0.2 ml chloroform were added and shaken vigorously for 15 sec by hand. Samples were then left standing at room temperature for 3 min. Samples were spun for 15 min (11,500 rpm) at 4°C. After centrifugation 3 phases were visible. The upper aqueous phase was transferred to a fresh tube and 500 µl of isopropyl alcohol were added per 600 µl aqueous phase for RNA precipitation. Samples were mixed and incubated for 10 min at room temperature. Afterwards samples were spun for 10 min (11,500 rpm) at 4°C, the supernatant was removed and the pellet was washed with 1ml 75% ethanol. After one more centrifugation (10 min, 9,200 rpm, 4°C) the ethanol was removed and the pellet dried for 10 min at room temperature. The dried pellet was dissolved in RNase-free H_2O and the concentration was measured with a NanoDrop (Thermo Scientific).

4.4.2. Reverse transcription

RNA was transcribed to cDNA using the RevertAid H Minus First Strand cDNA Synthesis Kit (Thermo Scientific) according to the manufacturers protocol; oligo $(dt)_{18}$ primers were used. cDNA was directly used or stored at 4°C for short time storage.

4.4.3. Quantitative RT-PCR

Quantification of RNA was done using the Universal Probe Library system from Roche. Measurements were done in technical duplicates in 96-well plates with the LightCycler480 Instrument II (Roche). Reactions were mixed according to the manufacturer's protocol (0.4 µM forward and reverse primer, 0.1 µM UPL probe, the LightCycler 480 MasterMix and 50 ng cDNA). The primers (Table 4.6) were designed using the 'Universal ProbeLibrary Assay Design Center' (Roche) with the standard settings, including the parameter 'intron spanning'. Following settings were used for amplification: Pre-incubation (10 min, 95°C), 45 cycles (10 sec 95°C [ramp rate 4.4°C/sec], 30 sec 60°C [ramp rate 2.2°C/sec] and 1 sec 72°C [ramp rate 4.4°C/sec]). Fluorescence measurements were

done after each cycle. The crossing point (CP) was obtained by the 'Second Derivative Maximum Method' (LightCylcer 480 Software, Roche).

Fold changes from one experiment were calculated according to (Pfaffl 2001) considering the efficiencies of the primers (Table 4.6). RNA samples from one experiment were compared to the mean CP value of all control (solvent) replicates from that experiment (Figure 4.2). Fold changes were calculated for all control samples ($control_{mean}$ vs. $control_{individual}$) and stimulant samples ($control_{mean}$ vs. $stimulant_{individual}$). Calculations were done with samples from one cell culture experiment. Nevertheless, results from different cell culture experiments are presented together in one graph if stated in the legend. Data is presented as mean and the standard error of the mean.

$$\frac{\mathrm{E\ (gene\ of\ interest)}^{[\mathrm{meanCP\ (control)-CP\ (sample\ of\ interest)}]}}{\mathrm{E\ (GAPDH)}^{[\mathrm{meanCP\ (control)-CP\ (sample\ of\ interest)}]}}$$

Figure 4.2 Equation for fold change calculations from qRT-PCR.
E: Efficiency. CP: crossing point. Control: OTC treated with respective solvent. Sample of interest: RNA samples from OTCs treated with DMSO, PBS, CsA, UV, UV+CsA, CXCL14, DEFB4B or IGFL1.

Table 4.6 qRT-PCR primer

Gene name	Forward primer	Reverse primer	Probe	Efficiencies
ATF3	cgtgagtcctcggtgctc	gcctgggtgttgaagcat	#1	1.985
ATF4	ccagcgacaaggctaagg	tctccaacatccaatctgtcc	#76	1.912
ATF5	gctcccaccttctttcttcag	caaggcgaaagtggaagact	#70	2
CRNN	caactgcacagcgctcac	tccacagttgctggatcgt	#24	1.949
CSF2	tctcagaaatgtttgacctcca	gcccttgagcttggtgag	#1	2
CXCL14	acgtgaagaagctggaaatga	tgacctcggtacctggacac	#9	2
DEFB4A	tcagccatgagggtcttgta	ggatcgcctataccaccaaa	#35	1.948
EGF	catccattggcaaaaccag	aacaccaagcagttccaagc	#75	2
ELF3	ttggtactgaccctgagcaa	ttggtagctgatccagtccag	#45	1.915
FGF7	aagggacccaagagatgaaga	cctttgattgccacaattcc	#59	1.93
FLG	ggactctgagaggcgatctg	tgctcccgagaagatccat	#38	1.958
GAPDH	agccacatcgctcagacac	gcccaatacgaccaaatcc	#60	1.948
HGF	cagcatgtcctcctgcatc	tcttttcctttgtccctctgc	#15	1.87
IGFL1	ggctgcatcgtagctgtctt	gcacagcatcaggtaaggagt	#80	1.944
KRT10	atgagctgaccctgaccaag	cagtggacacatttcgaagg	#80	1.923
LCE1B	ctgctgtggaggagggagt	tttggccatttgtgttcttct	#75	2
LCE2A	ggagaaacttgcaaccagga	tgtgtcagcccaaggaaag	#2	2
LCE3A	cagcagaaccagcagcagt	ggaagctggaggcagacac	#75	2
MMP1	gctaacctttgatgctataactacga	tttgtgcgcatgtagaatctg	#7	1.62
MMP3	cagtttgctcagcctatcca	tcacatctttttcgaggtcgt	#58	1.9
MMP10	gtgctgttgtgtctgccagt	tcacatccttttcgaggttgta	#13	2
SPRR2B	tgctgcccaactcctaaact	tgcactgctgctgttgataa	#67	2

4.4.4. Whole genome RNA expression profiles

Whole genome RNA expression profiling was done from three samples per condition. In order to get very pure samples, RNA isolated by TRIzol was additional processed using the RNeasy Mini kit (Qiagen) according to the manufacturer's protocol 'RNA Cleanup' including the DNase steps.

Subsequent cDNA synthesis, labeling, hybridization and image acquisition was performed by the DKFZ Genomics and Proteomics Core Facility. The following Chip was used: Illumina HumanHT-12 v 4.0 Expression BeadChip.

4.4.5. Analysis of whole genome RNA expression profiles

4.4.5.1. Chipster

Raw gene expression data was analyzed with the open source software Chipster 3.8.1 (http://chipster.csc.fi/). If not stated otherwise, standard settings were applied. For normalization the Illumina function was used with the following settings: normalization method (quantile), Illumina software version (GenomeStudio or BeadStudio 3), Chip type (Human-HT12v4), Identifier type (ProbeID). Subsequently, the data was preprocessed by 'Remove missing values'. Finally, differential gene expression was determined by 'Two groups tests' with the following settings: Test (empirical Bayes), p-value adjustment method (BH), p-value threshold (0.01).

Non-metric multidimensional scaling (NMDS) and visualization of hierarchical clustering (dendrogram based on Pearson correlation and average linking method) were performed from normalized data.

4.4.5.2. Ingenuity® Pathway Analysis (IPA)

If not stated otherwise, standard settings were applied. Data sets with differentially expressed genes created with Chipster were imported into IPA®. Data sets were analyzed using the 'Core Analysis' using 'HumanHT-12 v 4.0' as reference gene set. With the function 'Comparison Analysis' different data sets were compared to each other.

4.4.5.3. Heat maps of 'epidermal development' genes

Data sets of differentially expressed genes were filtered by the GO-term (GO-0008544) 'epidermal development' using Chipster. These filtered data sets were imported to IPA. Using the function 'Compare' the gene sets were aligned and sorted. Afterwards the data sets were exported to Excel. The heat maps were created by Lars-Lennart Oettl (ZI Mannheim) using MATLAB (The MAthWorks).

5. REFERENCES

Abikhair M, Mitsui H, Yanofsky V, Roudiani N, Ovits C, Bryan T, Oberyszyn TM, Tober KL, Gonzalez J, Krueger JG, Felsen D, Carucci JA (2016). Cyclosporine A immunosuppression drives catastrophic squamous cell carcinoma through IL-22. *JCI Insight*. **1**.

Abiko Y, Nishimura M, Kusano K, Yamazaki M, Arakawa T, Takuma T, Kaku T (2003). Upregulated expression of human beta defensin-1 and -3 mRNA during differentiation of keratinocyte immortalized cell lines, HaCaT and PHK16-0b. *J Dermatol Sci*. **31**, 225-228.

Adami J, Gabel H, Lindelof B, Ekstrom K, Rydh B, Glimelius B, Ekbom A, Adami HO, Granath F (2003). Cancer risk following organ transplantation: a nationwide cohort study in Sweden. *Br J Cancer*. **89**, 1221-1227.

Aramburu J, Heitman J, Crabtree GR (2004). Calcineurin: a central controller of signalling in eukaryotes. *EMBO Rep*. **5**, 343-348.

Aramburu J, Yaffe MB, Lopez-Rodriguez C, Cantley LC, Hogan PG, Rao A (1999). Affinity-driven peptide selection of an NFAT inhibitor more selective than cyclosporin A. *Science*. **285**, 2129-2133.

Bahner JD, Bordeaux JS (2013). Non-melanoma skin cancers: photodynamic therapy, cryotherapy, 5-fluorouracil, imiquimod, diclofenac, or what? Facts and controversies. *Clinics in dermatology*. **31**, 792-798.

Benjamin CL, Melnikova VO, Ananthaswamy HN (2008). P53 protein and pathogenesis of melanoma and nonmelanoma skin cancer. *Adv Exp Med Biol*. **624**, 265-282.

Berg D, Otley CC (2002). Skin cancer in organ transplant recipients: Epidemiology, pathogenesis, and management. *Journal of the American Academy of Dermatology*. **47**, 1-20.

Bergboer JG, Tjabringa GS, Kamsteeg M, van Vlijmen-Willems IM, Rodijk-Olthuis D, Jansen PA, Thuret JY, Narita M, Ishida-Yamamoto A, Zeeuwen PL, Schalkwijk J (2011). Psoriasis risk genes of the late cornified envelope-3 group are distinctly expressed compared with genes of other LCE groups. *Am J Pathol*. **178**, 1470-1477.

Bergboer JG, Zeeuwen PL, Schalkwijk J (2012). Genetics of psoriasis: evidence for epistatic interaction between skin barrier abnormalities and immune deviation. *J Invest Dermatol*. **132**, 2320-2331.

Berning M, Pratzel-Wunder S, Bickenbach JR, Boukamp P (2015). Three-Dimensional In Vitro Skin and Skin Cancer Models Based on Human Fibroblast-Derived Matrix. *Tissue engineering. Part C, Methods*. **21**, 958-970.

Bhora FY, Dunkin BJ, Batzri S, Aly HM, Bass BL, Sidawy AN, Harmon JW (1995). Effect of growth factors on cell proliferation and epithelialization in human skin. *J Surg Res*. **59**, 236-244.

Biniek K, Levi K, Dauskardt RH (2012). Solar UV radiation reduces the barrier function of human skin. *Proc Natl Acad Sci U S A*. **109**, 17111-17116.

Bordea C, Wojnarowska F, Millard PR, Doll H, Welsh K, Morris PJ (2004). Skin cancers in renal-transplant recipients occur more frequently than previously recognized in a temperate climate. *Transplantation*. **77**, 574-579.

Borel JF, Feurer C, Gubler HU, Stahelin H (1976). Biological effects of cyclosporin A: a new antilymphocytic agent. *Agents Actions*. **6**, 468-475.

Bornstein S, Schmidt M, Choonoo G, Levin T, Gray J, Thomas CR, Jr., Wong M, McWeeney S (2016). IL-10 and integrin signaling pathways are associated with head and neck cancer progression. *BMC Genomics*. **17**, 38.

Boukamp P (2005a). Non-melanoma skin cancer: what drives tumor development and progression? *Carcinogenesis*. **26**, 1657-1667.

Boukamp P (2005b). UV-induced skin cancer: similarities--variations. *J Dtsch Dermatol Ges*. **3**, 493-503.

Boukamp P, Petrussevska RT, Breitkreutz D, Hornung J, Markham A, Fusenig NE (1988). Normal keratinization in a spontaneously immortalized aneuploid human keratinocyte cell line. *J Cell Biol*. **106**, 761-771.

Boukamp P, Stanbridge EJ, Foo DY, Cerutti PA, Fusenig NE (1990). c-Ha-ras oncogene expression in immortalized human keratinocytes (HaCaT) alters growth potential in vivo but lacks correlation with malignancy. *Cancer Res*. **50**, 2840-2847.

Bouwes Bavinck JN, Hardie DR, Green A, Cutmore S, MacNaught A, O'Sullivan B, Siskind V, Van Der Woude FJ, Hardie IR (1996). The risk of skin cancer in renal transplant recipients in Queensland, Australia. A follow-up study. *Transplantation*. **61**, 715-721.

Boyd S, Virolainen S, Parssinen J, Skoog T, van Hogerlinden M, Latonen L, Kyllonen L, Toftgard R, Saarialho-Kere U (2009). MMP-10 (Stromelysin-2) and MMP-21 in human and murine squamous cell cancer. *Exp Dermatol*. **18**, 1044-1052.

Brash DE, Rudolph JA, Simon JA, Lin A, McKenna GJ, Baden HP, Halperin AJ, Ponten J (1991). A role for sunlight in skin cancer: UV-induced p53 mutations in squamous cell carcinoma. *Proc Natl Acad Sci U S A*. **88**, 10124-10128.

Brockbank EC, Bridges J, Marshall CJ, Sahai E (2005). Integrin beta1 is required for the invasive behaviour but not proliferation of squamous cell carcinoma cells in vivo. *Br J Cancer*. **92**, 102-112.

Brougham ND, Dennett ER, Cameron R, Tan ST (2012). The incidence of metastasis from cutaneous squamous cell carcinoma and the impact of its risk factors. *J Surg Oncol*. **106**, 811-815.

Brummer C, Nerlich A, Rabes HM (1993). Excessive basement membrane material production by epithelial tumors induced by dimethylnitrosamine in rat kidneys. *Virchows Arch B Cell Pathol Incl Mol Pathol*. **63**, 271-276.

Burnworth B, Arendt S, Muffler S, Steinkraus V, Brocker EB, Birek C, Hartschuh W, Jauch A, Boukamp P (2007). The multi-step process of human skin carcinogenesis: a role for p53, cyclin D1, hTERT, p16, and TSP-1. *Eur J Cell Biol*. **86**, 763-780.

Burnworth B, Popp S, Stark HJ, Steinkraus V, Brocker EB, Hartschuh W, Birek C, Boukamp P (2006). Gain of 11q/cyclin D1 overexpression is an essential early step in skin cancer development and causes abnormal tissue organization and differentiation. *Oncogene*. **25**, 4399-4412.

Cabral A, Sayin A, de Winter S, Fischer DF, Pavel S, Backendorf C (2001). SPRR4, a novel cornified envelope precursor: UV-dependent epidermal expression and selective incorporation into fragile envelopes. *J Cell Sci*. **114**, 3837-3843.

Campistol JM, Eris J, Oberbauer R, Friend P, Hutchison B, Morales JM, Claesson K, Stallone G, Russ G, Rostaing L, Kreis H, Burke JT, Brault Y, Scarola JA, Neylan JF (2006). Sirolimus therapy after early cyclosporine withdrawal reduces the risk for cancer in adult renal transplantation. *J Am Soc Nephrol*. **17**, 581-589.

Candi E, Schmidt R, Melino G (2005). The cornified envelope: a model of cell death in the skin. *Nat Rev Mol Cell Biol*. **6**, 328-340.

Caroti L, Zanazzi M, Paudice N, Tsalouchos A, Carta P, Larti A, Pimpinelli N, Moscarelli L, Salvadori M, Bertoni E (2012). Conversion from calcineurin inhibitors to everolimus with low-dose cyclosporine in renal transplant recipients with squamous cell carcinoma of the skin. *Transplant Proc*. **44**, 1926-1927.

Carucci JA (2004). Cutaneous oncology in organ transplant recipients: meeting the challenge of squamous cell carcinoma. *J Invest Dermatol*. **123**, 809-816.

Chang LK, Johnson EM, Jr. (2002). Cyclosporin A inhibits caspase-independent death of NGF-deprived sympathetic neurons: a potential role for mitochondrial permeability transition. *J Cell Biol*. **157**, 771-781.

Chen JD, Lapiere JC, Sauder DN, Peavey C, Woodley DT (1995). Interleukin-1 alpha stimulates keratinocyte migration through an epidermal growth factor/transforming growth factor-alpha-independent pathway. *J Invest Dermatol*. **104**, 729-733.

Cherpelis BS, Marcusen C, Lang PG (2002). Prognostic factors for metastasis in squamous cell carcinoma of the skin. *Dermatol Surg*. **28**, 268-273.

Chmielowiec J, Borowiak M, Morkel M, Stradal T, Munz B, Werner S, Wehland J, Birchmeier C, Birchmeier W (2007). c-Met is essential for wound healing in the skin. *J Cell Biol*. **177**, 151-162.

Chrysalyne D. Schmults M, MSCE; Pritesh S. Karia, MPH; Joi B. Carter, MD; Jiali Han, PhD; Abrar A. Qureshi, MD, MPH (2013). Factors Predictive of Recurrence and Death From Cutaneous Squamous Cell CarcinomaA 10-Year, Single-Institution Cohort Study.

Coghill AE, Johnson LG, Berg D, Resler AJ, Leca N, Madeleine MM (2016). Immunosuppressive Medications and Squamous Cell Skin Carcinoma: Nested Case-Control Study Within the Skin Cancer after Organ Transplant (SCOT) Cohort. *Am J Transplant*. **16**, 565-573.

Crabtree GR (1999). Generic signals and specific outcomes: signaling through Ca2+, calcineurin, and NF-AT. *Cell*. **96**, 611-614.

Crabtree GR, Schreiber SL (2009). SnapShot: Ca2+-calcineurin-NFAT signaling. *Cell*. **138**, 210, 210 e211.

Cravedi P, Ruggenenti P, Remuzzi G (2010). Sirolimus for calcineurin inhibitors in organ transplantation: contra. *Kidney Int*. **78**, 1068-1074.

Dannewitz B, Edrich C, Tomakidi P, Kohl A, Gabbert O, Eickholz P, Steinberg T (2006). Elevated gene expression of MMP-1, MMP-10, and TIMP-1 reveal changes of molecules involved in turn-over of extracellular matrix in cyclosporine-induced gingival overgrowth. *Cell Tissue Res*. **325**, 513-522.

Dantal J, Hourmant M, Cantarovich D, Giral M, Blancho G, Dreno B, Soulillou J-P (1998). Effect of long-term immunosuppression in kidney-graft recipients on cancer incidence: randomised comparison of two cyclosporin regimens. *The Lancet*. **351**, 623-628.

de Oliveira VL, Keijsers RR, van de Kerkhof PC, Seyger MM, Fasse E, Svensson L, Latta M, Norsgaard H, Labuda T, Hupkens P, van Erp PE, Joosten I, Koenen HJ (2012). Humanized mouse model of skin inflammation is characterized by disturbed keratinocyte differentiation and influx of IL-17A producing T cells. *PLoS One*. **7**, e45509.

Dinehart SM, Nelson-Adesokan P, Cockerell C, Russell S, Brown R (1997). Metastatic cutaneous squamous cell carcinoma derived from actinic keratosis. *Cancer*. **79**, 920-923.

Donehower LA, Harvey M, Slagle BL, McArthur MJ, Montgomery CA, Jr., Butel JS, Bradley A (1992). Mice deficient for p53 are developmentally normal but susceptible to spontaneous tumours. *Nature*. **356**, 215-221.

Duncan FJ, Wulff BC, Tober KL, Ferketich AK, Martin J, Thomas-Ahner JM, Allen SD, Kusewitt DF, Oberyszyn TM, Vanbuskirk AM (2007). Clinically relevant immunosuppressants influence UVB-induced tumor size through effects on inflammation and angiogenesis. *Am J Transplant*. **7**, 2693-2703.

Durando B, Reichel J (2005). The relative effects of different systemic immunosuppressives on skin cancer development in organ transplant patients. *Dermatol Ther*. **18**, 1-11.

Durinck S, Ho C, Wang NJ, Liao W, Jakkula LR, Collisson EA, Pons J, Chan SW, Lam ET, Chu C, Park K, Hong SW, Hur JS, Huh N, Neuhaus IM, Yu SS, Grekin RC, Mauro TM, Cleaver JE, Kwok PY, LeBoit PE, Getz G, Cibulskis K, Aster JC, Huang H, Purdom E, Li J, Bolund L, Arron ST, Gray JW, Spellman PT, Cho RJ (2011). Temporal dissection of tumorigenesis in primary cancers. *Cancer Discov*. **1**, 137-143.

Dziunycz PJ, Lefort K, Wu X, Freiberger SN, Neu J, Djerbi N, Iotzowa-Weiss G, French LE, Dotto GP, Hofbauer GF (2014). The oncogene ATF3 is potentiated by cyclosporine A and ultraviolet light A. *J Invest Dermatol*. **134**, 1998-2004.

Eccles SA, Heckford SE, Alexander P (1980). Effect of cyclosporin A on the growth and spontaneous metastasis of syngeneic animal tumours. *Br J Cancer*. **42**, 252-259.

El Ghalbzouri A, Hensbergen P, Gibbs S, Kempenaar J, van der Schors R, Ponec M (2004). Fibroblasts facilitate re-epithelialization in wounded human skin equivalents. *Lab Invest*. **84**, 102-112.

Emtage P, Vatta P, Arterburn M, Muller MW, Park E, Boyle B, Hazell S, Polizotto R, Funk WD, Tang YT (2006). IGFL: A secreted family with conserved cysteine residues and similarities to the IGF superfamily. *Genomics*. **88**, 513-520.

Ensley RD, Bristow MR, Olsen SL, Taylor DO, Hammond EH, O'Connell JB, Dunn D, Osburn L, Jones KW, Kauffman RS, et al. (1993). The use of mycophenolate mofetil (RS-61443) in human heart transplant recipients. *Transplantation*. **56**, 75-82.

Errasti P, Izquierdo D, Martin P, Errasti M, Slon F, Romero A, Lavilla FJ (2010). Pneumonitis associated with mammalian target of rapamycin inhibitors in renal transplant recipients: a single-center experience. *Transplant Proc*. **42**, 3053-3054.

Espinosa JR, Samy KP, Kirk AD (2016). Memory T cells in organ transplantation: progress and challenges. *Nature reviews. Nephrology*. **12**, 339-347.

Eun HM, Pak CY, Kim CJ, McArthur RG, Yoon JW (1987). Role of cyclosporin A in macromolecular synthesis of beta-cells. *Diabetes*. **36**, 952-958.

Euvrard S, Kanitakis J, Claudy A (2003). Skin cancers after organ transplantation. *N Engl J Med*. **348**, 1681-1691.

Euvrard S, Kanitakis J, Decullier E, Butnaru AC, Lefrancois N, Boissonnat P, Sebbag L, Garnier JL, Pouteil-Noble C, Cahen R, Morelon E, Touraine JL, Claudy A, Chapuis F (2006). Subsequent skin cancers in kidney and heart transplant recipients after the first squamous cell carcinoma. *Transplantation*. **81**, 1093-1100.

Feldmeyer L, Hofbauer GF, Boni T, French LE, Hafner J (2012). Mammalian target of rapamycin (mTOR) inhibitors slow skin carcinogenesis, but impair wound healing. *Br J Dermatol*. **166**, 422-424.

Ferreira M, Fujiwara H, Morita K, Watt FM (2009). An activating beta1 integrin mutation increases the conversion of benign to malignant skin tumors. *Cancer Res*. **69**, 1334-1342.

Fisher GJ, Duell EA, Nickoloff BJ, Annesley TM, Kowalke JK, Ellis CN, Voorhees JJ (1988). Levels of cyclosporin in epidermis of treated psoriasis patients differentially inhibit growth of keratinocytes cultured in serum free versus serum containing media. *J Invest Dermatol*. **91**, 142-146.

Fortina AB, Piaserico S, Alaibac M, Peserico A (2009). Squamous cell carcinoma. *Cancer treatment and research*. **146**, 241-261.

Freije A, Molinuevo R, Ceballos L, Cagigas M, Alonso-Lecue P, Rodriguez R, Menendez P, Aberdam D, De Diego E, Gandarillas A (2014). Inactivation of p53 in Human Keratinocytes Leads to Squamous Differentiation and Shedding via Replication Stress and Mitotic Slippage. *Cell Rep*. **9**, 1349-1360.

Frye M, Bargon J, Gropp R (2001). Expression of human beta-defensin-1 promotes differentiation of keratinocytes. *J Mol Med (Berl)*. **79**, 275-282.

Fuentes JJ, Genesca L, Kingsbury TJ, Cunningham KW, Perez-Riba M, Estivill X, de la Luna S (2000). DSCR1, overexpressed in Down syndrome, is an inhibitor of calcineurin-mediated signaling pathways. *Hum Mol Genet*. **9**, 1681-1690.

Fung J, Abu-Elmagd K, Jain A, Gordon R, Tzakis A, Todo S, Takaya S, Alessiani M, Demetris A, Bronster O, et al. (1991). A randomized trial of primary liver transplantation under immunosuppression with FK 506 vs cyclosporine. *Transplant Proc*. **23**, 2977-2983.

Ganz T (2005). Defensins and other antimicrobial peptides: a historical perspective and an update. *Comb Chem High Throughput Screen*. **8**, 209-217.

Garrett GL, Lowenstein SE, Singer JP, He SY, Arron ST (2016). Trends of skin cancer mortality after transplantation in the United States: 1987 to 2013. *J Am Acad Dermatol*. **75**, 106-112.

Geigl JB, Uhrig S, Speicher MR (2006). Multiplex-fluorescence in situ hybridization for chromosome karyotyping. *Nat Protoc*. **1**, 1172-1184.

Goldstein J, Roth E, Roberts N, Zwick R, Lin S, Fletcher S, Tadeu A, Wu C, Beck A, Zeiss C, Suarez-Farinas M, Horsley V (2015). Loss of endogenous Nfatc1 reduces the rate of DMBA/TPA-induced skin tumorigenesis. *Mol Biol Cell*. **26**, 3606-3614.

Group TCMTS (1986). A randomized clinical trial of cyclosporine in cadaveric renal transplantation. Analysis at three years. The Canadian Multicentre Transplant Study Group. *N Engl J Med*. **314**, 1219-1225.

Guba M, von Breitenbuch P, Steinbauer M, Koehl G, Flegel S, Hornung M, Bruns CJ, Zuelke C, Farkas S, Anthuber M, Jauch KW, Geissler EK (2002). Rapamycin inhibits primary and metastatic tumor growth by antiangiogenesis: involvement of vascular endothelial growth factor. *Nat Med*. **8**, 128-135.

Gutschalk CM, Herold-Mende CC, Fusenig NE, Mueller MM (2006). Granulocyte colony-stimulating factor and granulocyte-macrophage colony-stimulating factor promote malignant growth of cells from head and neck squamous cell carcinomas in vivo. *Cancer Res*. **66**, 8026-8036.

Haider AS, Peters SB, Kaporis H, Cardinale I, Fei J, Ott J, Blumenberg M, Bowcock AM, Krueger JG, Carucci JA (2006). Genomic analysis defines a cancer-specific gene expression signature for human squamous cell carcinoma and distinguishes malignant hyperproliferation from benign hyperplasia. *J Invest Dermatol*. **126**, 869-881.

Han W, Ming M, He TC, He YY (2010). Immunosuppressive cyclosporin A activates AKT in keratinocytes through PTEN suppression: implications in skin carcinogenesis. *J Biol Chem*. **285**, 11369-11377.

Han W, Soltani K, Ming M, He YY (2012). Deregulation of XPC and CypA by cyclosporin A: an immunosuppression-independent mechanism of skin carcinogenesis. *Cancer Prev Res (Phila)*. **5**, 1155-1162.

Hanlon A, O'Neill M, Fang F, Chen H, Lott J, Wigger M, Stasko T (2013). Gene expression profiling for cardiac rejection surveillance is not predictive of post-transplantation skin cancer. *Dermatol Surg*. **39**, 1507-1513.

Haratake A, Uchida Y, Schmuth M, Tanno O, Yasuda R, Epstein JH, Elias PM, Holleran WM (1997). UVB-induced alterations in permeability barrier function: roles for epidermal hyperproliferation and thymocyte-mediated response. *J Invest Dermatol*. **108**, 769-775.

Hardinger KL, Brennan DC (2013). Novel immunosuppressive agents in kidney transplantation. *World J Transplant*. **3**, 68-77.

Harwood CA, Mesher D, McGregor JM, Mitchell L, Leedham-Green M, Raftery M, Cerio R, Leigh IM, Sasieni P, Proby CM (2013). A surveillance model for skin cancer in organ transplant recipients: a 22-year prospective study in an ethnically diverse population. *Am J Transplant*. **13**, 119-129.

Harwood CA, Proby CM, Inman GJ, Leigh IM (2016). The Promise of Genomics and the Development of Targeted Therapies for Cutaneous Squamous Cell Carcinoma. *Acta Derm Venereol*. **96**, 3-16.

Herman M, Weinstein T, Korzets A, Chagnac A, Ori Y, Zevin D, Malachi T, Gafter U (2001). Effect of cyclosporin A on DNA repair and cancer incidence in kidney transplant recipients. *J Lab Clin Med*. **137**, 14-20.

Hermann-Kleiter N, Baier G (2010). NFAT pulls the strings during CD4+ T helper cell effector functions. *Blood*. **115**, 2989-2997.

Hiesse C, Larue JR, Kriaa F, Blanchet P, Bellamy J, Benoit G, Charpentier B (1995). Incidence and type of malignancies occurring after renal transplantation in conventionally and in cyclosporine-treated recipients: single-center analysis of a 20-year period in 1600 patients. *Transplant Proc*. **27**, 2450-2451.

Ho VC (2004). The use of ciclosporin in psoriasis: a clinical review. *Br J Dermatol*. **150 Suppl 67**, 1-10.

Hodge MR, Ranger AM, Charles de la Brousse F, Hoey T, Grusby MJ, Glimcher LH (1996). Hyperproliferation and dysregulation of IL-4 expression in NF-ATp-deficient mice. *Immunity*. **4**, 397-405.

Hofbauer G (2010). [Immunosuppressive therapy after transplantation. Dermatologic relevance and pathomechanisms]. *Hautarzt*. **61**, 214-219.

Hojo M, Morimoto T, Maluccio M, Asano T, Morimoto K, Lagman M, Shimbo T, Suthanthiran M (1999). Cyclosporine induces cancer progression by a cell-autonomous mechanism. *Nature*. **397**, 530-534.

Horsley V, Aliprantis AO, Polak L, Glimcher LH, Fuchs E (2008). NFATc1 balances quiescence and proliferation of skin stem cells. *Cell*. **132**, 299-310.

Huang C, Mattjus P, Ma WY, Rincon M, Chen NY, Brown RE, Dong Z (2000). Involvement of nuclear factor of activated T cells activation in UV response. Evidence from cell culture and transgenic mice. *J Biol Chem*. **275**, 9143-9149.

Huang YH, Ma YL, Ma L, Mao JL, Zhang Y, Du MR, Li DJ (2014). Cyclosporine A improves adhesion and invasion of mouse preimplantation embryos via upregulating integrin beta3 and matrix metalloproteinase-9. *Int J Clin Exp Pathol*. **7**, 1379-1388.

Ikoma T, Ozawa S, Suzuki K, Kondo T, Maehata Y, Lee MC, Hata R, Kubota E (2012). Calcium-calmodulin signaling induced by epithelial cell differentiation upregulates BRAK/CXCL14 expression via the binding of SP1 to the BRAK promoter region. *Biochem Biophys Res Commun*. **420**, 217-222.

Ingvar A, Smedby KE, Lindelof B, Fernberg P, Bellocco R, Tufveson G, Hoglund P, Adami J (2010). Immunosuppressive treatment after solid organ transplantation and risk of post-transplant cutaneous squamous cell carcinoma. *Nephrol Dial Transplant*. **25**, 2764-2771.

Jackson B, Tilli CM, Hardman MJ, Avilion AA, MacLeod MC, Ashcroft GS, Byrne C (2005). Late cornified envelope family in differentiating epithelia--response to calcium and ultraviolet irradiation. *J Invest Dermatol*. **124**, 1062-1070.

Janes SM, Watt FM (2006). New roles for integrins in squamous-cell carcinoma. *Nat Rev Cancer*. **6**, 175-183.

Jensen JM, Pfeiffer S, Witt M, Brautigam M, Neumann C, Weichenthal M, Schwarz T, Folster-Holst R, Proksch E (2009). Different effects of pimecrolimus and betamethasone on the skin barrier in patients with atopic dermatitis. *J Allergy Clin Immunol*. **123**, 1124-1133.

Ji C, Yang B, Yang Z, Tu Y, Yang YL, He L, Bi ZG (2012). Ultra-violet B (UVB)-induced skin cell death occurs through a cyclophilin D intrinsic signaling pathway. *Biochem Biophys Res Commun*. **425**, 825-829.

Johansson A, Moller E (1990). Evidence that the immunosuppressive effects of FK506 and cyclosporine are identical. *Transplantation*. **50**, 1001-1007.

Johnson JL, Koetsier JL, Sirico A, Agidi AT, Antonini D, Missero C, Green KJ (2014). The desmosomal protein desmoglein 1 aids recovery of epidermal differentiation after acute UV light exposure. *J Invest Dermatol*. **134**, 2154-2162.

Kakazu A, Chandrasekher G, Bazan HE (2004). HGF protects corneal epithelial cells from apoptosis by the PI-3K/Akt-1/Bad- but not the ERK1/2-mediated signaling pathway. *Invest Ophthalmol Vis Sci*. **45**, 3485-3492.

Karia PS, Han J, Schmults CD (2013). Cutaneous squamous cell carcinoma: estimated incidence of disease, nodal metastasis, and deaths from disease in the United States, 2012. *J Am Acad Dermatol*. **68**, 957-966.

Karimkhani C, Boyers LN, Dellavalle RP, Weinstock MA (2015). It's time for "keratinocyte carcinoma" to replace the term "nonmelanoma skin cancer". *J Am Acad Dermatol*. **72**, 186-187.

Kartasova T, van de Putte P (1988). Isolation, characterization, and UV-stimulated expression of two families of genes encoding polypeptides of related structure in human epidermal keratinocytes. *Mol Cell Biol*. **8**, 2195-2203.

Kashyap T, Rabinovitz I (2012). The calcium/calcineurin pathway promotes hemidesmosome stability through inhibition of beta4 integrin phosphorylation. *J Biol Chem*. **287**, 32440-32449.

Katsanos G, Donickier V (2009). Introduction - Historical Perspective. In *Skin Cancer after Organ Transplantation*. (TSC Group, ed): Springer, pp. 1-4.

Kawahara T, Kashiwagi E, Ide H, Li Y, Zheng Y, Ishiguro H, Miyamoto H (2015). The role of NFATc1 in prostate cancer progression: cyclosporine A and tacrolimus inhibit cell proliferation, migration, and invasion. *Prostate*. **75**, 573-584.

Kelly GE, Meikle W, Sheil AG (1987). Effects of immunosuppressive therapy on the induction of skin tumors by ultraviolet irradiation in hairless mice. *Transplantation*. **44**, 429-434.

Khorshid SM, Glover MT, Churchill L, McGregor JM, Proby CM (1996). p53 immunoreactivity in non-melanoma skin cancer from immunosuppressed and immunocompetent individuals: a comparative study of 246 tumours. *J Cutan Pathol*. **23**, 229-233.

Kim CH, Choi YS, Cheong KA, Lee AY (2013). Mechanism underlying the effect of combined therapy using glucosamine and low-dose cyclosporine A on the development of atopic dermatitis-like skin lesions in NC/Nga mice. *International immunopharmacology*. **15**, 424-432.

Kim M, Murrell DF (2015). Update on the pathogenesis of squamous cell carcinoma development in recessive dystrophic epidermolysis bullosa. *Eur J Dermatol*. **25 Suppl 1**, 30-32.

Koria P, Brazeau D, Kirkwood K, Hayden P, Klausner M, Andreadis ST (2003). Gene expression profile of tissue engineered skin subjected to acute barrier disruption. *J Invest Dermatol*. **121**, 368-382.

Krynitz B, Edgren G, Lindelof B, Baecklund E, Brattstrom C, Wilczek H, Smedby KE (2013). Risk of skin cancer and other malignancies in kidney, liver, heart and lung transplant recipients 1970 to 2008--a Swedish population-based study. *Int J Cancer*. **132**, 1429-1438.

Krynitz B, Lundh Rozell B, Lindelof B (2010). Differences in the peritumoural inflammatory skin infiltrate between squamous cell carcinomas in organ transplant recipients and immunocompetent patients. *Acta Derm Venereol*. **90**, 379-385.

Krynitz B, Olsson H, Lundh Rozell B, Lindelof B, Edgren G, Smedby KE (2016). Risk of basal cell carcinoma in Swedish organ transplant recipients: a population-based study. *Br J Dermatol*. **174**, 95-103.

Kubica AW, Brewer JD (2012). Melanoma in immunosuppressed patients. *Mayo Clin Proc*. **87**, 991-1003.

Kuivanen T, Jeskanen L, Kyllonen L, Isaka K, Saarialho-Kere U (2009). Matrix metalloproteinase-26 is present more frequently in squamous cell carcinomas of immunosuppressed compared with immunocompetent patients. *J Cutan Pathol*. **36**, 929-936.

Kupper TS, Lee F, Birchall N, Clark S, Dower S (1988). Interleukin 1 binds to specific receptors on human keratinocytes and induces granulocyte macrophage colony-stimulating factor mRNA and protein. A potential autocrine role for interleukin 1 in epidermis. *J Clin Invest*. **82**, 1787-1792.

Lambert SR, Mladkova N, Gulati A, Hamoudi R, Purdie K, Cerio R, Leigh I, Proby C, Harwood CA (2014). Key differences identified between actinic keratosis and cutaneous squamous cell carcinoma by transcriptome profiling. *Br J Cancer*. **110**, 520-529.

LeBoeuf NR, Schmults CD (2011). Update on the management of high-risk squamous cell carcinoma. *Seminars in cutaneous medicine and surgery*. **30**, 26-34.

Leigh IM, Eady RA, Heagerty AH, Purkis PE, Whitehead PA, Burgeson RE (1988). Type VII collagen is a normal component of epidermal basement membrane, which shows altered expression in recessive dystrophic epidermolysis bullosa. *J Invest Dermatol*. **90**, 639-642.

Leufke C, Leykauf J, Krunic D, Jauch A, Holtgreve-Grez H, Bohm-Steuer B, Brocker EB, Mauch C, Utikal J, Hartschuh W, Purdie KJ, Boukamp P (2014). The telomere profile distinguishes two classes of genetically distinct cutaneous squamous cell carcinomas. *Oncogene*. **33**, 3506-3518.

Lindelöf B, Jarnvik J, Ternesten-Bratel A, Granath F, Hedblad MA (2006). Mortality and Clinicopathological Features of Cutaneous Squamous Cell Carcinoma in Organ Transplant Recipients: A Study of the Swedish Cohort. *Acta Dermato-Venereologica*. **86**, 219-222.

Lindelof B, Sigurgeirsson B, Gabel H, Stern RS (2000). Incidence of skin cancer in 5356 patients following organ transplantation. *Br J Dermatol*. **143**, 513-519.

Lobito AA, Ramani SR, Tom I, Bazan JF, Luis E, Fairbrother WJ, Ouyang W, Gonzalez LC (2011). Murine insulin growth factor-like (IGFL) and human IGFL1 proteins are induced in inflammatory skin conditions and bind to a novel tumor necrosis factor receptor family member, IGFLR1. *J Biol Chem*. **286**, 18969-18981.

Lott DG, Manz R, Koch C, Lorenz RR (2010). Aggressive behavior of nonmelanotic skin cancers in solid organ transplant recipients. *Transplantation*. **90**, 683-687.

Maas-Szabowski N, Fusenig NE (1996). Interleukin-1-induced growth factor expression in postmitotic and resting fibroblasts. *J Invest Dermatol*. **107**, 849-855.

Maas-Szabowski N, Stark HJ, Fusenig NE (2000). Keratinocyte growth regulation in defined organotypic cultures through IL-1-induced keratinocyte growth factor expression in resting fibroblasts. *J Invest Dermatol*. **114**, 1075-1084.

Mackenzie KA, Wells JE, Lynn KL, Simcock JW, Robinson BA, Roake JA, Currie MJ (2010). First and subsequent nonmelanoma skin cancers: incidence and predictors in a population of New Zealand renal transplant recipients. *Nephrol Dial Transplant*. **25**, 300-306.

Mammucari C, Tommasi di Vignano A, Sharov AA, Neilson J, Havrda MC, Roop DR, Botchkarev VA, Crabtree GR, Dotto GP (2005). Integration of Notch 1 and calcineurin/NFAT signaling pathways in keratinocyte growth and differentiation control. *Dev Cell*. **8**, 665-676.

Manohar A, Shome SG, Lamar J, Stirling L, Iyer V, Pumiglia K, DiPersio CM (2004). Alpha 3 beta 1 integrin promotes keratinocyte cell survival through activation of a MEK/ERK signaling pathway. *J Cell Sci*. **117**, 4043-4054.

Marcil I, Stern RS (2000). Risk of developing a subsequent nonmelanoma skin cancer in patients with a history of nonmelanoma skin cancer: a critical review of the literature and meta-analysis. *Arch Dermatol*. **136**, 1524-1530.

Martincorena I, Roshan A, Gerstung M, Ellis P, Van Loo P, McLaren S, Wedge DC, Fullam A, Alexandrov LB, Tubio JM, Stebbings L, Menzies A, Widaa S, Stratton MR, Jones PH, Campbell PJ (2015). Tumor evolution. High burden and pervasive positive selection of somatic mutations in normal human skin. *Science*. **348**, 880-886.

Martinez-Cruz AB, Santos M, Lara MF, Segrelles C, Ruiz S, Moral M, Lorz C, Garcia-Escudero R, Paramio JM (2008). Spontaneous squamous cell carcinoma induced by the somatic inactivation of retinoblastoma and Trp53 tumor suppressors. *Cancer Res*. **68**, 683-692.

Martins VL, Vyas JJ, Chen M, Purdie K, Mein CA, South AP, Storey A, McGrath JA, O'Toole EA (2009). Increased invasive behaviour in cutaneous squamous cell carcinoma with loss of basement-membrane type VII collagen. *J Cell Sci*. **122**, 1788-1799.

Medyouf H, Ghysdael J (2008). The calcineurin/NFAT signaling pathway: a novel therapeutic target in leukemia and solid tumors. *Cell Cycle*. **7**, 297-303.

Mildner M, Eckhart L, Lengauer B, Tschachler E (2002). Hepatocyte growth factor/scatter factor inhibits UVB-induced apoptosis of human keratinocytes but not of keratinocyte-derived cell lines via the phosphatidylinositol 3-kinase/AKT pathway. *J Biol Chem*. **277**, 14146-14152.

Mildner M, Jin J, Eckhart L, Kezic S, Gruber F, Barresi C, Stremnitzer C, Buchberger M, Mlitz V, Ballaun C, Sterniczky B, Fodinger D, Tschachler E (2010). Knockdown of filaggrin impairs diffusion barrier function and increases UV sensitivity in a human skin model. *J Invest Dermatol*. **130**, 2286-2294.

Mitsui H, Suarez-Farinas M, Gulati N, Shah KR, Cannizzaro MV, Coats I, Felsen D, Krueger JG, Carucci JA (2014). Gene expression profiling of the leading edge of cutaneous squamous cell carcinoma: IL-24-driven MMP-7. *J Invest Dermatol*. **134**, 1418-1427.

Mueller AR, Platz KP, Bechstein WO, Schattenfroh N, Stoltenburg-Didinger G, Blumhardt G, Christe W, Neuhaus P (1994). Neurotoxicity after orthotopic liver transplantation. A comparison between cyclosporine and FK506. *Transplantation*. **58**, 155-170.

Ng YZ, Pourreyron C, Salas-Alanis JC, Dayal JH, Cepeda-Valdes R, Yan W, Wright S, Chen M, Fine JD, Hogg FJ, McGrath JA, Murrell DF, Leigh IM, Lane EB, South AP (2012). Fibroblast-derived dermal matrix drives development of aggressive cutaneous squamous cell carcinoma in patients with recessive dystrophic epidermolysis bullosa. *Cancer Res*. **72**, 3522-3534.

Niehues H, van Vlijmen-Willems IM, Bergboer JG, Kersten FF, Narita M, Hendriks WJ, van den Bogaard EH, Zeeuwen PL, Schalkwijk J (2015). Late cornified envelope (LCE) proteins: Distinct expression patterns of LCE2 and LCE3 members suggest non-redundant roles in human epidermis and other epithelia. *Br J Dermatol*.

Nuutila K, Siltanen A, Peura M, Bizik J, Kaartinen I, Kuokkanen H, Nieminen T, Harjula A, Aarnio P, Vuola J, Kankuri E (2012). Human skin transcriptome during superficial cutaneous wound healing. *Wound Repair Regen*. **20**, 830-839.

Obermueller E, Vosseler S, Fusenig NE, Mueller MM (2004). Cooperative autocrine and paracrine functions of granulocyte colony-stimulating factor and granulocyte-macrophage colony-stimulating factor in the progression of skin carcinoma cells. *Cancer Res*. **64**, 7801-7812.

Oliveira VD, Zankl H, Rath T (2004). Mutagenic and cytotoxic effects of immunosuppressive drugs on human lymphocyte cultures. *Exp Clin Transplant*. **2**, 273-279.

Ong CS, Keogh AM, Kossard S, Macdonald PS, Spratt PM (1999). Skin cancer in Australian heart transplant recipients. *J Am Acad Dermatol*. **40**, 27-34.

Ozturk S, Ayna TK, Cefle K, Palanduz S, Ciftci HS, Kaya SA, Diler AS, Turkmen A, Gurtekin M, Sever MS, Carin M (2008). Effect of cyclosporin A and tacrolimus on sister chromatid exchange frequency in renal transplant patients. *Genet Test*. **12**, 427-430.

Palmer CN, Irvine AD, Terron-Kwiatkowski A, Zhao Y, Liao H, Lee SP, Goudie DR, Sandilands A, Campbell LE, Smith FJ, O'Regan GM, Watson RM, Cecil JE, Bale SJ, Compton JG, DiGiovanna JJ, Fleckman P, Lewis-Jones S, Arseculeratne G, Sergeant A, Munro CS, El Houate B, McElreavey K, Halkjaer LB, Bisgaard H, Mukhopadhyay S, McLean WH (2006). Common loss-of-function variants of the epidermal barrier protein filaggrin are a major predisposing factor for atopic dermatitis. *Nat Genet*. **38**, 441-446.

Paul CF, Ho VC, McGeown C, Christophers E, Schmidtmann B, Guillaume JC, Lamarque V, Dubertret L (2003). Risk of malignancies in psoriasis patients treated with cyclosporine: a 5 y cohort study. *J Invest Dermatol*. **120**, 211-216.

Pena JA, Losi-Sasaki JL, Gooch JL (2010). Loss of calcineurin Aalpha alters keratinocyte survival and differentiation. *J Invest Dermatol*. **130**, 135-140.

Perez Ferriols A, Aguilera J, Aguilera P, de Argila D, Barnadas MA, de Cabo X, Carrrascosa JM, de Galvez Aranda MV, Gardeazabal J, Gimenez-Arnau A, Lecha M, Lorente J, Martinez-Lozano JA, Rodriguez Granados MT, Sola Y, Utrillas MP (2014). Determination of minimal erythema dose and anomalous reactions to UVA radiation by skin phototype. *Actas Dermosifiliogr*. **105**, 780-788.

Perez HC, Benavides X, Perez JS, Pabon MA, Tschen J, Maradei-Anaya SJ, Lopez L, Lozano E (2016). Basic aspects of the pathogenesis and prevention of non-melanoma skin cancer in solid organ transplant recipients: a review. *International journal of dermatology*.

Petter Jensen M, Svein Hansen, MDb, Bjørn Møller, MScb, Torbjørn Leivestad, MD, PhDc, Per Pfeffer, MD, PhDd, Odd Geiran, MD, PhDd, Per Fauchald, MD, PhDe, Svein Simonsen, MD, PhDe (1999). Skin cancer in kidney and heart transplant recipients and different long-term immunosuppressive therapy regimens.

Pfaffl MW (2001). A new mathematical model for relative quantification in real-time RT-PCR. *Nucleic Acids Res*. **29**, e45.

Pierceall WE, Goldberg LH, Tainsky MA, Mukhopadhyay T, Ananthaswamy HN (1991). Ras gene mutation and amplification in human nonmelanoma skin cancers. *Mol Carcinog*. **4**, 196-202.

Ponticelli C, Cucchiari D, Bencini P (2014). Skin cancer in kidney transplant recipients. *J Nephrol*. **27**, 385-394.

Popp FC, Eggenhofer E, Renner P, Slowik P, Lang SA, Kaspar H, Geissler EK, Piso P, Schlitt HJ, Dahlke MH (2008). Mesenchymal stem cells can induce long-term acceptance of solid organ allografts in synergy with low-dose mycophenolate. *Transpl Immunol*. **20**, 55-60.

Queille S, Luron L, Spatz A, Avril MF, Ribrag V, Duvillard P, Hiesse C, Sarasin A, Armand JP, Daya-Grosjean L (2007). Analysis of skin cancer risk factors in immunosuppressed renal transplant patients shows high levels of UV-specific tandem CC to TT mutations of the p53 gene. *Carcinogenesis*. **28**, 724-731.

Ramsay HM, Fryer AA, Hawley CM, Smith AG, Harden PN (2002). Non-melanoma skin cancer risk in the Queensland renal transplant population. *Br J Dermatol*. **147**, 950-956.

Ratushny V, Gober MD, Hick R, Ridky TW, Seykora JT (2012). From keratinocyte to cancer: the pathogenesis and modeling of cutaneous squamous cell carcinoma. *J Clin Invest*. **122**, 464-472.

Rival-Tringali AL1 ES, Decullier E, Claudy A, Faure M, Kanitakis J. (2009). Conversion from calcineurin inhibitors to sirolimus reduces vascularization and thickness of post-transplant cutaneous squamous cell carcinomas.

Rogers HW, Weinstock MA, Feldman SR, Coldiron BM (2015). Incidence Estimate of Nonmelanoma Skin Cancer (Keratinocyte Carcinomas) in the U.S. Population, 2012. *JAMA Dermatol*. **151**, 1081-1086.

Roh MR, Zheng Z, Kim HS, Kwon JE, Jeung HC, Rha SY, Chung KY (2012). Differential expression patterns of MMPs and their role in the invasion of epithelial premalignant tumors and invasive cutaneous squamous cell carcinoma. *Exp Mol Pathol*. **92**, 236-242.

Rubio-Casadevall J, Hernandez-Pujol AM, Ferreira-Santos MC, Morey-Esteve G, Vilardell L, Osca-Gelis G, Vilar-Coromina N, Marcos-Gragera R (2016). Trends in incidence and survival analysis in non-melanoma skin cancer from 1994 to 2012 in Girona, Spain: A population-based study. *Cancer Epidemiol*. **45**, 6-10.

Ruegg CP, Graf N, Muhleisen B, Szucs TD, French LE, Surber C, Hofbauer GF (2012). Squamous cell carcinoma of the skin induces considerable sustained cost of care in organ transplant recipients. *J Am Acad Dermatol*. **67**, 1242-1249.

Sachewsky N, Hunt J, Cooke MJ, Azimi A, Zarin T, Miu C, Shoichet MS, Morshead CM (2014). Cyclosporin A enhances neural precursor cell survival in mice through a calcineurin-independent pathway. *Dis Model Mech*. **7**, 953-961.

Saigal S, Norris S, Muiesan P, Rela M, Heaton N, O'Grady J (2002). Evidence of differential risk for posttransplantation malignancy based on pretransplantation cause in patients undergoing liver transplantation. *Liver Transpl*. **8**, 482-487.

Sakai M, Miyake H, Tashiro S, Okumura Y, Kido H (2004). Inhibitory effect of FK506 and cyclosporine A on the growth and invasion of human liver cancer cells. *J Med Invest*. **51**, 63-69.

Santini MP, Talora C, Seki T, Bolgan L, Dotto GP (2001). Cross talk among calcineurin, Sp1/Sp3, and NFAT in control of p21(WAF1/CIP1) expression in keratinocyte differentiation. *Proc Natl Acad Sci U S A*. **98**, 9575-9580.

Sapijaszko M, Zloty D, Bourcier M, Poulin Y, Janiszewski P, Ashkenas J (2015). Non-melanoma Skin Cancer in Canada Chapter 5: Management of Squamous Cell Carcinoma. *J Cutan Med Surg*. **19**, 249-259.

Sardarian A, Andisheh Tadbir A, Zal F, Amini F, Jafarian A, Khademi F, Mostafavi-Pour Z (2015). Altered oxidative status and integrin expression in cyclosporine A-treated oral epithelial cells. *Toxicol Mech Methods*. **25**, 98-104.

Savoia P, Trusolino L, Pepino E, Cremona O, Marchisio PC (1993). Expression and topography of integrins and basement membrane proteins in epidermal carcinomas: basal but not squamous cell carcinomas display loss of alpha 6 beta 4 and BM-600/nicein. *J Invest Dermatol*. **101**, 352-358.

Schlage P, Kockmann T, Sabino F, Kizhakkedathu JN, Auf dem Keller U (2015). Matrix Metalloproteinase 10 Degradomics in Keratinocytes and Epidermal Tissue Identifies Bioactive Substrates With Pleiotropic Functions. *Mol Cell Proteomics*. **14**, 3234-3246.

Schmidt C, Bladt F, Goedecke S, Brinkmann V, Zschiesche W, Sharpe M, Gherardi E, Birchmeier C (1995). Scatter factor/hepatocyte growth factor is essential for liver development. *Nature*. **373**, 699-702.

Servilla KS, Burnham DK, Daynes RA (1987). Ability of cyclosporine to promote the growth of transplanted ultraviolet radiation-induced tumors in mice. *Transplantation*. **44**, 291-295.

Sethi T, Rintoul RC, Moore SM, MacKinnon AC, Salter D, Choo C, Chilvers ER, Dransfield I, Donnelly SC, Strieter R, Haslett C (1999). Extracellular matrix proteins protect small cell lung cancer cells against apoptosis: a mechanism for small cell lung cancer growth and drug resistance in vivo. *Nat Med*. **5**, 662-668.

Sliwa M, Markovic D, Gabrusiewicz K, Synowitz M, Glass R, Zawadzka M, Wesolowska A, Kettenmann H, Kaminska B (2007). The invasion promoting effect of microglia on glioblastoma cells is inhibited by cyclosporin A. *Brain*. **130**, 476-489.

Smith KJ, Hamza S, Skelton H (2004). Histologic features in primary cutaneous squamous cell carcinomas in immunocompromised patients focusing on organ transplant patients. *Dermatol Surg*. **30**, 634-641.

Sollinger HW (1995). Mycophenolate mofetil for the prevention of acute rejection in primary cadaveric renal allograft recipients. U.S. Renal Transplant Mycophenolate Mofetil Study Group. *Transplantation*. **60**, 225-232.

Sommerer C, Konstandin M, Dengler T, Schmidt J, Meuer S, Zeier M, Giese T (2006). Pharmacodynamic monitoring of cyclosporine a in renal allograft recipients shows a quantitative relationship between immunosuppression and the occurrence of recurrent infections and malignancies. *Transplantation*. **82**, 1280-1285.

Speicher MR, Gwyn Ballard S, Ward DC (1996). Karyotyping human chromosomes by combinatorial multi-fluor FISH. *Nat Genet*. **12**, 368-375.

Stark LA, Arends MJ, McLaren KM, Benton EC, Shahidullah H, Hunter JA, Bird CC (1994). Accumulation of p53 is associated with tumour progression in cutaneous lesions of renal allograft recipients. *Br J Cancer*. **70**, 662-667.

Stegall MD, Simon M, Wachs ME, Chan L, Nolan C, Kam I (1997). Mycophenolate mofetil decreases rejection in simultaneous pancreas-kidney transplantation when combined with tacrolimus or cyclosporine. *Transplantation*. **64**, 1695-1700.

Suto H, Matsuda H, Mitsuishi K, Hira K, Uchida T, Unno T, Ogawa H, Ra C (1999). NC/Nga mice: a mouse model for atopic dermatitis. *Int Arch Allergy Immunol*. **120 Suppl 1**, 70-75.

Tang CL, Zhao HB, Li MQ, Du MR, Meng YH, Li DJ (2012). Focal adhesion kinase signaling is necessary for the Cyclosporin A-enhanced migration and invasion of human trophoblast cells. *Placenta*. **33**, 704-711.

Tiu J, Li H, Rassekh C, van der Sloot P, Kovach R, Zhang P (2006). Molecular basis of posttransplant squamous cell carcinoma: the potential role of cyclosporine a in carcinogenesis. *Laryngoscope*. **116**, 762-769.

Tremblay F, Fernandes M, Habbab F, de BEMD, Loertscher R, Meterissian S (2002). Malignancy after renal transplantation: incidence and role of type of immunosuppression. *Ann Surg Oncol*. **9**, 785-788.

Uehara Y, Minowa O, Mori C, Shiota K, Kuno J, Noda T, Kitamura N (1995). Placental defect and embryonic lethality in mice lacking hepatocyte growth factor/scatter factor. *Nature*. **373**, 702-705.

Ulrich C, Jurgensen JS, Degen A, Hackethal M, Ulrich M, Patel MJ, Eberle J, Terhorst D, Sterry W, Stockfleth E (2009). Prevention of non-melanoma skin cancer in organ transplant patients by regular use of a sunscreen: a 24 months, prospective, case-control study. *Br J Dermatol*. **161 Suppl 3**, 78-84.

Verdolini R, Amerio P, Goteri G, Bugatti L, Lucarini G, Mannello B, Filosa G, Offidani A, Brancorsini D, Biagini G, Giangiacomi M (2001). Cutaneous carcinomas and preinvasive neoplastic lesions. Role of MMP-2 and MMP-9 metalloproteinases in neoplastic invasion and their relationship with proliferative activity and p53 expression. *J Cutan Pathol*. **28**, 120-126.

Voskamp P, Bodmann CA, Koehl GE, Rebel HG, Van Olderen MG, Gaumann A, El Ghalbzouri A, Tensen CP, Bavinck JN, Willemze R, Geissler EK, De Gruijl FR (2013). Dietary immunosuppressants do not enhance UV-induced skin carcinogenesis, and reveal discordance between p53-mutant early clones and carcinomas. *Cancer Prev Res (Phila)*. **6**, 129-138.

Walter A, Barysch MJ, Behnke S, Dziunycz P, Schmid B, Ritter E, Gnjatic S, Kristiansen G, Moch H, Knuth A, Dummer R, van den Broek M (2010). Cancer-testis antigens and immunosurveillance in human cutaneous squamous cell and basal cell carcinomas. *Clin Cancer Res*. **16**, 3562-3570.

Wang NJ, Sanborn Z, Arnett KL, Bayston LJ, Liao W, Proby CM, Leigh IM, Collisson EA, Gordon PB, Jakkula L, Pennypacker S, Zou Y, Sharma M, North JP, Vemula SS, Mauro TM, Neuhaus IM, Leboit PE, Hur JS, Park K, Huh N, Kwok PY, Arron ST, Massion PP, Bale AE, Haussler D, Cleaver JE, Gray JW, Spellman PT, South AP, Aster JC, Blacklow SC, Cho RJ (2011). Loss-of-function mutations in Notch receptors in cutaneous and lung squamous cell carcinoma. *Proc Natl Acad Sci U S A*. **108**, 17761-17766.

Watson CJ, Dark JH (2012). Organ transplantation: historical perspective and current practice. *Br J Anaesth*. **108 Suppl 1**, i29-42.

Watt FM (2002). Role of integrins in regulating epidermal adhesion, growth and differentiation. *EMBO J*. **21**, 3919-3926.

Weaver VM, Lelievre S, Lakins JN, Chrenek MA, Jones JC, Giancotti F, Werb Z, Bissell MJ (2002). beta4 integrin-dependent formation of polarized three-dimensional architecture confers resistance to apoptosis in normal and malignant mammary epithelium. *Cancer Cell*. **2**, 205-216.

Wisgerhof HC, Edelbroek JR, de Fijter JW, Haasnoot GW, Claas FH, Willemze R, Bavinck JN (2010). Subsequent squamous- and basal-cell carcinomas in kidney-transplant recipients after the first skin cancer: cumulative incidence and risk factors. *Transplantation*. **89**, 1231-1238.

Wu H, Peisley A, Graef IA, Crabtree GR (2007). NFAT signaling and the invention of vertebrates. *Trends Cell Biol*. **17**, 251-260.

Wu X, Nguyen BC, Dziunycz P, Chang S, Brooks Y, Lefort K, Hofbauer GF, Dotto GP (2010). Opposing roles for calcineurin and ATF3 in squamous skin cancer. *Nature*. **465**, 368-372.

Wulff BC, Kusewitt DF, VanBuskirk AM, Thomas-Ahner JM, Duncan FJ, Oberyszyn TM (2008). Sirolimus reduces the incidence and progression of UVB-induced skin cancer in SKH mice even with co-administration of cyclosporine A. *J Invest Dermatol*. **128**, 2467-2473.

Yajima Y, Sueki H, Oguro T, Yoshida T, Iijima M (2008). Effects of oral administration of ciclosporin A on skin carcinogenesis: a study using the two-stage carcinogenesis protocol in mice. *Clin Exp Dermatol*. **33**, 478-483.

Yarosh DB, Pena AV, Nay SL, Canning MT, Brown DA (2005). Calcineurin inhibitors decrease DNA repair and apoptosis in human keratinocytes following ultraviolet B irradiation. *J Invest Dermatol*. **125**, 1020-1025.

Zheng X, Baker H, Hancock WS, Fawaz F, McCaman M, Pungor E, Jr. (2006). Proteomic analysis for the assessment of different lots of fetal bovine serum as a raw material for cell culture. Part IV. Application of proteomics to the manufacture of biological drugs. *Biotechnol Prog*. **22**, 1294-1300.

Zhou AY, Ryeom S (2014). Cyclosporin A promotes tumor angiogenesis in a calcineurin-independent manner by increasing mitochondrial reactive oxygen species. *Mol Cancer Res*. **12**, 1663-1676.

6. ABBREVIATIONS

µm	Micrometre
ATF3	Activating transcription factor 3
ATF4	Activating transcription factor 4
ATF5	Activating transcription factor 5
BCC	Basal cell carcinoma
BSA	Bovine serum albumin
CDKN2A	Cyclin dependent kinase inhibitor 2A
cm	Centimetre
CO2	Carbon dioxide
ColIV	Collagen type IV
ColVII	Collagen type VII
CRNN	Cornulin
CsA	Cyclosporine A
cSCC	Cutaneous squamous cell carcinoma
CSF2	Colony stimulating factor 2
CXCL14	C-X-C motif chemokine ligand 14
ddH2O	Double distilled water
DEFB4A	Defensin, beta 4A
DMEM	Dulbecco's modified eagle's medium
EGF	Epidermal growth factor
ELF3	E74 like ETS transcription factor 3
EtOH	Ethanol
FAT1	FAT atypical cadherin 1
FGF7	Fibroblast growth factor 7
FLG	Filaggrin
GAPDH	Glyceraldehyde-3-phosphate dehydrogenase
GM-CSF	Granulocyte-macrophage colony-stimulating factor
HaCaT	Human adult Calcium Temperature
H&E	Haematoxylin & eosin
HGF	Hepatocyte growth factor
HRAS	Hras proto-oncogene, GTpase
IGFL1	IGF-like family member 1
IL-1α	Interleukin-1α
IPA	Ingenuity pathway analysis
ITGA6	Integrin subunit alpha 6
ITGB1	Integrin subunit beta 3
KGF	Keratinocyte growth factor
KRT10	Keratin 10
LCE1B	Late cornified envelope 1B
LCE2	Late cornified envelope 2
LCE2A	Late cornified envelope 2A
LCE3	Late cornified envelope 3
LCE3A	Late cornified envelope 3A

LCE3E	Late cornified envelope 3E
min	Minutes
Mio	Million
ml	Millilitre
MMP1	Matrix metallopeptidase 1
MMP3	Matrix metallopeptidase 3
MMP10	Matrix metallopeptidase 10
MYC	V-myc avian myelocytomatosis viral oncogene homolog
N_2	Nitrogen
NHDF	Normal human dermal fibroblasts
NHEK	Normal human epidermal keratinocytes
NMDS	Non-metric multidimensional scaling
O2	Oxygen
OTC	Organotypic culture
OTK	Organotypische Kultur
OTR	Organ transplant recipient
PBS	Phosphate buffered saline
PCR	Polymerase chain reaction
qRT-PCR	Quantitative reverse transcription PCR
RCAN1	Regulator of calcineurin 1
RNA	Ribonucleic acid
SPRR2B	Small proline-rich protein 2B
TEER	Transepithelial electrical resistance

7. APPENDIX

Table 7.1 List of 20 TOP up- and down-regulated genes from a genome wide RNA expression profile from HaCaT epithelia (DMSO vs. CsA)[1]

TOP 20 Up-regulated Genes				TOP 20 Down-regulated Genes			
Symbol	**Gene Name**	**p-value[2]**	**Fold Change[3]**	**Symbol**	**Gene Name**	**p-value[2]**	**Fold Change[3]**
LCE3A	late cornified envelope 3A	0	3.0	**CRNN**	cornulin	0	-4.8
DEFB4A	defensin, beta 4A	0	2.8	**KRT13**	keratin 13	1.0E-06	-3.6
LCE3E	late cornified envelope 3E	0	2.6	**RCAN1**	regulator of calcineurin 1	0	-3.5
CDSN	corneodesmosin	5.0E-06	2.3	**NR4A2**	nuclear receptor subfamily 4, group A, member 2	0	-3.4
CPA4	carboxypeptidase A4	0	2.2	**CCL2**	chemokine (C-C motif) ligand 2	3.0E-06	-2.9
EMP3	epithelial membrane protein 3	0	2.1	**NR4A2**	nuclear receptor subfamily 4, group A, member 2	0	-2.9
IGFL1	IGF-like family member 1	0	2.1	**STC1**	stanniocalcin 1	0	-2.8
LCE3D	late cornified envelope 3D	2.0E-06	2.1	**SLC2A3**	solute carrier family 2 (facilitated glucose transporter), member 3	0	-2.7
LY6D	lymphocyte antigen 6 complex, locus D	0	2.1	**OLFM4**	olfactomedin 4	0	-2.6
SPRR2B	small proline-rich protein 2B	0	2.0	**CES1**	carboxylesterase 1	0	-2.5
FADS1	fatty acid desaturase 1	0	1.9	**TMPRSS11D**	transmembrane protease, serine 11D	0	-2.5
GPSM1	G-protein signaling modulator 1	2.0E-05	1.9	**MAL**	mal, T-cell differentiation protein	2.0E-06	-2.5
IL36G	interleukin 36, gamma	5.0E-06	1.9	**PLIN2**	perilipin 2	0	-2.3
PRODH	proline dehydrogenase (oxidase) 1	0	1.8	**DIO2**	deiodinase, iodothyronine, type II	1.0E-06	-2.1
MYADM	myeloid-associated differentiation marker	3.3E-05	1.8	**HES1**	hairy and enhancer of split 1, (Drosophila)	1.0E-06	-2.0
GRHL3	grainyhead-like 3	1.0E-06	1.8	**UBE2C**	ubiquitin-	6.0E-06	-2.0

	(Drosophila)				conjugating enzyme E2C		
CRCT1	cysteine-rich C-terminal 1	1.0E-06	1.7	**SFTPD**	surfactant protein D	4.0E-06	-2.0
GSDMA	gasdermin A	7.8E-04	1.7	**KRT4**	keratin 4	2.0E-06	-1.9
EDN1	endothelin 1	2.1E-04	1.7	**IFI27**	interferon, alpha-inducible protein 27	3.0E-05	-1.9
PTGS2	prostaglandin-endoperoxide synthase 2 (prostaglandin G/H synthase and cyclooxygenase)	4.1E-05	1.7	**CD70**	CD70 molecule	0	-1.9

[1] OTCs were treated for 2 weeks

[2] 0 = p-value ≤ 0.000001

[3] fold changes were calculated with Chipster. The table shows numbers recalculated from log2. Values below 1 (negative fold changes) were converted by the following formula: fold change= –(1/x).

Underlined gene symbols: part of the GO-term: GO-0008544 (‘epidermal development’).

Table 7.2 List of 20 TOP up- and down-regulated genes from a genome wide RNA expression profile from HaCaT-RAS A-5 epithelia (DMSO vs. CsA)[1]

TOP 20 Up-regulated Genes				TOP 20 Down-regulated Genes			
Symbol	**Gene Name**	**p-value[2]**	**Fold Change[3]**	**Symbol**	**Gene Name**	**p-value[2]**	**Fold Change[3]**
SPRR2G	small proline-rich protein 2G	1.4E-04	8.5	**SCGB1A1**	secretoglobin, family 1A, member 1 (uteroglobin)	0	-17.9
LCE3D	late cornified envelope 3D	9.8E-05	6.2	**RARRES3**	retinoic acid receptor responder (tazarotene induced) 3	2.0E-06	-5.1
AADACL2	arylacetamide deacetylase-like 2	9.0E-06	5.8	**CEACAM 1**	carcinoembryonic antigen-related cell adhesion molecule 1 (biliary glycoprotein)	2.0E-06	-4.5
LCE2B	late cornified envelope 2B	3.9E-05	5.6	**KRT24**	keratin 24	1.0E-06	-4.3
LCE2D	late cornified envelope 2D	5.2E-05	5.6	**CEACAM 5**	carcinoembryonic antigen-related cell adhesion molecule 5	8.0E-06	-4.1
SPRR2B	small proline-rich protein 2B	6.7E-04	5.6	**MAL**	mal, T-cell differentiation protein	2.9E-03	-4.1
SBSN	suprabasin	1.7E-05	5.4	**MUC4**	mucin 4, cell surface associated	0	-4.1
SPRR2C	small proline-rich protein 2C (pseudogene)	3.2E-04	5.3	**GABRP**	gamma-aminobutyric acid (GABA) A receptor, pi	1.0E-06	-4.1
ASPRV1	aspartic peptidase, retroviral-like 1	5.4E-05	5.2	**MUC20**	mucin 20, cell surface associated	6.0E-06	-4.0
DSG1	desmoglein 1	1.7E-05	4.9	**CAPN13**	calpain 13	0	-3.9
LCE2A	late cornified envelope 2A	1.3E-04	4.4	**IGFBP3**	insulin-like growth factor binding protein 3	0	-3.7
KPRP	keratinocyte proline-rich protein	2.8E-04	4.4	**KYNU**	kynureninase	0	-3.7
SERPINA12	serpin peptidase inhibitor, clade A (alpha-1 antiproteinase, antitrypsin), member 12	1.5E-04	4.2	**FOXA1**	forkhead box A1	3.4E-05	-3.7

CDSN	corneodesmosin	4.8E-04	4.2	**ELF3**	E74-like factor 3 (ets domain transcription factor, epithelial-specific)	0	-3.6
SPRR2E	small proline-rich protein 2E	5.2E-05	4.1	**IGFBP3**	insulin-like growth factor binding protein 3	0	-3.5
LCE1B	late cornified envelope 1B	4.3E-05	4.1	**MDK**	midkine (neurite growth-promoting factor 2)	6.0E-06	-3.5
LCE6A	late cornified envelope 6A	1.8E-04	3.9	**ALOX5**	arachidonate 5-lipoxygenase	1.0E-06	-3.4
FLG	filaggrin	2.5E-04	3.8	**MAL**	mal, T-cell differentiation protein	7.0E-04	-3.4
ALOX12B	arachidonate 12-lipoxygenase, 12R type	1.3E-04	3.8	**ADIRF**	adipogenesis regulatory factor	7.1E-05	-3.2
LCE2C	late cornified envelope 2C	3.5E-04	3.7	**STC1**	stanniocalcin 1	0	-3.1

[1] OTCs were treated for 3 weeks

[2] 0 = p-value ≤ 0.000001

[3] fold changes were calculated with Chipster. The table shows numbers recalculated from log2. Values below 1 (negative fold changes) were converted by the following formula: fold change= –(1/x).

Underlined gene symbols: part of the GO-term: GO-0008544 ('epidermal development').

Table 7.3 Genes differentially expressed in HaCaT and HaCaT-RAS A-5 epithelia [taken from genome wide RNA expression profiles (DMSO vs. CsA)][1]

		HaCaT		HaCaT-RAS A-5			
Symbol	**Entrez Gene Name**	**p-value[2]**	**Fold change (log2)**	**p-value[2]**	**Fold change (log2)**	**Location**	**Type(s)**
DEFB4A/DEFB4B[3]	defensin beta 4A	0	1.48	0.016	1.207	Extracellular Space	other
XK	X-linked Kx blood group	0	1.47	0	-2.717	Plasma Membrane	transporter
LCE3E	late cornified envelope 3E	0	1.397	0.002	1.533	Other	other
CDSN	corneodesmosin	0	1.213	0	2.063	Plasma Membrane	other
CPA4	carboxypeptidase A4	0	1.157	0	1.613	Extracellular Space	peptidase
IGFL1[3]	IGF like family member 1	0	1.093	0	1.29	Extracellular Space	other
LCE3D	late cornified envelope 3D	0	1.093	0	2.627	Other	other
SPRR2B	small proline rich protein 2B	0	0.987	0.001	2.48	Cytoplasm	other
GPSM1	G-protein signaling modulator 1	0	0.927	0.016	0.707	Cytoplasm	other
LOC102724788/PRODH	proline dehydrogenase 1	0	0.87	0	0.667	Cytoplasm	enzyme
CRCT1	cysteine rich C-terminal 1	0	0.787	0	1.703	Other	other
GSDMA	gasdermin A	0.001	0.777	0.003	0.917	Cytoplasm	other
CXCL14[3]	C-X-C motif chemokine ligand 14	0	0.747	0	1.783	Extracellular Space	cytokine
SPRR2C	small proline rich protein 2C (pseudogene)	0	0.73	0	2.397	Cytoplasm	other
CST6	cystatin E/M	0	0.713	0	1.207	Extracellular Space	other
SLC5A1	solute carrier family 5 member 1	0	0.707	0.005	0.757	Plasma Membrane	transporter
ELOVL4	ELOVL fatty acid elongase 4	0	0.7	0	1.733	Cytoplasm	enzyme
CDH16	cadherin 16	0	0.687	0	1.27	Plasma Membrane	enzyme
LCE2C/LCE2D	late cornified envelope 2D	0	0.677	0	2.483	Other	other
CLCF1	cardiotrophin-like cytokine factor 1	0	0.633	0.003	0.85	Extracellular Space	cytokine
LCE2B	late cornified envelope 2B	0.001	0.613	0	2.497	Other	other
LCE6A	late cornified envelope 6A	0.004	0.607	0	1.947	Other	other
KPRP	keratinocyte proline rich protein	0.001	0.603	0	2.137	Cytoplasm	other
PSORS1C2	psoriasis susceptibility 1 candidate 2	0.002	0.603	0	1.327	Extracellular Space	other
IGFL2	IGF like family member 2	0	-0.623	0	1.507	Other	other
C17orf53	chromosome 17 open reading frame 53	0	-0.637	0.007	-0.63	Other	other
PHLDA1	pleckstrin homology like domain family A member 1	0	-0.64	0	-1.093	Cytoplasm	other
ELF3	E74 like ETS transcription factor 3	0.001	-0.64	0	-1.843	Nucleus	transcription regulator
SLC16A3	solute carrier family 16 member 3	0	-0.647	0	-0.887	Plasma Membrane	transporter
FGG	fibrinogen gamma chain	0	-0.65	0	1.17	Extracellular Space	other
PRC1	protein regulator of cytokinesis 1	0	-0.66	0	-0.663	Nucleus	other
TSPAN6	tetraspanin 6	0	-0.687	0.006	-0.837	Plasma Membrane	other
CEACAM5	carcinoembryonic antigen related cell adhesion molecule 5	0	-0.693	0	-2.04	Plasma Membrane	other

CEACAM1	carcinoembryonic antigen related cell adhesion molecule 1	0	-0.703	0	-2.16	Plasma Membrane	other
PHGR1	proline/histidine/glycine-rich 1	0	-0.74	0	-0.96	Other	other
PPP1R1B	protein phosphatase 1 regulatory inhibitor subunit 1B	0	-0.743	0.001	-0.737	Cytoplasm	phosphatase
TOP2A	topoisomerase (DNA) II alpha	0	-0.75	0	-0.977	Nucleus	enzyme
CAPN5	calpain 5	0	-0.763	0	-1.27	Cytoplasm	peptidase
CXCL2	C-X-C motif chemokine ligand 2	0.001	-0.793	0.007	0.647	Extracellular Space	cytokine
AOC1	amine oxidase. copper containing 1	0	-0.8	0.004	-1.367	Extracellular Space	enzyme
MDK	midkine (neurite growth-promoting factor 2)	0	-0.843	0	-1.8	Extracellular Space	growth factor
HILPDA	hypoxia inducible lipid droplet associated	0	-0.85	0	-1.157	Cytoplasm	other
CDCA5	cell division cycle associated 5	0	-0.86	0	-0.717	Cytoplasm	other
SPRR3	small proline rich protein 3	0	-0.867	0.047	-0.923	Cytoplasm	other
CCNB2	cyclin B2	0	-0.883	0.001	-0.703	Cytoplasm	other
HIST1H4C	histone cluster 1. H4c	0	-0.907	0	-0.64	Nucleus	other
FOXQ1	forkhead box Q1	0	-0.93	0.002	-1.187	Nucleus	transcription regulator
IFI27	interferon alpha inducible protein 27	0	-0.96	0	-1.55	Cytoplasm	other
KRT4	keratin 4	0	-0.963	0.001	-1.347	Cytoplasm	other
UBE2C	ubiquitin conjugating enzyme E2 C	0	-0.987	0.001	-0.81	Cytoplasm	enzyme
PLIN2	perilipin 2	0	-1.197	0	-0.687	Plasma Membrane	other
MAL	mal T-cell differentiation protein	0	-1.307	0.003	-2.04	Plasma Membrane	transporter
OLFM4	olfactomedin 4	0	-1.38	0	-0.793	Extracellular Space	other
STC1	stanniocalcin 1	0	-1.487	0	-1.623	Extracellular Space	kinase
CCL2	C-C motif chemokine ligand 2	0	-1.557	0	1.043	Extracellular Space	cytokine
KRT13	keratin 13	0	-1.847	0.022	-0.873	Cytoplasm	other
CRNN	cornulin	0	-2.273	0.015	-1.01	Cytoplasm	other

[1] the rows of the table are sorted by the fold change of HaCaT
[2] 0 = p-value ≤ 0.000001
[3] candidate genes for validation and stimulation experiments

Table 7.4 List of 20 TOP up- and down-regulated genes from a genome wide RNA expression profile from HaCaT-OLD epithelia (DMSO vs. CsA treatment)[1]

TOP 20 Up-regulated Genes				TOP 20 Down-regulated Genes			
Symbol	**Gene Name**	**p-value[2]**	**Fold Change[3]**	**Symbol**	**Gene Name**	**p-value[2]**	**Fold Change[3]**
DHRS9	dehydrogenase/reductase (SDR family) member 9	0	2.8	**IFI27**	interferon, alpha-inducible protein 27	0	-3.2
PTGS2	prostaglandin-endoperoxide synthase 2 (prostaglandin G/H synthase and cyclooxygenase)	0	2.5	**TCN1**	transcobalamin I (vitamin B12 binding protein, R binder family)	1.0E-06	-2.9
DHRS9	dehydrogenase/reductase (SDR family) member 9	0	2.4	**ALDH3A1**	aldehyde dehydrogenase 3 family, member A1	0	-2.8
IL1RL1	interleukin 1 receptor-like 1	0	2.3	**KRT2**	keratin 2	0	-2.8
EMP3	epithelial membrane protein 3	0	2.2	**SPRR3**	small proline-rich protein 3	0	-2.6
THBS1	thrombospondin 1	0	2.1	**S100A7A**	S100 calcium binding protein A7A	0	-2.5
LEPREL1	leprecan-like 1	0	2.0	**HTR3A**	5-hydroxytryptamine (serotonin) receptor 3A, ionotropic	0	-2.5
MYADM	myeloid-associated differentiation marker	3.0E-06	2.0	**S100P**	S100 calcium binding protein P	0	-2.4
TNC	tenascin C	2.0E-06	2.0	**HRNR**	hornerin	2.4E-03	-2.4
RGCC	regulator of cell cycle	0	1.9	**DEFB1**	defensin, beta 1	1.0E-06	-2.3
CLCF1	cardiotrophin-like cytokine factor 1	0	1.9	**CD36**	CD36 molecule (thrombospondin receptor)	4.0E-06	-2.3
PTGS2	prostaglandin-endoperoxide synthase 2 (prostaglandin G/H synthase and cyclooxygenase)	2.3E-05	1.9	**GCNT3**	glucosaminyl (N-acetyl) transferase 3, mucin type	0	-2.2
CREB3L2	cAMP responsive element binding protein 3-like 2	0	1.9	**SERPINB4**	serpin peptidase inhibitor, clade B (ovalbumin), member 4	0	-2.1
FBN2	fibrillin 2	5.0E-06	1.8	**TMPRSS11D**	transmembrane protease, serine 11D	0	-2.1
EDN1	endothelin 1	2.1E-05	1.8	**IFIT2**	interferon-induced protein with tetratricopeptide repeats 2	0	-2.1
GPSM1	G-protein signaling modulator 1	1.0E-06	1.8	**AKR1B10**	aldo-keto reductase family 1, member B10 (aldose reductase)	0	-2.1
FOS	FBJ murine osteosarcoma viral oncogene homolog	0	1.8	**LOR**	loricrin	1.6E-05	-2.0
PHACTR3	phosphatase and actin regulator 3	3.0E-06	1.8	**GBP2**	guanylate binding protein 2, interferon-inducible	0	-2.0
LCE3E	late cornified envelope 3E	1.3E-05	1.8	**GPNMB**	glycoprotein (transmembrane) nmb	0	-2.0
MYADM	myeloid-associated differentiation marker	1.0E-06	1.8	**CRNN**	cornulin	0	-2.0

[1] OTCs were treated for 4 weeks

[2] 0 = p-value ≤ 0.000001

[3] fold changes were calculated with Chipster. The table shows numbers recalculated from log2. Values below 1 (negative fold changes) were converted by the following formula: fold change= –(1/x). Underlined gene symbols: part of the GO-term: GO-0008544.

Table 7.5 List of 20 TOP up- and down-regulated genes from a genome wide RNA expression profile from HaCaT epithelia (DMSO vs. UV+CsA)[1]

TOP 20 Up-regulated Genes				TOP 20 Down-regulated Genes			
Symbol	**Gene Name**	**p-value[2]**	**Fold Change[3]**	**Symbol**	**Gene Name**	**p-value[2]**	**Fold Change[3]**
MYADM	myeloid-associated differentiation marker	0	3.2	**KRT13**	keratin 13	0	-10.3
DEFB4A	defensin, beta 4A	0	2.6	**CRNN**	cornulin	0	-7.4
CDSN	corneodesmosin	1.0E-06	2.4	**MAL**	mal, T-cell differentiation protein	0	-6.4
DSC1	desmocollin 1	4.0E-05	2.4	**CCL2**	chemokine (C-C motif) ligand 2	0	-6.3
CXCL14	chemokine (C-X-C motif) ligand 14	3.0E-06	2.4	**OLFM4**	olfactomedin 4	0	-5.7
SPRR2B	small proline-rich protein 2B	0	2.3	**STC1**	stanniocalcin 1	0	-5.6
LCE3E	late cornified envelope 3E	0	2.3	**KRT4**	keratin 4	0	-5.6
TYMP	thymidine phosphorylase	0	2.1	**CES1**	carboxylesterase 1	0	-5.0
COL17A1	collagen, type XVII, alpha 1	5.0E-06	2.1	**HTR3A**	5-hydroxytryptamine (serotonin) receptor 3A, ionotropic	0	-4.7
EMP3	epithelial membrane protein 3	0	2.1	**SPINK7**	serine peptidase inhibitor, Kazal type 7 (putative)	0	-3.9
IL36G	interleukin 36, gamma	0	2.1	**NR4A2**	nuclear receptor subfamily 4, group A, member 2	0	-3.9
GPSM1	G-protein signaling modulator 1	1.0E-06	2.1	**MAL**	mal, T-cell differentiation protein	0	-3.8
CPA4	carboxypeptidase A4	0	2.0	**TMPRSS11D**	transmembrane protease, serine 11D	0	-3.8
PFKFB4	6-phosphofructo-2-kinase/fructose-2,6-biphosphatase 4	1.0E-06	2.0	**CD36**	CD36 molecule (thrombospondin receptor)	0	-3.7
PTGS2	prostaglandin-endoperoxide synthase 2 (prostaglandin G/H synthase and cyclooxygenase)	0	2.0	**DIO2**	deiodinase, iodothyronine, type II	0	-3.6
IGFL1	IGF-like family member 1	1.0E-06	2.0	**ID1**	inhibitor of DNA binding 1, dominant negative helix-loop-helix protein	0	-3.3
DSC1	desmocollin 1	2.8E-04	2.0	**SFTPD**	surfactant protein D	0	-3.2
RGS20	regulator of G-protein signaling 20	0	2.0	**GCNT3**	glucosaminyl (N-acetyl) transferase 3, mucin type	0	-3.1
LAMC2	laminin, gamma 2	0	1.9	**SLC2A3**	solute carrier family 2 (facilitated glucose transporter), member 3	1.0E-06	-3.1
LCE3A	late cornified envelope 3A	3.1E-05	1.9	**VS.IG8**	V-set and immunoglobulin domain containing 8	0	-3.0

[1] OTCs were treated for 2 weeks

[2] 0 = p-value ≤ 0.000001

[3] fold changes were calculated with Chipster. The table shows numbers recalculated from log2. Values below 1 (negative fold changes) were converted by the following formula: fold change= –(1/x).

Table 7.6 List of 20 TOP up- and down-regulated genes from a genome wide RNA expression profile from HaCaT-RAS A-5 epithelia (DMSO vs. UV+CsA)[1]

TOP 20 Up-regulated Genes				TOP 20 Down-regulated Genes			
Symbol	**Gene Name**	**p-value[2]**	**Fold Change[3]**	**Symbol**	**Gene Name**	**p-value[2]**	**Fold Change[3]**
DSC1	desmocollin 1	0	26.2	**KRT13**	keratin 13	0	-82.9
DEFB4A	defensin, beta 4A	0	20.3	**MAL**	mal, T-cell differentiation protein	0	-40.9
SPRR2B	small proline-rich protein 2B	0	18.9	**SCGB1A1**	secretoglobin, family 1A, member 1 (uteroglobin)	0	-33.8
SPRR2G	small proline-rich protein 2G	0	16.0	**NA**	NA	0	-30.0
SPRR2C	small proline-rich protein 2C (pseudogene)	0	15.3	**KRT4**	keratin 4	0	-21.7
KRT2	keratin 2	0	15.0	**SPRR3**	small proline-rich protein 3	0	-15.8
SERPINA12	serpin peptidase inhibitor, clade A (alpha-1 antiproteinase, antitrypsin), member 12	0	14.4	**ADIRF**	adipogenesis regulatory factor	0	-15.2
DSG1	desmoglein 1	0	13.3	**AOC1**	amine oxidase, copper containing 1	0	-11.5
AADACL2	arylacetamide deacetylase-like 2	0	12.2	**CLDN8**	claudin 8	0	-11.4
CDSN	corneodesmosin	0	11.5	**CEACAM1**	carcinoembryonic antigen-related cell adhesion molecule 1 (biliary glycoprotein)	0	-10.5
LCE3D	late cornified envelope 3D	0	8.0	**ELF3**	E74-like factor 3 (ets domain transcription factor, epithelial-specific)	0	-10.4
SBSN	suprabasin	0	7.9	**MAL**	mal, T-cell differentiation protein	0	-10.0
KRT3	keratin 3	0	7.9	**HIST1H4C**	histone cluster 1, H4c	0	-9.9
ELOVL4	ELOVL fatty acid elongase 4	0	6.2	**KRT15**	keratin 15	0	-9.3
ALOX12B	arachidonate 12-lipoxygenase, 12R type	0	6.1	**S100A4**	S100 calcium binding protein A4	0	-9.3
HRNR	hornerin	0	6.0	**S100P**	S100 calcium binding protein P	0	-9.2
SPRR2E	small proline-rich protein 2E	0	6.0	**CLDN8**	claudin 8	0	-9.1
TMEM45A	transmembrane protein 45A	0	5.6	**CRNN**	cornulin	0	-9.1
FLG	filaggrin	0	5.6	**FOXA1**	forkhead box A1	0	-8.3
SPRR2E	small proline-rich protein 2E	0	5.5	**CEACAM1**	carcinoembryonic antigen-related cell adhesion molecule 1 (biliary glycoprotein)	0	-8.1

[1] OTCs were treated for 3 weeks

[2] 0 = p-value ≤ 0.000001

[3] fold changes were calculated with Chipster. The table shows numbers recalculated from log2. Values below 1 (negative fold changes) were converted by the following formula: fold change= –(1/x).

Table 7.7 List of 20 TOP up- and down-regulated genes from a genome wide RNA expression profile from HaCaT epithelia (DMSO vs. UV)[1]

TOP 20 Up-regulated Genes				TOP 20 Down-regulated Genes			
Symbol	**Gene Name**	**p-value[2]**	**Fold Change[3]**	**Symbol**	**Gene Name**	**p-value[2]**	**Fold Change[3]**
DSC1	desmocollin 1	3.0E-06	3.1	**MAL**	mal, T-cell differentiation protein	0	-5.6
SERPINA12	serpin peptidase inhibitor, clade A (alpha-1 antiproteinase, antitrypsin), member 12	4.7E-05	2.7	**KRT13**	keratin 13	0	-5.3
CDSN	corneodesmosin	6.5E-05	2.0	**CCL2**	chemokine (C-C motif) ligand 2	0	-4.2
ARG1	arginase 1	3.7E-05	1.9	**KRT4**	keratin 4	0	-3.3
SPRR2B	small proline-rich protein 2B	7.0E-06	1.9	**DCN**	decorin	0	-3.0
ADAP2	ArfGAP with dual PH domains 2	8.0E-05	1.8	**KLK12**	kallikrein-related peptidase 12	0	-2.9
FLG	filaggrin	1.1E-04	1.8	**HTR3A**	5-hydroxytryptamine (serotonin) receptor 3A, ionotropic	0	-2.8
DEFB4A	defensin, beta 4A	2.1E-05	1.8	**TMPRSS11D**	transmembrane protease, serine 11D	0	-2.7
COL17A1	collagen, type XVII, alpha 1	6.6E-05	1.7	**SPINK7**	serine peptidase inhibitor, Kazal type 7 (putative)	0	-2.6
PSAT1	phosphoserine aminotransferase 1	1.4E-04	1.7	**CES1**	carboxylesterase 1	0	-2.6
ASNS	asparagine synthetase (glutamine-hydrolyzing)	5.4E-05	1.7	**ELF3**	E74-like factor 3 (ets domain transcription factor, epithelial-specific)	0	-2.5
HRNR	hornerin	2.6E-03	1.7	**HTR3A**	5-hydroxytryptamine (serotonin) receptor 3A, ionotropic	0	-2.5
TRIB3	tribbles homolog 3 (Drosophila)	1.3E-05	1.7	**KLK13**	kallikrein-related peptidase 13	0	-2.5
MAP2	microtubule-associated protein 2	6.1E-05	1.7	**CD70**	CD70 molecule	0	-2.3
SH3KBP1	SH3-domain kinase binding protein 1	2.9E-05	1.6	**OLFM4**	olfactomedin 4	0	-2.3
RCAN1	regulator of calcineurin 1	6.6E-05	1.6	**C6orf15**	chromosome 6 open reading frame 15	0	-2.1
SPRR2C	small proline-rich protein 2C (pseudogene)	1.3E-05	1.6	**STC1**	stanniocalcin 1	0	-2.1
COL17A1	collagen, type XVII, alpha 1	6.0E-06	1.6	**ID1**	inhibitor of DNA binding 1, dominant negative helix-loop-helix protein	0	-2.1
SLPI	secretory leukocyte peptidase inhibitor	7.0E-06	1.6	**GBP6**	guanylate binding protein family, member 6	0	-2.1
TNFRSF21	tumor necrosis factor receptor superfamily, member 21	1.1E-05	1.6	**DHRS9**	dehydrogenase/reductase (SDR family) member 9	1.0E-06	-2.1

[1] OTCs were treated for 2 weeks

[2] 0 = p-value ≤ 0.000001

[3] fold changes were calculated with Chipster. The table shows numbers recalculated from log2. Values below 1 (negative fold changes) were converted by the following formula: fold change= –(1/x)

Table 7.8 List of 20 TOP up- and down-regulated genes from a genome wide RNA expression profile from HaCaT-RAS A-5 epithelia (DMSO vs. UV)[1]

TOP 20 Up-regulated Genes				TOP 20 Down-regulated Genes			
Symbol	**Gene Name**	**p-value[2]**	**Fold Change[3]**	**Symbol**	**Gene Name**	**p-value[2]**	**Fold Change[3]**
KRT2	keratin 2	0	26.5	**KRT13**	keratin 13	0	-46.6
DSC1	desmocollin 1	0	23.2	**MAL**	mal, T-cell differentiation protein	0	-38.1
DEFB4A	defensin, beta 4A	0	20.4	**SCGB1A1**	secretoglobin, family 1A, member 1 (uteroglobin)	0	-32.2
SPRR2B	small proline-rich protein 2B	0	19.8	**KRT4**	keratin 4	0	-21.3
SERPINA12	serpin peptidase inhibitor, clade A (alpha-1 antiproteinase, antitrypsin), member 12	0	17.6	**CLDN8**	claudin 8	0	-14.2
SPRR2G	small proline-rich protein 2G	1.0E-06	17.3	**ADIRF**	adipogenesis regulatory factor	1.0E-06	-9.3
SPRR2C	small proline-rich protein 2C (pseudogene)	0	16.0	**SPRR3**	small proline-rich protein 3	0	-8.3
LCE3D	late cornified envelope 3D	0	11.0	**KRT15**	keratin 15	0	-8.2
HRNR	hornerin	0	10.6	**CEACAM1**	carcinoembryonic antigen-related cell adhesion molecule 1 (biliary glycoprotein)	0	-7.9
AADACL2	arylacetamide deacetylase-like 2	0	10.2	**FOXA1**	forkhead box A1	0	-7.8
CDSN	corneodesmosin	0	9.2	**GCNT3**	glucosaminyl (N-acetyl) transferase 3, mucin type	0	-7.4
DSG1	desmoglein 1	0	9.0	**ELF3**	E74-like factor 3 (ets domain transcription factor, epithelial-specific)	0	-7.2
LCE2B	late cornified envelope 2B	1.0E-06	7.9	**RARRES3**	retinoic acid receptor responder (tazarotene induced) 3	0	-7.1
LCE2D	late cornified envelope 2D	1.0E-06	7.9	**CEACAM5**	carcinoembryonic antigen-related cell adhesion molecule 5	0	-6.9
KRT3	keratin 3	0	7.3	**CEACAM1**	carcinoembryonic antigen-related cell adhesion molecule 1 (biliary glycoprotein)	0	-6.8
SBSN	suprabasin	0	6.9	**AOC1**	amine oxidase, copper containing 1	0	-6.7
SPRR2E	small proline-rich protein 2E	0	6.8	**DHRS9**	dehydrogenase/reductase (SDR family) member 9	0	-6.6
LCE2A	late cornified envelope 2A	0	6.7	**KRT19**	keratin 19	0	-6.5
ALOX12B	arachidonate 12-lipoxygenase, 12R type	0	6.5	**MUC20**	mucin 20, cell surface associated	0	-5.9
FGG	fibrinogen gamma chain	0	6.4	**S100A4**	S100 calcium binding protein A4	4.0E-06	-5.8

[1] OTCs were treated for 3 weeks

[2] 0 = p-value ≤ 0.000001

[3] fold changes were calculated with Chipster. The table shows numbers recalculated from log2. Values below 1 (negative fold changes) were converted by the following formula: fold change= –(1/x)

Table 7.9 Genes differentially expressed in HaCaT and HaCaT-RAS A-5 epithelia treated with CsA or UV or UV+CsA

		Fold Change (log2)						
		HaCaT			HaCaT-RAS A-5			
Symbol	**Gene Name**	**CsA**	**UV**	**UV+CsA**	**CsA**	**UV**	**UV+CsA**	**Protein type**
ANGPTL4	angiopoietin like 4	-0.42	-0.46	-0.68	-1.42	-1.01	-1.81	other
AOC1	amine oxidase, copper containing 1	-0.80	-0.65	-0.88	-1.37	-2.74	-3.52	enzyme
ARRDC4	arrestin domain containing 4	0.44	0.49	0.52	0.50	0.76	1.31	other
BPIFC	BPI fold containing family C	0.42	0.42	0.56	0.62	0.72	0.72	transporter
CAPN5	calpain 5	-0.76	-0.99	-1.27	-1.27	-1.68	-2.07	peptidase
CD14	CD14 molecule	-0.37	-0.54	-0.59	-0.69	-1.86	-2.24	transmembrane receptor
CD36	CD36 molecule	-0.73	-0.93	-1.90	0.51	0.47	-0.70	transmembrane receptor
CDH16	cadherin 16	0.69	0.42	0.83	1.27	0.86	1.42	enzyme
CDSN	corneodesmosin	1.21	0.99	1.29	2.06	3.20	3.53	other
CEACAM1	carcinoembryonic antigen related cell adhesion molecule 1	-0.70	-0.91	-0.91	-2.16	-2.99	-3.40	transporter
CEACAM5	carcinoembryonic antigen related cell adhesion molecule 5	-0.69	-0.95	-1.39	-2.04	-2.78	-3.00	other
CLDN7	claudin 7	-0.33	-0.48	-0.63	-1.13	-1.88	-2.06	other
CPA4	carboxypeptidase A4	1.16	0.45	1.03	1.61	1.53	1.36	peptidase
CTSV	cathepsin V	0.40	0.65	0.65	1.31	1.39	1.26	peptidase
ELF3	E74 like ETS transcription factor 3	-0.64	-1.35	-1.30	-1.84	-2.85	-3.38	transcription regulator
ELOVL4	ELOVL fatty acid elongase 4	0.70	0.54	0.91	1.73	2.35	2.62	enzyme
FAM3D	family with sequence similarity 3 member D	-0.40	-0.53	-0.75	-0.66	-0.77	-1.15	cytokine
FGG	fibrinogen gamma chain	-0.65	-0.63	-0.84	1.17	2.68	1.06	other
FOXC1	forkhead box C1	-0.40	-0.37	-0.46	-1.00	-1.12	-1.27	transcription regulator
GCHFR	GTP cyclohydrolase I feedback regulator	-0.58	-0.44	-0.77	-1.01	-1.52	-1.73	other
GCNT3	glucosaminyl (N-acetyl) transferase 3, mucin type	-0.53	-1.04	-1.64	-1.35	-2.89	-2.99	enzyme
GLDC	glycine decarboxylase	-0.35	-0.37	-0.45	-1.27	-1.24	-2.17	enzyme
GSTA2	glutathione S-transferase alpha 2	-0.54	-0.51	-0.50	-0.45	-0.39	-0.96	enzyme
HP	haptoglobin	-0.50	-0.39	-0.50	-0.88	-0.71	-1.40	peptidase
IGFBP3	insulin like growth factor binding protein 3	-0.52	-0.45	-0.54	-1.89	-1.64	-1.02	other
ISG15	ISG15 ubiquitin-like modifier	-0.52	-0.49	-0.62	-1.28	-1.71	-1.93	other
KRT4	keratin 4	-0.96	-1.72	-2.47	-1.35	-4.41	-4.44	other
KRT7	keratin 7	-0.43	-0.35	-0.44	-0.98	-1.64	-1.57	other
LAMA3	laminin subunit alpha 3	0.45	0.55	0.77	0.70	0.79	1.19	other
LCN2	lipocalin 2	-0.35	-0.64	-1.24	-1.17	-2.03	-2.56	transporter

LYPD2	LY6/PLAUR domain containing 2	0.36	-0.76	-0.76	-0.75	-1.54	-2.35	other
MAL	mal, T-cell differentiation protein	-1.31	-2.49	-2.67	-2.04	-5.25	-5.35	transporter
MDK	midkine (neurite growth-promoting factor 2)	-0.84	-0.55	-0.89	-1.80	-2.02	-2.30	growth factor
MUC4	mucin 4, cell surface associated	-0.55	-0.68	-0.71	-2.02	-2.40	-2.52	other
PHGR1	proline, histidine and glycine rich 1	-0.74	-0.62	-0.96	-0.96	-1.29	-1.53	other
PITX1	paired like homeodomain 1	-0.56	-0.58	-0.75	-0.79	-0.94	-1.30	transcription regulator
PPP1R1B	protein phosphatase 1 regulatory inhibitor subunit 1B	-0.74	-0.98	-1.39	-0.74	-1.11	-1.39	phosphatase
S100P	S100 calcium binding protein P	-0.55	-0.77	-1.38	-0.96	-2.15	-3.20	other
SBSN	suprabasin	0.39	0.43	0.52	2.43	2.80	2.98	other
SLC16A3	solute carrier family 16 member 3	-0.65	-0.39	-0.54	-0.89	-0.74	-1.18	transporter
SLC5A1	solute carrier family 5 member 1	0.71	0.50	0.92	0.76	1.51	2.05	transporter
SOX7	SRY-box 7	-0.69	-0.48	-1.17	-0.51	-0.47	-0.98	transcription regulator
SPRR2B	small proline rich protein 2B	0.99	0.90	1.23	2.48	4.31	4.24	other
SPRR2C	small proline rich protein 2C (pseudogene)	0.73	0.69	0.78	2.40	4.00	3.94	other
SPRR2G	small proline rich protein 2G	0.40	0.39	0.40	3.08	4.11	4.00	other
SRPX2	sushi repeat containing protein, X-linked 2	-0.50	-0.78	-0.74	-1.52	-1.75	-1.95	other
STC1	stanniocalcin 1	-1.49	-1.07	-2.48	-1.62	-1.35	-2.37	kinase
TMPRSS11D	transmembrane protease, serine 11D	-1.31	-1.44	-1.91	-0.56	-0.93	-1.31	peptidase
TSPAN6	tetraspanin 6	-0.69	-0.72	-0.98	-0.84	-1.23	-1.36	other
TYMP	thymidine phosphorylase	0.69	0.65	1.10	-0.58	-0.52	-0.49	growth factor
XK	X-linked Kx blood group	1.47	-1.22	-1.79	-2.72	-5.14	-4.91	transporter
XKRX	XK related, X-linked	0.58	0.54	0.62	0.77	1.21	1.24	other

Table 7.10 List of 20 TOP up- and down-regulated genes from genome wide RNA expression profile from HaCaT-GOLD epithelia (DMSO vs. CsA)[1]

TOP 20 Up-regulated Genes				TOP 20 Down-regulated Genes			
Symbol	**Gene Name**	**p-value[2]**	**Fold Change[3]**	**Symbol**	**Gene Name**	**p-value[2]**	**Fold Change[3]**
DEFB103B	defensin, beta 103B	0	8.1	**KRT2**	keratin 2	0	-19.6
CRCT1	cysteine-rich C-terminal 1	0	7.5	**OLFM4**	olfactomedin 4	0	-12.3
UPP1	uridine phosphorylase 1	0	6.6	**DAPL1**	death associated protein-like 1	0	-11.2
FAM25A	family with sequence similarity 25, member A	0	6.0	**DSC1**	desmocollin 1	0	-8.9
SERPINE2	serpin peptidase inhibitor, clade E (nexin, plasminogen activator inhibitor type 1), member 2	0	5.8	**KRT13**	keratin 13	0	-7.0
IL1A	interleukin 1, alpha	0	5.4	**HRNR**	hornerin	0	-6.7
IL1B	interleukin 1, beta	0	5.3	**SPRR3**	small proline-rich protein 3	0	-6.6
LCE3D	late cornified envelope 3D	0	5.2	**CD36**	CD36 molecule (thrombospondin receptor)	0	-6.5
TM4SF19	transmembrane 4 L six family member 19	0	5.1	**ALDH3A1**	aldehyde dehydrogenase 3 family, member A1	0	-6.3
LAMC2	laminin, gamma 2	0	4.5	**LOR**	loricrin	0	-6.1
LCE3E	late cornified envelope 3E	0	4.5	**AADACL2**	arylacetamide deacetylase-like 2	0	-5.4
RNASE7	ribonuclease, RNase A family, 7	0	4.1	**KRT3**	keratin 3	1.0E-06	-5.1
LAMC2	laminin, gamma 2	0	4.1	**TMEM45A**	transmembrane protein 45A	0	-4.8
PTGS2	prostaglandin-endoperoxide synthase 2 (prostaglandin G/H synthase and cyclooxygenase)	0	4.1	**CRNN**	cornulin	0	-4.7
TGFBI	transforming growth factor, beta-induced, 68kDa	0	4.0	**FLG**	filaggrin	0	-4.3
PTGS2	prostaglandin-endoperoxide synthase 2 (prostaglandin G/H synthase and cyclooxygenase)	0	3.9	**TMEM45A**	transmembrane protein 45A	0	-4.2
GPSM1	G-protein signaling modulator 1	0	3.9	**VIPR1**	vasoactive intestinal peptide receptor 1	0	-4.2
SERPINE1	serpin peptidase inhibitor, clade E (nexin, plasminogen activator inhibitor type 1), member 1	0	3.7	**FLG**	filaggrin	0	-4.2
ACKR3	atypical chemokine receptor 3	0	3.6	**LOC645638**	WDNM1-like pseudogene	0	-4.0
SERPINB1	serpin peptidase inhibitor, clade B (ovalbumin), member 1	0	3.6	**RPTN**	repetin	0	-4.0

[1] OTCs were treated for 2 weeks

[2] 0 = p-value ≤ 0.000001

[3] fold changes were calculated with Chipster. The table shows numbers recalculated from log2. Values below 1 (negative fold changes) were converted by the following formula: fold change= –(1)/x